



A Comprehensive Review on Analysis and Implementation of Recent Image Dehazing Methods

Subhash Chand Agrawal¹ · Anand Singh Jalal¹

Received: 22 April 2021 / Accepted: 18 April 2022 / Published online: 12 May 2022

© The Author(s) under exclusive licence to International Center for Numerical Methods in Engineering (CIMNE) 2022

Abstract

Images acquired in poor weather conditions (haze, fog, smog, mist, etc.) are often severely degraded. In the atmosphere, there exists two types of particles: dry particles (dust, smoke, etc.) and wet particles (water droplets, rain, etc.) Due to the scattering and absorption of these particles, various adverse effects, including reduced visibility and contrast, color distortions, etc. are introduced in the image. These degraded images are not acceptable for many computer vision applications such as smart transportation, video surveillance, weather forecasting, remote sensing, etc. The computer vision task associated with the mitigation of this effect is known as image dehazing. A high-quality input image (haze-free) is required to ensure the accurate working of these applications, supplied by image dehazing methods. The haze effect in the captured image is dependent on the distance from the observer to the scene. Besides, the scattering of particles adds non-linear and data-dependent noise to the captured image. Single image dehazing utilizes the physical model of hazy image formation in which estimation of depth or transmission is an important parameter to obtain a haze-free image. This review article groups the recent dehazing methods into different categories and elaborates the popular dehazing methods of each category. This category-wise analysis of different dehazing methods reveals that the deep learning and the restoration-based methods with priors have attracted the attention of the researchers in recent years in solving two challenging problems of image dehazing: dense haze and non-homogeneous haze. Also, recently, hardware implementation-based methods are introduced to assist smart transportation systems. This paper provides in-depth knowledge of this field; progress made to date and compares performance (both qualitative and quantitative) of the latest works. It covers a detailed description of dehazing methods, motivation, popular, and challenging datasets used for testing, metrics used for evaluation, and issues/challenges in this field from a new perspective. This paper will be useful to all types of researchers from novice to highly experienced in this field. It also suggests research gaps in this field where recent methods are lacking.

1 Introduction

The computer vision is defined as a field of study that deals in developing techniques to help computers gain high-level understanding from digital images or videos. It automates various tasks and extracts useful information from images/videos with the help of artificial intelligence systems. There are numerous computer vision applications, including smart transportation systems, video surveillance, object detection, weather forecasting, etc. [1] that require high-quality input images or videos to “see” and analyze the contents. Unfortunately, poor weather conditions (haze, fog, rain, etc.)

diminish the visibility and lead to the failure of these applications. The image captured under these circumstances suffers from various degradations, namely low contrast, faded colors and most importantly reduced visibility. These degradations occur in the captured image due to the scattering of atmospheric particles (aerosols, water droplets, molecules, etc.) suspended in the atmosphere.

The role of image dehazing is to improve the visual quality of a degraded image and remove the influence of the weather. Therefore, the image dehazing algorithm acts as preprocessing tool for many computer vision applications, as shown in Fig. 1.

Fog, mist, and haze are the atmospheric phenomena that reduce the visibility of the image. Fog and mist both occur when the air has wet particles or water droplets. Both the terms are almost the same and the only difference is how far we can see. Fog is the term generally referred to when

✉ Subhash Chand Agrawal
subhash.agrawal@glau.ac.in

¹ Department of Computer Engineering and Applications,
GLA University, Mathura, UP 281406, India

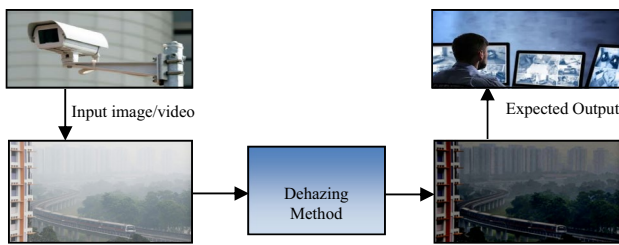


Fig. 1 An application of image dehazing

visibility is less than 1 km. If we can see more than 1 km away, it is considered as mist. Haze is a slightly different phenomenon, in which extremely small, dry particles, for example, air pollutants, dust, smoke, chemicals, etc. are suspended in the air. These dry particles are invisible to the naked eyes but sufficient to degrade the quality of the image in terms of visibility, contrast, and color. The visibility is less than 1.25 miles in the presence of haze. These dry particles are generated through various sources including farming, traffic, industry, and wildfires. Figure 2 shows the example image of fog, mist, and haze and also various sources of hazy image formation.

The hazy effect in the captured image is expressed by the atmospheric scattering model (ASM) or the physical

model of hazy image formation, as shown in Fig. 3. When incident light is reflected from the object, reflected light is attenuated due to the distance between observer and scene. In addition, due to the scattering of particles, airlight is also introduced into the camera. Therefore, a hazy image is composed of direct attenuation and airlight. Direct attenuation distorts the color whereas airlight reduces the visibility. The physical model is given as follows [2]:

$$I_{\text{hazy}}^c(x) = J_{\text{haze-free}}^c T_r(x) + A_t^c(1 - T_r(x)) \quad (1)$$

where $c \in \{r, g, b\}$ is the color channel, I_{hazy}^c is the captured hazy image, $J_{\text{haze-free}}^c$ is the haze-free image, A_t^c is the atmospheric light, T_r is the transmission medium, and x is a pixel position. The transmission describes the portion of light, directly reaching the camera without scattering. The value of the transmission medium lies in the range of $[0, 1]$. Furthermore, it is expressed as an exponential function of distance and depends on two parameters: distance d and scattering coefficient β , as follows:

$$T_r(x) = e^{-\beta d(x)} \quad (2)$$

Haze-free image $J_{\text{haze-free}}^c$ can be obtained in the inverse way as follows:

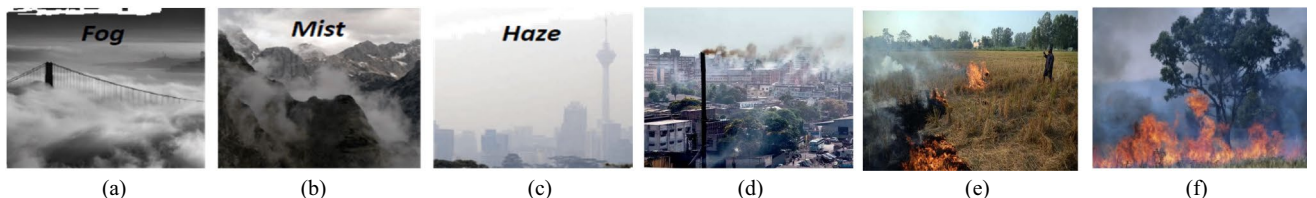


Fig. 2 Images of **a** fog, **b** mist, **c** haze, **d** Source: air pollutants, **e** Source: farming, **f** Source: wildfires

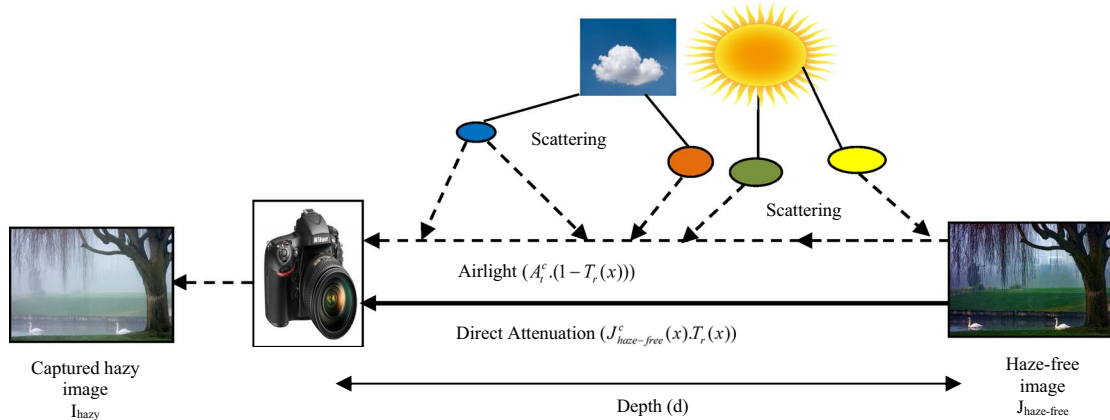


Fig. 3 Physical model of hazy image formation

$$J_{\text{haze-free}}^c(x) = \frac{I_{\text{hazy}}^c(x) - A_t^c}{T_r(x)} + A_t^c \quad (3)$$

Single image dehazing (SID) is an ill-posed problem because we have to estimate two key parameters A_t^c and T_r from I_{hazy}^c to find hazy-free image $J_{\text{haze-free}}^c$. The performance of a dehazing method depends on the estimation of key parameters.

In the past, many dehazing methods came into existence that utilizes various prior knowledge or assumptions to compute the depth information. However, the performance of these methods depends on the validity of these priors and may lead to various issues, such as color distortions, incomplete haze removal, halo artifacts, etc. In the literature, image enhancement based dehazing methods were also reported which do not require the estimation of the transmission and its costly refinement process. Since it does not consider the degradation mechanism into account while recovering an image. They suffer from the problem of over/under enhancement, over-saturation, and loss of information and are also unable to deal with dense hazy images. To overcome the problem of restoration and enhancement-based methods, many machine learning and deep learning methods are successfully implemented to compute an accurate transmission map. These methods require a vast amount of hazy and corresponding clean images to train the model. However, it is very difficult to obtain hazy images and their GT image in the real world. The related work section describes the recent dehazing methods of each category along with their pros and cons.

In this review article, we have mainly focused on haze removal methods from a single image proposed in 2016 and onwards. The major contributions are as follows:

- (1) This paper provides an extensive study of various recent the state-of-the-art dehazing methods. It classifies these methods into twelve categories: Image enhancement, Image restoration with prior, Image fusion, Superpixel, Machine learning, Deep learning, Polarization, DCP based, Airlight estimation, Hardware implementation, Non-homogenous and Miscellaneous. All these methods are investigated on various dehazing parameters, namely key technique, dataset, issues of dehazing, evaluation metrics, etc.
- (2) It provides a comprehensive study of various datasets used in image dehazing to date. It also discusses datasets of various haze densities from thin haze to very dense haze including real hazy images and synthetic hazy images. These datasets are assessed on various parameters, namely haze concentrations, number of images, and performance of recent dehazing methods.

- (3) This paper also explores different metrics introduced in recent works for the evaluation of dehazing algorithms with their merits and demerits.
- (4) Furthermore, this paper focuses on the latest technology advancement and development in this field from the perspective of non-homogenous haze removal, dense haze, hardware architecture, ensemble networks and deep learning methods.
- (5) Finally, it provides research gaps in single image dehazing where recent the state-of-the-art methods are lacking.

There are few papers available in the field of single image dehazing, however, they are limited to certain aspects. For instance, [3] concentrated on discussing various haze removal methods and quantitative results. Later, Wang et al. [4] added a description of different evaluation metrics. Singh et al. [5] explained numerous categories of dehazing methods with their pros and cons and analyzed methods based on issues of dehazing. However, it did not provide the qualitative and quantitative analysis of dehazing methods. In addition, it did not talk about standard dehazing datasets available for assessment. In the year 2020, two survey papers [6, 7] were reported. However, they take into consideration only a few recent papers from the year 2017 to 2020. This article considers approximately 150 recent papers in comparison to 46 in [7] and 51 in [6]. The comparison with existing survey/review papers is illustrated in Table 1. In this table, we can visualize the strength on various parameters of image dehazing. In addition to the previous research, this paper explores various untouched haze removal techniques for handling the most challenging problems of dehazing such as removal of non-homogeneous haze, superpixels, dense haze, and real-time applicability (hardware implementation). This article provides an extensive review of recent and popular dehazing techniques based on qualitative and quantitative comparisons, challenges in dehazing, available datasets, and evaluation metrics. This paper aspires to serve as a guide in all aspects of image dehazing for the researchers to find a path for their work.

2 Applications of Image Dehazing

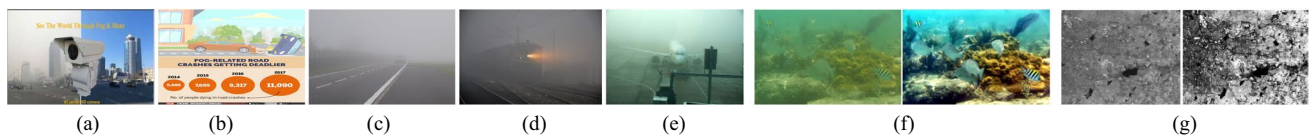
Image dehazing is an important area of research. The output of dehazing algorithms acts as an input to various vision applications. Some of the motivations are shown in Fig. 4 and discussed as follows:

2.1 Video Surveillance

A video surveillance system is a key component in the field of security. The effectiveness and accuracy of the visual

Table 1 Comparison with existing survey/review papers

| Survey/review paper | [4] (2017) | [3] (2017) | [5] (2019) | [6] (2020) | [7] (2020) | The proposed |
|---|--|---|---|--|--|---|
| (1) Year coverage | 2000 to 2015 | 1997 to 2016 | from 2008 to 2017 | 2008 to 2019 | 2012 to 2020 | from 2015 onward |
| (2) Motivation | No | No | Yes | No | No | Yes |
| (3) Classification | (1) Image Enhancement (2) Image Fusion (3) Image Restoration | (1) Depth estimation (2) Multi-images (3) Polarizing filters (4) Known depth (5) single image | (1) Depth Estimation (2) Wavelet Based (3) Enhancement (4) Filtering (5) Supervised learning (6) Fusion (7) Variational Image (8) Meta-heuristic | (1) Depth Estimation (2) Filtering (3) Fusion (4) Enhancement (5) Meta-Heuristic (6) Transform (7) Variational (8) Learning | (1) Filter (2) Color correction (3) Simple learning (4) Deep learning | (1) Image Enhancement (2) Image fusion (3) Restoration with priors (4) Polarization (5) DCP based (6) Airlight Estimation (7) Hardware (8) Machine Learning (9) Deep learning (10) Non-homogeneous (11) Miscellaneous (12) Superpixels |
| (4) Dehazing datasets | No | No | No | Yes | Limited | Yes |
| (5) Evaluation metrics | Yes | No | Yes | Yes | Limited | Yes |
| (6) Analysis based on issues of dehazing | No | No | Yes | Yes | No | Yes |
| (7) Qualitative and quantitative analysis | Yes | Yes | No | No | Yes | Yes |
| (8) Analysis based on standard datasets | No | No | No | Yes | Limited | Yes |
| (9) Future direction | Yes | No | Yes | Yes | Limited | Yes |

**Fig. 4** Applications of image dehazing, **a** video surveillance, **b** fog related road accidents, **c** road transportation, **d** railway transportation, **e** air transportation, **f** underwater image enhancement, **g** remote sensing

surveillance system depend on the quality of visual input. However, the poor weather condition affects the quality of input. The video captured by the camera of a surveillance system degrades due to scattering and absorption of light by the atmosphere. For example, video recorded in hazy weather has limited visibility which could be problematic for police, investigating a crime. Thus, these systems do perform poorly in hazy weather conditions. Hence, a robust surveillance system is required.

2.2 Intelligent Transportation System

The foggy weather conditions affect the driver's capabilities and increase the risk of accidents and the travel time significantly due to limited visibility. In past years, fog-related road fatalities have increased significantly. Road crashes, injuries or deaths on account of poor weather conditions like thick fog run in thousand every year on highways. The bad news is that this number is increasing every year [8].

In addition to roads or highways, fog also affects other transportation systems like airplanes and railways. Generally, takeoff and landing of airplanes become a very challenging task in a hazy environment. Due to which many flights get delayed or sometimes, they are canceled. Similarly, in the case of railway transportation, thick foggy conditions are a hazard to the passengers and crew members that could easily result in loss of life. The driver may miss the signals due to impaired visibility. Therefore, we require an intelligent transportation system that can provide a clear view to the driver in these transports to save life and property.

2.3 Underwater Image Enhancement

Underwater imaging often suffers poor visibility and color distortions. The poor visibility is produced by the haze effect due to the scattering of light by water particles multiple times. Color distortion is due to the attenuation of light and makes an image bluish. Therefore, an underwater vision system requires an image dehazing algorithm as a preprocessing so that a human can see the underwater objects.

2.4 Remote Sensing

In remote sensing, images are captured to obtain information about objects or areas. These images are usually taken from satellites or aircraft. Due to the high difference of distance in the camera and the scene, the haze effect is introduced in the captured scene. Therefore, this application also demands image dehazing as a preprocessing tool to improve the visual quality of an image before analysis.

Besides these applications, image dehazing also plays an important role in other applications, such as astronomy, medical science, agronomy, border security, archaeology, environmental studies and many more.

Therefore, it is important for computer vision applications to improve the visual quality of the image and highlight the image details. With respect to hardware aspects of camera sensors, many super-telephoto lenses are designed to incorporate scientific filtering and coating to enhance the contrast of the image. However, these lenses are very expensive and bulky and not applicable in daily life. Therefore, the restoration of hazy images or videos has attracted increasing interest in the last few years.

3 Issues/Challenges of Image Dehazing

The dehazed image may suffer from various types of issues like color shift, over enhancement, structure damage or incomplete haze removal, as shown in Fig. 5.

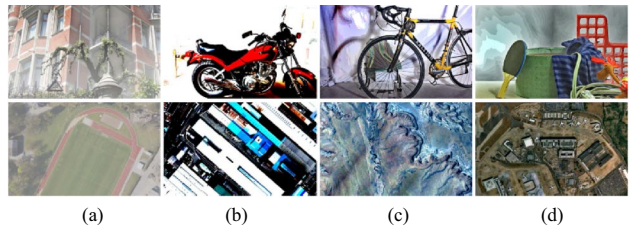


Fig. 5 [9]: Various issues of image dehazing **a** incomplete haze removal, **b** structure damage, **c** color shift, **d** over enhancement

3.1 Under/Over Enhancement

Restoration of hazy images often leads to two phenomena: under enhancement and over enhancement, as shown in Fig. 6. In under enhancement, haze is not completely removed from the original image. Hence, the visibility is not improved as desired. In case of over enhancement, the original information is changed in haze-free regions and color shift is caused in hazy regions during dehazing process [9]. This problem is generally observed in dense hazy regions which are having low contrast. Over dehazing makes the color much darker and causes saturation of pixels.

The image dehazing algorithms must keep the information of haze-free regions unchanged, meanwhile, capable enough to improve the visibility in hazy regions without color distortions.

3.2 Halo Artifact and Noise Amplification

The existing image dehazing method generally used patch-based method to estimate the transmission to recover the hazy image. Inaccurate estimation of the transmission may lead to distortions in the dehazed image, as shown in Fig. 7. Most of the method is also based on the assumption that local patches have similar depth. Depth discontinuities or abrupt jumps in an image will cause halo artifacts. To remove the problem of halo artifacts various refinement methods like Guided filtering, contextual regularization, total variation, etc. are utilized in many works. Still, the problem exists, halo artifacts are reduced but they are not completely removed.

Moreover, in presence of dense haze, noises and artifacts are not visible in the hazy images. The existing methods may amplify these noises and artifacts depending upon the depth and concentration of the haze during dehazing process [10]. Some of them introduce other distortion like the blurring effect in the dehazed images.

3.3 Dense Fog Removal/ Different Foggy Weather Conditions

In state-of-the-art dehazing methods, till now, there is not even a single method that can remove the effect of varying and challenging weather conditions like removal of all types of haze ranging from thin haze to very thick haze, night-time haze removal, non-homogenous haze (uneven distribution of haze), etc. as shown in Fig. 8.

Most of the methods work well in daytime scenes; they fail in night-time hazy conditions due to inaccurate estimation of the airlight. Generally, an airlight is estimated by the brightest pixels. This estimator faces two challenges when it is applied to night-time scenes (1) it is estimated globally over the entire image, whereas there are multiple local sources of light and they are non-uniform in nature. (2) It selects the white pixels which are the brightest pixels in the hazy image. But, it is not true for night-time scenes that exhibit strong color lighting [11].

The majority of the methods are able to remove the mild or thin haze. In presence of dense haze, either they fail to remove the haze completely or may result in loss of

information in form of saturation of pixels. In the case of thick fog, scene reflection becomes very small due to the small value of the transmission. The reason for small transmission is due to the large scattering coefficient, meanwhile, the proportion of airlight increases significantly. Therefore, it is a very challenging task to remove the thick haze considering minuscule reflection.

3.4 Adaptive Parameter Setting

The performance of the dehazing methods greatly depends on the selection of the different parameters, namely patch size, dehazing controlling parameter, Gamma correction, size of the filter, regularization term, scaling factor, number of superpixels, etc. For e.g., if the patch size is small, it may underestimate the transmission, especially for the regions with bright and white objects and may lead to over enhancement. By contrast, if the patch size is large, it may introduce the halo artifacts at depth discontinuities and also will increase the computation [12]. Therefore, for a good recovery result, patch size must be selected adaptively depending upon the pixels. Another parameter



Fig. 6 Hazy and haze-free images related to over/under enhancement problems. **a** Much darker color by dehazing method [15]. **b** Under enhancement problem by method [64]. **c** Saturation of pixels by method [51]. **d** Distortion of colors by method [13]

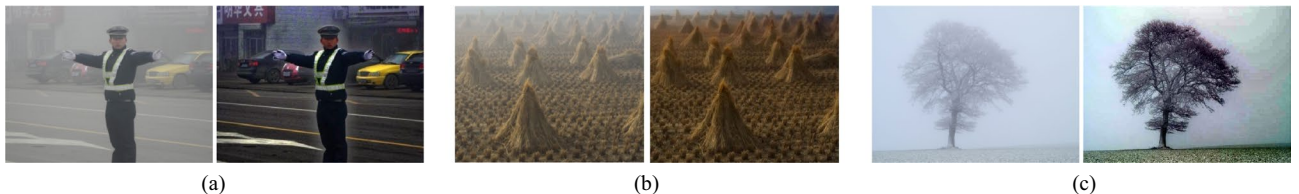


Fig. 7 Various distortion in dehazed image. **a** Halo artifacts by method [63]. **b** Blurring effect by method [51]. **c** Noise amplification by method [66]

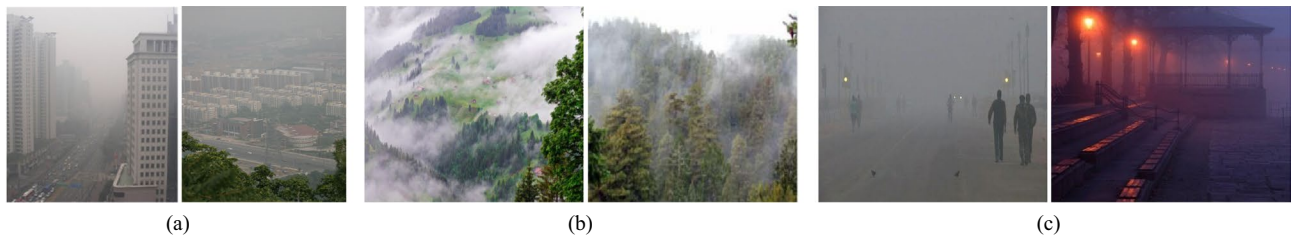


Fig. 8 Examples of challenging weather conditions. **a** Dense hazy images. **b** Non-homogenous hazy images. **c** Night-time hazy images

that is used by most of the methods is dehazing controlling parameter, as shown in Fig. 9.

All these parameters are set manually according to the experimental setup. They may not fit for different degrees of haze present in images. These parameters must be set adaptively to improve the performance because haze density on a given image varies from image to image and atmospheric veil.

3.5 Speed of Dehazing

Another drawback with existing dehazing methods is the computational complexity of the dehazing process. It is still a very challenging task to dehaze an image/video in real-time by which various vision applications, such as intelligent transportation systems or video surveillance can be benefited. The time complexity can be reduced by joint

estimation of airlight and transmission and to avoid the costly refinement process of the transmission.

4 Related Works

In recent years, significant progress is made in the field of image dehazing. We present recent and popular dehazing methods in this section. For convenience, we have divided these methods into the following categories: (1) image enhancement based, (2) image restoration with priors (3) image fusion based (4) non-homogeneous haze (5) hardware implementation based (6) polarization based (7) traditional learning based (8) deep learning based (9) superpixel based. Furthermore, subcategories of each category are identified, as shown in Fig. 10.

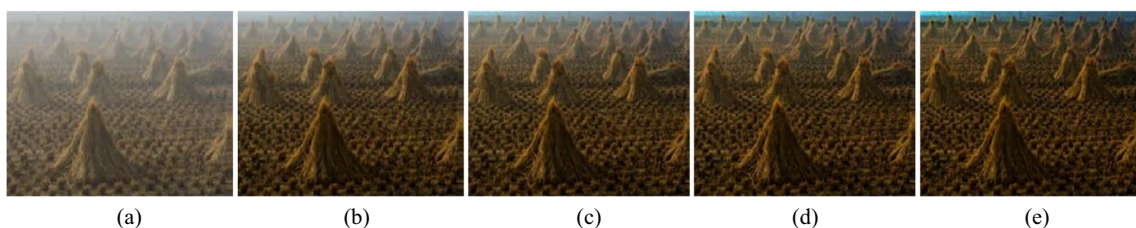


Fig. 9 Restored images with different δ by method [30]. **a** Original image, **b** $\delta=1.0$, **c** $\delta=0.8$, **d** $\delta=0.6$, **e** $\delta=0.4$

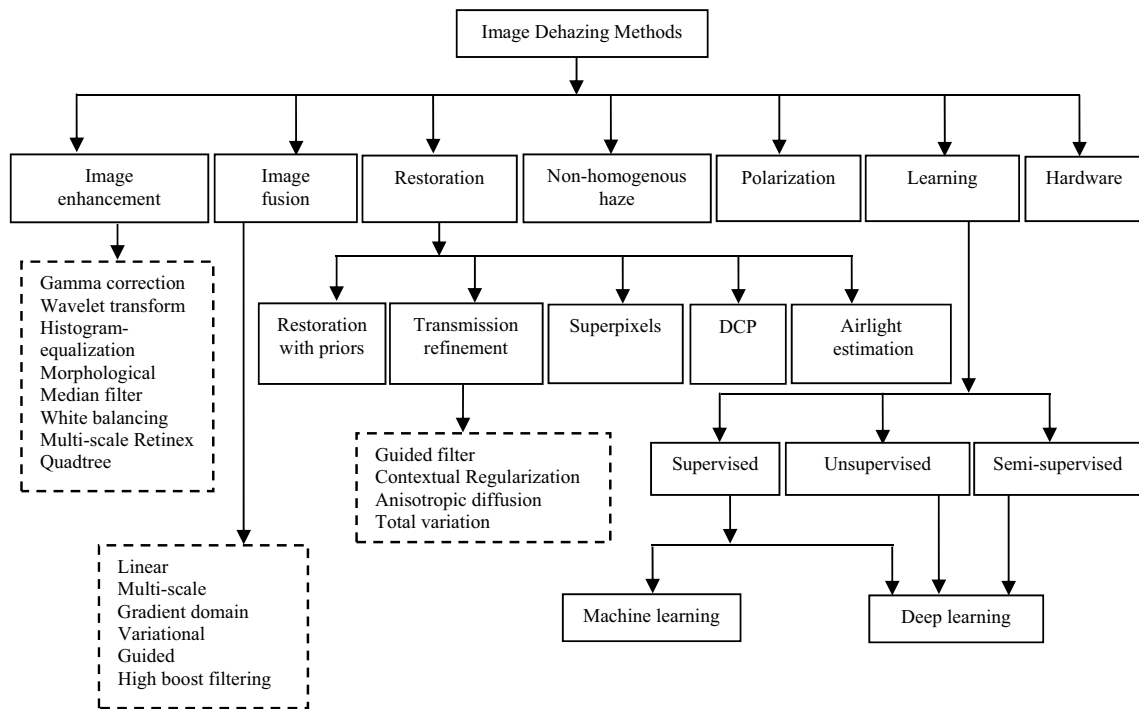


Fig. 10 Different categories of image dehazing methods

4.1 Image Enhancement based Methods

Image enhancement-based method can be divided in two sub-categories (1) the methods do not consider the atmospheric scattering model or degradation mechanism to enhance the visual quality of the hazy images. Therefore, they do not estimate the transmission and atmospheric light. (2) image enhancement operations are utilized in estimation of transmission or airlight. Hence, they may fall in methods of other categories too, such as restoration or fusion-based. Both sub-categories use various image enhancement techniques, including histogram equalization [13, 14], Bi-histogram modification [15], weighted histograms[16], Gamma correction [13, 17–20], multi-scale retinex [21], wavelet decomposition [22–25], multi-scale gradient domain contrast enhancement [17], texture filtering [26], bilateral filter [26, 27], white balance method [26, 28], median filtering [28, 29], Linear Transformation [30], morphological constructions [31], Discrete cosine transform [14], Guided filter [32–39], anisotropic diffusion [40, 41], contrast enhancement [42–44], quadtree Decomposition: [30, 45, 46], Contextual Regularization: [45, 47–49], weighted L1-norm regularization [50], and total variation [51–53] (Table 2).

Wang et al. [21] proposes a multi-scale Retinex based algorithm with color restoration to compute the transmission. The author estimated the atmospheric light by dark channel image and a decision image according to a threshold. However, dehazed image contains small halos and also appears dark in the regions of small gradients and bright areas. Cui et al. [50] proposed a SID method based on the region segmentation which separates the hazy image into bright and non-bright regions. This removes the problem of overestimation of the transmission in non-bright regions and underestimation of the transmission in bright regions of the DCP method. Weighted L1-norm regularization is used for refining the transmission. However, this method suffers from over-saturation. Moreover, it underestimates the transmission for the object similar to the dense haze and leads to the over enhancement. Liu et al. [53] proposed a solution for two challenging problems of existing dehazing methods. These two challenges are (1) halo artifacts due to insufficiency of edges in estimated transmission and (2) amplification of noise and artifacts in presence of dense haze. This method estimates the initial transmission by boundary constraint and its refinement is done by non-local total variation (NLTV) regularization. However, this method fails in the presence of white objects such as clouds, dense haze, etc. and as a result, the dehazed image looks darker. Furthermore, to improve the quality of the haze-free image, a post-processing method is required. Moreover, lower values

of SSIM AND CIEDE2000 indicate that performance of this method is not satisfactory on synthetic hazy images. Raikwar et al. [47] estimate a lower bound on the transmission by considering the difference between the minimum channel of a hazy and haze-free image. A lower bound is characterized by a bounding function and a quality control parameter. The bounding function is estimated by a non-linear model and a control parameter is used to control the degree of dehazing. However, this method is unable to increase the contrast of dense hazy images. Wu et al. [54] proposed a variational model to remove artifacts due to noise present in the hazy image. They proposed a transmission-aware non-local regularization that suppresses the noises and provides the fine details of the dehazed image without amplification of noises. In addition, to smooth the transmission, semantic-guided regularization is proposed. This method provides satisfactory results without amplification of noises. However, this method fails on non-homogeneous hazy images. Furthermore, when objects are in the same plane and look similar, vanishing lines are falsely estimated and unable to update the segmentation process. In this case, it wrongly estimates the transmission, scene radiance and the segmentation map of a hazy image.

In summary, the image enhancement-based methods don't use the physical model of haze formation and also don't concentrate on the image quality. They only highlight certain details of the image while may reduce or remove some information from the dehazed image. These methods suffer from the problem of over-saturation of pixels and over enhancement. In addition, they are not able to remove the dense haze. However, when image enhancement-based techniques are combined with a physical model like [22, 30, 45], their performance is improved a lot.

4.2 Image Fusion Based Methods

Image fusion is an image processing technique that selects the best regions from multiple images and combines them into a single high-quality image. A fused image is generated in a transformed domain such as Gaussian and Laplacian pyramids, Gradient-domain, Linear, High boost filtering, Guided filtering, Variation based, etc.(Table 3).

In [52] proposed a multiple prior based method to estimate the global atmospheric light. Three priors: color saturation, brightness and gradient map are combined to judge a pixel whether it belongs to an atmospheric light or not. This method computes two coarse transmission maps: pixel-based transmission (PTM) and block level transmission map (BTM). A fusion procedure is employed to combine these two transmissions as follows:

Table 2 Comparison of existing image enhancement-based methods

| Ref. (Year) | Key methodology | Performance/characteristics | Speed | Over-enhancement | Artifacts | Dense fog removal |
|-------------|---|--|---------|------------------|-----------|-------------------|
| [15] (2015) | Bi-Histogram Modification to handle uneven haze density | The restored image looks dark when there are brighter objects in the scene such as a headlight or sunlight | Good | Yes | Yes | Yes |
| [14] (2015) | Regularized-Histogram equalization and discrete cosine transform | This method improves the global contrast and local details of the image. However, it may lead to noise amplification in some hazy images | Good | No | No | No |
| [17] (2016) | Multi-scale gradient domain contrast enhancement | (1) Decomposition is performed in the gradient domain; therefore, the restored image may become dark or overexposed (2) Slightly blurs part of the details in the restored image (3) May fail when a color cast exists in the hazy image | Poor | Yes | Yes | No |
| [45] (2016) | Quadtree decomposition, boundary constraints, weighted contextual based regularization method | Handles blocking and halo artifacts. However, suffers from the problem of color distortions and saturation of pixels | Poor | Yes | Yes | Yes |
| [22] (2017) | Multi-scale correlated wavelet | Improves the visibility significantly and removes the noise. However, it is unable to preserve the edges in the restored image | Good | Yes | Yes | Yes |
| [30] (2017) | Linear Transformation, Gaussian Filtering, Quadtree decomposition | This method is computationally very fast. However, potential edges may be degraded and the color of the restored image is darkened in long-range regions | Good | Yes | No | Yes |
| [20] (2018) | Proposed a gamma correction based dehazing model and proved that a relationship exists between the scattering model and gamma correction | This method is free from artifacts, color distortion; however, haze exists in a small portion of the image | Average | No | No | No |
| [33] (2018) | A globally guided image filtering (G-GIF) | This algorithm recovers the fine structure of the image. However, this algorithm lacks computational efficiency | Average | No | No | Yes |
| [41] (2019) | The Anisotropic diffusion process is used to estimate atmospheric light | This method does not apply to dense hazy images. It also requires post-processing histogram stretching) to restore a haze-free image | Average | No | No | No |
| [24] (2019) | Multilevel wavelet transforms, Discrete Haar wavelet transform, Regularized optimization | This method removes the problem of over-saturation and halos. However, it is unable to increase the contrast of distant objects | Good | No | No | No |
| [23] (2020) | A deep CNN method called Y-net introduces a wavelet structure similarity loss function in the training step | It restores the image with high quality, reduced noise, artifacts and visibility | Average | Yes | No | No |
| [43] (2020) | This method works in the HSV color space. Local Contrast enhancement is performed in the value component and saturation is modified to retain the colorfulness of the image | This method is fast and does not introduce any artifact in the dehazed image. However, it is not able to remove haze completely | Good | Yes | No | No |

Table 3 Comparison of existing image fusion-based methods

| Ref. (Year) | Key methodology | Performance/characteristics | Speed | Over-enhancement | Artifacts | Dense fog removal |
|--------------|---|--|---------|------------------|-----------|-------------------|
| [52] (2017) | Multiple priors: color saturation, brightness and gradient map are combined to estimate the global atmospheric light | This method has a residual haze and is unable to highlight the local details of the image | Poor | No | No | No |
| [19] (2017) | Local linear fusion combines two images obtained after (1) subtracting haze layers and (2) Gamma correction and detail enhancement | (1) Heavily dependent on different parameters (2) Color distortions | Average | Yes | No | Yes |
| [143] (2017) | A fusion based variational image dehazing that removes the over enhancement artifacts problem of enhanced variation image dehazing (EVID) using progressive diffsat maps (difference of saturation) | It retains high contrast and colors in faraway regions without changing in nearby regions. However, it requires several parameters to be adjusted | Average | No | No | No |
| [13] (2018) | Multi-scale Laplacian fusion is used to combine images generated through gamma corrections and CLAHE | Avoid the need of estimating the transmission map | Average | Yes | No | No |
| [135] (2018) | Estimated the transmission by the fusion of luminance and dark channel prior (F-LDCP) | Dehaze a long shot hazy image without color distortions or artifacts in sky regions. However, unable to increase the contrast of distant objects | Poor | Yes | No | Yes |
| [55] (2020) | Proposed a heterogeneous generative adversarial network (GAN), consisting of CycleGAN and a conditional GAN | Restore haze-free image with preservation of texture details. However, dehazed images are slightly darker | Average | Yes | No | Yes |
| [144] (2020) | Patch adaptive structure decomposition to fuse a high-quality patch of each under-exposed image, generated through Gamma correction and saturation adjustment | This method is expensive in terms of computational speed | Poor | No | No | No |
| [56] (2020) | The Guided filter is used to decompose under-exposed images into local components and global components | This method achieves satisfactory results with computational efficiency, clearer details and color quality | Good | No | No | Yes |
| [145] (2020) | Proposed a self-constructing image fusion method to fuse a set of images with different exposures. These images are constructed through segmentation to approximate global atmospheric light | Handles various issues of dehazing, such as halo artifacts, bright objects, edge blur in sky regions, etc | Poor | Yes | No | Yes |
| [146] (2020) | Proposed a color balance and fusion based method to restore color and visibility of images degraded by sandstorm weather conditions using gamma correction and CLAHE | This method can remove the color cast problem. However, in faraway regions visibility is not improved significantly | Average | No | No | No |
| [147] (2021) | Presented a fusion based algorithm by combining multi-scale fusion and prior knowledge | Performs satisfactorily on mild hazy images. However, it is unable to reveal the details in presence of dense haze or images were taken in the night-time | Average | Yes | No | No |
| [148] (2021) | Generates various latent images using global constant transmission values. Finally, all latent images are combined into a single haze-free image with patch based fusion method | This method is simple and effective. However, it is unable to remove the effect of dense haze and also it suffers from the problem of saturation of pixels | Average | Yes | No | No |

$$F_i = P_i \left(1 - \left(\frac{i}{N} \right)^3 \right) + B_i \left(\frac{i}{N} \right)^3 \quad (4)$$

Laplacian Pyramid is used to compute the transmission map in which N is the number of decomposition levels in the Laplacian pyramid. P_i and B_i denote the decomposition result of PTM and BTM, respectively. F_i is the linear fusion of two transmissions P_i and B_i . Furthermore, fused transmission is refined by a total variation. This method suffers from various problems-e.g., incomplete haze removal, unable to highlight the local details of the image and also not being able to remove dense haze.

The existing deep learning methods are trained on synthetic indoor hazy images. Therefore, their performance is not satisfactory on outdoor hazy images. Park et al. [55] proposed a heterogeneous generative adversarial network (GAN), consisting of a CycleGAN and a conditional GAN for restoring a haze-free image with the preservation of texture details. In Phase 1, a cycleGAN is trained on unpaired outdoor synthetic hazy images. Phase 2 utilizes various networks, such as atmospheric light estimation, transmission map estimation, and a fusion CNN. Finally, these three networks are trained through adversarial learning. Fusion CNN combines the output of Phase 1 and Phase 2 to achieve the dehazed image.

Zhu et al. [56] proposed a fusion-based algorithm to solve the image dehazing problem without considering the degradation mechanism. A set of under-exposed images are generated using Gamma correction coefficients. A Guided filter is used to decompose an under-exposed image into local components and global components. For the local components, the exposure quality of the image is measured by applying the average filter to the luminance component. Global components reflect the structure information of the

image and its weight is calculated using initial global components and quadratic function of average luminance. Once the weights are ready for under-exposed images, they are fused in a pixel-wise manner. Global components B_i and global components D_i of multiple gammas corrected input images are fused as shown:

$$F = \sum_{i=1}^n W_i^B B_i + \alpha \sum_{i=1}^n W_i^D D_i \quad (5)$$

where $\alpha \geq 1$ controls the local details in the fused image. Finally, to improve the quality of the dehazed image in terms of color quality, saturation adjustment is performed. The framework of this method is shown in Fig. 11. The overall performance of this method is good and achieves satisfactory results with computational efficiency.

Yuan et al. [57] proposed a transmission fusion strategy for handling normal and bright regions of the hazy image. They propose soft segmentation based on image matting to segment the image. Means and variances of local patches are calculated and binary classification is performed to generate the trimap. In the next step, image matting segments the hazy image into normal and bright regions. For normal regions, the transmission is calculated by DCP while transmission for bright regions is calculated by the atmospheric veil correction method. Finally, the fuzzy fusion method fuses these two transmissions obtained by DCP and AVC. The proposed framework of the method [57] is shown in Fig. 12. This method is tested on various challenging hazy images. However, this method has high computation complexity due to the estimation of two transmissions, binary classification and fuzzy fusion. It also suffers from the problem of over enhancement and halo artifacts.

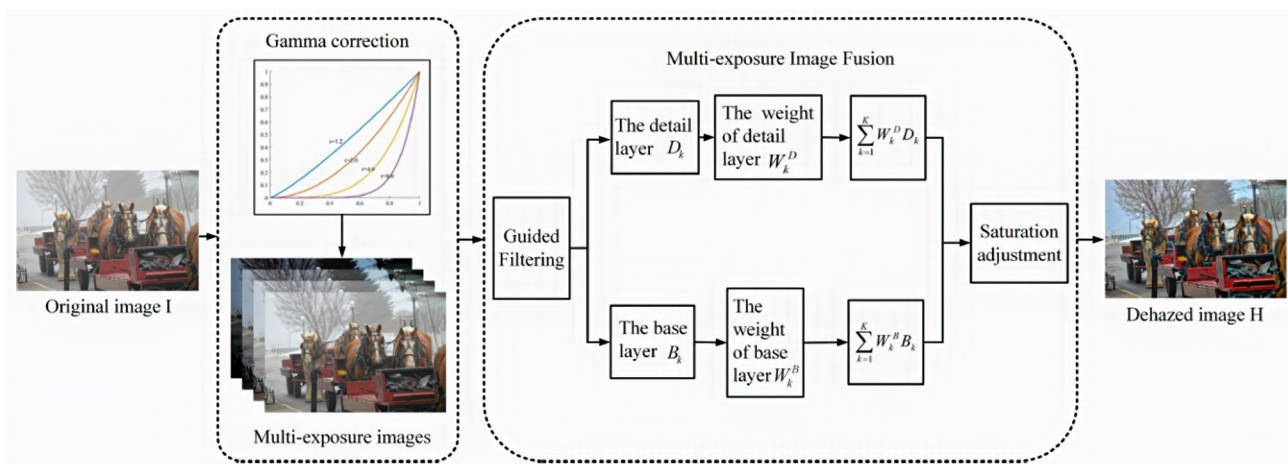


Fig. 11 The framework of the method [56]

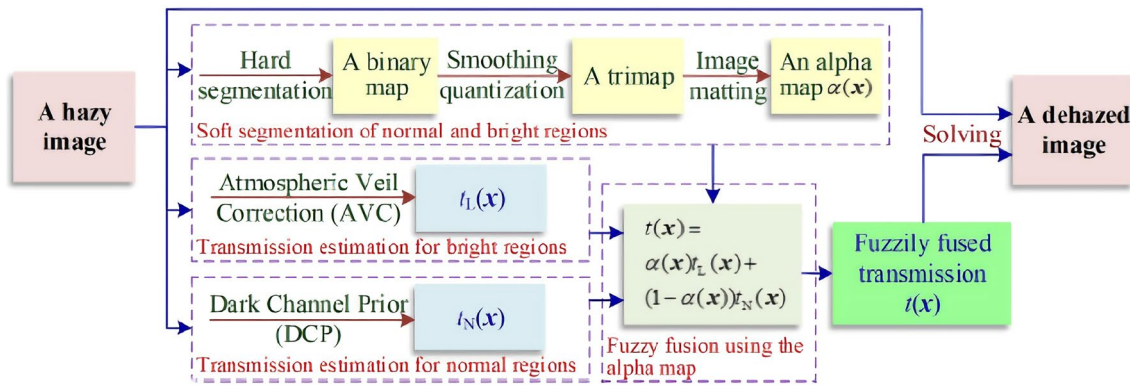


Fig. 12 The framework of the method [57]

Ma et al. [58] proposed a method to enhance the visibility of sea fog images. In the fusion process, the first image is obtained by a linear transformation. The second image is generated by a high-boost filtering algorithm based on a Guided filter. A simple fusion process is followed to combine these two images. The dehazed image is obtained by performing white balancing on a fused image. However, this method produces halo artifacts and is unable to remove noises in the dehazed image.

Son et al. [59] proposed a near-infrared fusion model to deal with the color distortions and removal of haze. This method develops the color and depth regularizations with the traditional degradation model of haze. The color regularization assigns colors to the haze-free image based on colors from the colorized near-infrared image and visible color image. The depth regularization estimates the depth of the colorized near-infrared image. Finally, both regularizations transfer the visibility and colors into a dehazed version of the captured visible image. Shibata et al. [60] focused on developing an application adaptive importance measure image fusion method that can be applied to many applications, including night vision, temperature-perceptible fusion, depth-perceptible fusion, haze removal, image restoration, etc. This method is a learning-based framework that extracts various features (Gabor, intensity, local contrast, gradient) from the decomposed images and learns the important area of the image without knowing the application. Zhao et al. [61] handle two problems of dehazing: misestimation of transmission and oversaturation. It first identified the edges called TME which are misestimating the transmission. Accordingly, a hazy image is divided into two regions: TME and non-TME regions. Multi-scale fusion is used to fuse both patch-wise transmission and pixel-wise transmission. This method greatly enhances the visibility of the hazy image. However, it has a high computation time. Moreover, two post-processing methods (Fast Gradient Domain GIF and exposure enhancement) are utilized on a fused image to obtain the final haze-free image.

Agrawal et al. [62] proposed a fusion based method based on the joint cumulative distribution function (JCDF). This method dehazed the long shot hazy image without color distortions in nearby regions and at the same time, it can enhance the visibility in faraway regions. This method generates multiple images from different modules, such as faraway, nearby, CLAHE. Finally, these multiple images are fused into a single high-quality and artifacts-free image in the gradient domain.

The method uses the following JCDF equation to generate multiple images in nearby and faraway modules:

$$F_Z(z) = e^{-\lambda z}(-1 - \lambda z) + 1 \quad (6)$$

where $z = x_1 + x_2 = x^{d_{\min}} + x^{d_{\max}}$, d_{\min} deals with the fog in nearby regions whereas d_{\max} deals with the fog in faraway regions. The parameters d_{\min} and d_{\max} are set to 2 and 10, respectively. λ is the dehazing parameter and used to generate the images for the fusion process. It generates 1 image with $\lambda = 2$ in faraway region and 3 images in the nearby region with $\lambda = 5, 8, 40$ to avoid the problem of over-saturation and color distortions. Furthermore, to increase the contrast, CLAHE is used to generate 1 more image. Finally, all these images are fused in a single dehazed image in the gradient domain, as shown in Fig. 13.

Recently, several effective fusion-based techniques were introduced which combine the multiple images generated from image enhancement or restoration-based methods. These methods successfully solve the problem of DCP, edge preservation, dense haze removal and halo artifacts. However, the fusion procedure may be complex and the dehazing speed may be decreased due to the generation of multiple images from enhancement-based operators.

4.3 Superpixel Based Dehazing

Another category of dehazing method introduced recently is superpixel based. The superpixels are utilized in dehazing

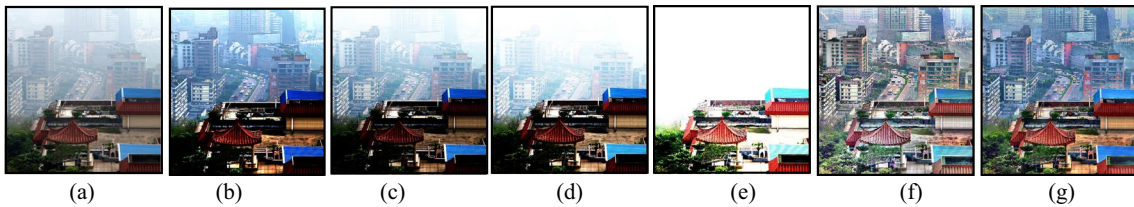


Fig. 13 Image generation in each module. **a** Hazy image, **b** Image generated in faraway region. **c–e** Images generated in nearby region. **f** CLAHE image, **g** Dehazed image

methods in two ways. First, they are used to segment the sky and non-sky regions to remove the problem of color distortions or color artifacts of DCP in sky regions. Another use of superpixel segmentation is to replace the patch-based operations with a superpixel. It offers two advantages: good dehazing speed and reduction of the halo artifacts (Table 4).

The two problems are associated with superpixels based approaches: over enhancement and time complexity. In superpixel based approaches, the number of superpixels is decided manually. The higher number of superpixels may introduce the problem of darkening of color while a smaller number may not sufficient to remove the haze. Another problem is the selection of a superpixel segmentation algorithm. Some algorithms have high computational complexity. Therefore, it is advised to select an algorithm that extracts the superpixels in real-time.

4.4 Prior Based Methods

The restoration-based method uses the physical model or haze formation. They compute the transmission map or depth map based on priors/ assumptions, such as dark channel prior [63], color attenuation prior [64], average saturation prior [65], non-local prior [66], gradient profile prior [27], color ellipsoid prior [67], etc.

Berman et al. [66] proposed a non-local prior as opposed to priors based on local patches. According to this prior, a haze-free image can be expressed by a few hundred colors from the RGB cluster and these pixels of RGB clusters are spread over the entire image. Each cluster in RGB space can be represented using lines termed haze-lines. These haze lines are used to estimate the atmospheric light, distance map and haze-free image. The failure case of this method is the non-uniform lighting which may lead to over enhancement and artifacts (Table 5).

Singh et al. [40] handles the problem of preserving the texture details in the presence of complex background and large haze gradient. They proposed a new prior called gradient profile prior to evaluate the depth map. The transmission map is refined by the anisotropic diffusion and iterative

learning base image filter. The image gradient gives the direction and magnitude and is calculated as follows:

$$\Delta I = \left(\frac{\partial I}{\partial m}, \frac{\partial I}{\partial n} \right) \quad (7)$$

where $\frac{\partial I}{\partial m}$ represents partial derivatives of an image in m direction while $\frac{\partial I}{\partial n}$ shows partial derivatives for n direction. $\frac{\partial I}{\partial m}$ is calculated as differences at one pixel, before it and after it and calculated as follows:

$$\frac{\partial I}{\partial m} = \frac{I(m+1, n) - I(m-1, n)}{2} \quad (8)$$

and similarly, $\frac{\partial I}{\partial n}$ is written as:

$$\frac{\partial I}{\partial n} = \frac{I(m, n+1) - I(m, n-1)}{2} \quad (9)$$

The maximum gradient values in I are considered as global atmospheric light and is estimated as follows:

$$A = I(\max_c(I_m^c)) \quad (10)$$

and transmission map is estimated as follows:

$$t(j) = 1 - \beta \Delta n \in \Omega(j) \left(\Delta c \frac{I_m^c(n)}{A_l^c} \right) \quad (11)$$

where $\Delta n \in \Omega(j) \left(\Delta c \frac{I_m^c(n)}{A_l^c} \right)$ is the gradient profile prior of the normalized image. It overcomes the sky region problem of the DCP method as it is computed toward 1 and t(j) will be toward 0. Some haze β is added to the image to look more natural.

Most of the prior based methods follow a physical model of haze formation which assumes single scattering under the homogeneous haze. However, in a realistic environment, haze behavior is non-homogeneous and there are multiple sources of scattering [68]. Besides, the dehazing results depend on the validity of priors. If assumptions or priors do not hold, it may result in various issues, such as incomplete haze removal, color distortions or artifacts due to the wrong estimation of the transmission.

Table 4 Comparison of existing superpixel based methods

| Ref. (Year) | Key methodology | Performance/characteristics | Speed | Over enhancement | Artifacts | Dense fog removal |
|--------------|---|--|---------|------------------|-----------|-------------------|
| [149] (2016) | Proposed a method using DCP and atmospheric point spread function (APSF) | This method generates a haze-free image without color distortions in sky regions and artifacts. However, it is not computationally efficient in terms of the speed of dehazing | Poor | No | No | Yes |
| [150] (2017) | Presented an adaptive bi-channel prior on superpixels to overcome the problems such as dark channel prior in white regions and bright channel prior in black regions | However, in some cases, it is unable to remove dense haze, if pixels of the hazy image are incorrectly classified | Average | No | No | No |
| [151] (2018) | Presented superpixel segmentation for night-time hazy image by decomposing it into the glow and glow-free image on the basis of smoothness | The dehazed image looks darker than the input image | Poor | Yes | Yes | Yes |
| [152] (2019) | Proposed a superpixel based method that partitions the image into regions of different haze densities for mobile devices | The method is unable to increase visibility in long-range regions | Average | No | No | No |
| [153] (2020) | Estimated the atmospheric light or hazy regions by segmenting the image using superpixels | It suffers from the problem of saturation of pixels and is also unable to estimate the accurate airlight in presence of bright white regions similar to dense haze | Average | Yes | No | Yes |
| [154] (2020) | A multi-scale fusion is used to fuse two transmissions obtained by the bright channel prior and dark channel prior to deal with bright and dark regions of a hazy image | It is inefficient in terms of the speed of dehazing due to the number of steps | Poor | No | No | No |
| [155] (2020) | This work utilized the superpixels to estimate the transmission to avoid blocking/halo artifacts and it is used to refine the transmission based on Markov random field | It is unable to remove the artifacts in sky regions in presence of dense haze | Average | Yes | Yes | No |
| [130] (2021) | Transform the minimum channel of a hazy image into a minimum channel of a haze-free image using superpixels and non-linear transformation | This method can remove the problem of over enhancement and artifacts. However, it is not applicable to non-homogeneous hazy images | Average | Yes | No | Yes |

Table 5 Comparison of existing restoration-based methods with priors

| Ref. (Year) | Key methodology | Performance/characteristics | Speed | Over enhancement | Artifacts | Dense fog removal |
|--------------|---|--|---------|------------------|-----------|-------------------|
| [64] (2015) | A linear model to approximate the depth by taking the difference between brightness and saturation | The method is fast but requires a number of parameters to adjust and is also applicable for mild haze only | Good | Yes | No | No |
| [65] (2017) | Average saturation prior based on the assumption that most of the pixels in the RGB histogram of a hazy image are identically distributed while the RGB histogram of a haze-free image differs significantly | This method can handle non-uniform atmospheric light. However, the accuracy of the method depends on the scene segmentation | Average | Yes | Yes | No |
| [156] (2018) | A scene prior that utilizes retrieved correlated haze-free image from the database as external information to dehaze an image | It is unable to perform registration and regularization for unknown hazy images and hence, details in the dehazed image are lost | Poor | Yes | No | Yes |
| [67] (2018) | Proposed a color ellipsoid prior (CEP), based on the observation that haze pixels in RGB clusters construct an ellipsoid image | This method enhances the visibility of a hazy image significantly. However, an over enhancement problem is seen in the dehazed image | Good | Yes | No | Yes |
| [40] (2019) | The gradient is used to evaluate the depth map and airlight. Transmission is refined by the anisotropic diffusion and iterative learning base image filter | Handle the problem of preserving the texture details in the presence of complex background and large haze gradient | Good | No | No | Yes |
| [27] (2019) | Moore neighborhood based gradient profile prior (GPP) to estimate the transmission and atmospheric light to resolve the various issues of image dehazing | However, GPP is unable to remove artifacts for the images having large sky regions | Good | No | Yes | Yes |
| [66] (2020) | Non-local prior states that a haze-free image can be expressed by a few hundred colors | Greatly enhances the visibility but fails in handling non-uniform lighting and leads to over enhancement and artifacts | Average | Yes | Yes | Yes |
| [138] (2020) | Proposed a Gamma correction prior and observed that inverted low light image looks similar to a hazy image | A global-wise strategy (without the refinement of the transmission) and vision indicator (rich texture details) are applied to achieve a high quality and haze-free image | Average | Yes | No | Yes |
| [157] (2020) | Based on the observation that the depth for all the pixels in a local patch is not the same rather it changes gradually. This method estimated the depth by patch similarity in the local neighborhoods | Sometimes dehazed images may have inconsistent contrast and glowing artifacts for the distant objects | Average | Yes | Yes | Yes |
| [136] (2021) | Proposed an enhancement ASM (EASM) model to remove the problem of dim effect in traditional ASM by introducing a new parameter called light absorption coefficient. This method is called IDE (image dehazing and exposure) and is based on gray world-assumption | The dehazed results are good. However, it is unable to remove haze under non-uniform illumination conditions and sometimes, more brightness in the haze-free image gives the illusion of residual haze | Good | No | No | Yes |

Table 6 Comparison of existing polarization-based methods

| Ref. (Year) | Key methodology | Performance/characteristics | Speed | Over enhancement | Artifacts | Dense fog removal |
|--------------|---|---|---------|------------------|-----------|-------------------|
| [158] (2017) | Proposed a polarized guided autoregressive model for estimation of depth | Depth estimation by this method is accurate without blurring edges and holes. However, objects in closer regions are wrong estimated as distant ones due to the illumination effect and a high degree of polarization | Poor | Yes | No | No |
| [159] (2018) | Presented a polarimetric image dehazing method by combining circularly polarized light and linearly polarized light in dense turbid media | The method is not suitable for highly polarized objects. It also takes a lot of time to search optimum value of parameters | Poor | Yes | No | Yes |
| [160] (2019) | An iterative dehazing method with two regularization schemes: depth-chromaticity for transmission map and chromaticity-depth for dehazing | This method suppresses noise amplification. However, visibility is less for distant objects | Poor | No | No | No |
| [161] (2019) | Presented a pseudo-polarimetric dehazing method for the removal of dense haze | Dehazing parameters are set according to the density of the haze | Poor | No | No | Yes |
| [161] (2019) | Proposed a polarimetric method, combined with synthetic aperture imaging | The polarization difference image is taken by manually rotating the polarizing place in front of the camera. Thus, real-time dehazing is not possible | Poor | No | No | No |
| [162] (2020) | Proposed a polarization-based method that describes the relationship between the angle of polarization (AOP) and the scattering light | The dehazed image is having better contrast and colors and lower noise | Average | No | No | Yes |
| [163] (2020) | Captured the hazy image with a polarization camera. Afterward, the darkest and brightest images are synthesized | Presented a method for lane detection in DAS with dense fog | Good | Yes | No | Yes |

4.5 Polarization Based Dehazing

The polarization-based methods utilized the polarized characteristic of the light. Therefore, it restores the depth information of the hazy image using multiple images with different degrees of polarization, generally represented as I_0 and I_{90} . Some methods based on this category are listed in Table 6.

Polarization based dehazing methods have a great advantage in terms of high efficiency and low computational complexity. These methods are effective in all kinds of turbid media, including haze, fog, water, etc. They are also capable to restore dense hazy images with detailed information. However, it requires a precise selection of image regions such as the sky region to estimate the key parameters which are not applicable in the real world. Also, a photon noise, a well-known quantum-mechanical effect is ignored by most of the existing polarization-based methods, resulting in amplification of noise in the dehazed image.

4.6 DCP Based Dehazing

Dark channel prior (DCP) is very simple and popular prior for haze removal. This prior is based on the observation of the haze-free images that at least one-color channel is significantly dark *i.e.* minimum color channel in a haze-free image is very close to 0 except the sky regions. This prior was introduced in the year 2010. Since 2010, a lot of research work is going on to improve the performance of DCP. In this section, we discuss recent methods based on DCP along with which problem of DCP they have solved (Table 7).

Atmospheric particles degrade the quality of the image in terms of blurring, distortion, color attenuation and cause low visibility. The method [69] proposed an improved version of DCP to handle the artifacts in the original DCP method. This method defines α as a square window of size 1 and calculates the dark channel as follows:

$$I_{(x-[l/2]\dots x+[l/2],y-[l/2]\dots y+[l/2])}^{dark} = \max \left(\alpha(1\dots l), (1\dots l), I_{(x-[l/2]\dots x+[l/2],y-[l/2]\dots y+[l/2])}^{dark} \right) \quad (12)$$

where α is a square window of size 1 and calculated as follows:

$$\alpha = \text{ones}(l, l) * \min_{z \in \Omega(x,y)} \left(\min_{c \in (R,G,B)} I^c(z) \right) \quad (13)$$

This method is managed to remove the artifact but it is not comparable to the DCP method in quantitative evaluation.

Chen et al. [51] proposed a DCP based method for suppressing artifacts and noises using gradient residual minimization. However, due to ambiguity between artifacts and

objects, it is unable to increase the contrast for the objects located at a far distance also slightly blurs the details.

In summary, many researchers addressed the problems of DCP and according presented their solution. For example, the method [31] proposed an alternative method for fast computation of the transmission map using morphological reconstruction. Since the performance of DCP is not good in the sky regions, the method [46] proposed a solution using quadtree decomposition and a region-wise transmission map. The method [70] removes the problem of color distortions for bright white objects using superpixels. The method [71] removes the problem of halo artifacts of DCP using energy minimization.

4.7 Airlight Based Methods

The existing dehazing methods focus on estimating the transmission only and ignore the contribution of airlight in the dehazing process. These methods produce over smoothed image without fine details. Two factors: wrong estimation of airlight and ignorance of multiple scattering contribute toward this problem. Besides, inaccurate airlight is also responsible for color distortions in the dehazed image. Therefore, recently, some works related to the estimation of airlight are reported in the literature (Table 8).

Therefore, the estimation of the airlight is as important as the estimation of the transmission. Inaccurate estimation of the atmospheric light may cause a haze-free image to look unrealistic and color distortions in the dehazed image.

4.8 Hardware Implementation Based Methods

In recent years, significant progress is made toward the development of real-time dehazing applications. Real-time dehazing is highly demanded in smart transportation systems and advanced driver assistance systems (ADAS). These applications demand a higher frame rate, low-cost hardware and power consumption. To date, the methods which fulfill

these requirements are very rare. Image dehazing consists of many steps: estimation of transmission, airlight, refinement of the transmission, recovery of haze-free image and an optional step post-processing operation on a haze-free image which leads to computational complexity. Many hardware such as Cortex A8 processor, field-programmable gate array (FPGA), TSMC 0.13-μm, TSMC 0.18-μm, DSP Processor, Graphics Processing Unit (GPU), application-specific integrated circuit (ASIC), etc. Therefore, dehazing method requires hardware implementation for resource-constrained embedded systems to meet the real-time challenge. This

Table 7 Comparison of existing DCP based methods

| Ref. (Year) | Key methodology | Performance/characteristics | Speed | Over enhancement | Artifacts | Dense fog removal |
|--------------|--|---|---------|------------------|-----------|-------------------|
| [63] (2010) | Based on the observation that the minimum of color channels in local patches of the haze-free image is near zero | DCP is the most popular and powerful prior. However, it is not valid in sky regions and also suffers from the problem of halo artifacts | Poor | Yes | Yes | Yes |
| [32] [2017] | Based on the observation that each haze-free image has at least one-color channel of higher brightness. It is called a brightness map | Able to remove the problem of DCP (halo artifacts and color distortions). However, it requires manual tuning of various parameters | Average | No | Yes | No |
| [46] (2017) | Quadtree based feature pixels for sky region segmentation. It calculates the dark channel based on edge detection in a hazy image then different patch size is selected for pixels in edges region and non-edges regions | Removes the problem of halo artifacts. However, the dehazed image suffers from color distortions in sky regions | Average | Yes | Yes | Yes |
| [70] (2018) | They proposed a saliency detection method that extracts the bright white objects using superpixels | A dehazed image has low contrast and gives the illusion of incomplete haze removal | Average | No | No | No |
| [71] (2018) | A method to remove artifacts. It uses the energy minimization function to estimate the transmission, sum of smoothness term and bound term | Due to patch-based prior, unable to estimate the transmissions of hollows smaller than the patch radius | Average | No | Yes | Yes |
| [31] (2019) | Proposed a DCP and morphological reconstruction for computation of the transmission map | Due to DCP as the base algorithm, it is unable to handle sky regions | Good | Yes | Yes | Yes |
| [44] (2019) | A luminance reconstruction method to achieve higher contrast on the basis of statistical properties of the haze-free image | This method is able to restore a haze-free image with good contrast. However, details are over-smoothed due to the degradation of edges | Good | Yes | No | Yes |
| [164] (2020) | Estimated the transmission as a function of saturation of scene radiance using a simple stretching method and color veil algorithm to deal with yellow and fine dust | A post-processing method is required to enhance the brightness of the dehazed image | Good | No | No | Yes |
| [88] (2020) | Proposed a completely unsupervised learning-based method in which training is performed using minimization of dark channel prior energy function | This method gives a better-dehazed result for the mild hazy images. However, it leaves some amount of haze in the dehazed image in presence of dense haze | Poor | No | No | No |
| [165] (2020) | Based on the observation that the dark channel is closely related to saturation and brightness | It recovers the hazy image without over-saturation and no need to compute DCP | Good | No | No | Yes |

Table 8 Comparison of existing airlight based methods

| Ref. (Year) | Key methodology | Performance/characteristics | Speed | Over-enhancement | Artifacts | Dense fog removal |
|--------------|--|---|---------|------------------|-----------|-------------------|
| [166] (2019) | They proposed two priors, namely the depth edge-aware prior (DEAP) and the airlight impact regularity prior (AIRP) | Remove the problems (missing fine details and over smoothed image) of existing methods | Average | No | Yes | Yes |
| [167] (2019) | Proposed an atmospheric illumination prior based on a deep CNN model | Three components of white hazy existence may result in unbalance in presence of worse weather conditions | Average | No | No | Yes |
| [168] (2020) | Proposed a method adaptable to different haze concentrations and lighting conditions using local-global illumination adjustment | This method is applicable to complex and varying illumination conditions | Average | No | No | Yes |
| [111] (2020) | Proposed a fusion based technique to recover haze-free images under night-time hazy conditions using local airlight estimation | This method suggests patches of multiple sizes in order to generate several images for the fusion process | Average | Yes | No | Yes |
| [169] (2020) | Proposed a method to remove color cast from sandstorms images. A color balancing algorithm and cast-adaptive refinement of airlight are proposed | This method first categorizes the image as cast or non-cast one on the basis of the spread of hue in a hazy image | Good | No | No | Yes |
| [109] (2020) | Approximate the airlight in local patches of a hazy image in YCbCr color space to preserve the local texture of the image | The nearest-neighbor regularization automatically increases the patch size for the sky regions to get the suitable intensity values | Average | Yes | No | Yes |

section discusses the state-of-the-art methods in aspects of hardware architecture (Table 9).

Shiau et al. [72] proposed an extremum approximate method to estimate the atmospheric light that uses a 3*3 minimum filter to obtain the dark channel and contour preserving estimation to calculate the transmission. This method is implemented on 11 stage pipeline architecture for real-time applications. The architecture is divided into four modules: register bank, atmospheric light estimation, transmission estimation and scene recovery, as shown in Fig. 14. It can process one pixel per clock cycle. It can achieve 200 MHZ with 12,816 Gate counts by TSMC 0.13- μ m technology. The power consumption is 11.9 mW.

The register bank modules provided 9-pixel values of the current 3*3 window as an input to the atmospheric light estimation module. Line buffers are used to store the pixel values of 2 rows of an input hazy image. Because of the independent nature of ALE and TE, clock gating help to switch between them for power saving.

4.9 Supervised Learning/Machine Learning Based Methods

Despite numerous methods proposed in the literature, they are restricted to only hand-crafted features. However, effective and reliable restoration of a hazy image is still an open challenge. The accuracy of the restoration-based methods depends on the validity of the prior. In a failure of prior, they may cause various issues, such as residual haze or an unrealistic hazy image. Therefore, the effort had been made toward developing machine learning methods for reliable estimation of the transmission for restoring a haze-free image. However, these techniques require a vast amount of data of hazy and their ground truth image, which is not available. For training the model, a lot of synthetic data using Eq. 1 is generated which limits the performance when they are tested on natural or realistic hazy images. For ease of understanding, machine learning methods are further categorized as traditional or simple learning and deep learning. This section focuses on simple learning techniques. These techniques used linear and non-linear regression, support vector regression, linear model, radial basis function, conditional random field, etc. (Table 10).

4.10 Deep Learning Based Methods

Recently deep learning based had attracted the researcher and successfully implemented in dehazing. These techniques not only remove the haze from an image but also offer a fast and quality dehazed image. Two types of methods exist in the literature for deep learning, one which utilize physical model [73–75], and another is without physical model [76–80]. Furthermore, some techniques [73–75, 77, 79]

Table 9 Comparison of existing hardware implementation-based methods

| Ref. (Year) | Key methodology | Performance/characteristics | Speed | Over-enhancement | Artifacts | Dense fog removal |
|--------------|--|---|---------|------------------|-----------|---------------------------|
| [72] (2013) | Based on minimum filter and DCP | This method is implemented on 11 stage pipeline architecture for real-time applications | Good | Yes | No | Yes |
| [131] (2017) | DCP method to estimate the airlight and transmission results | Satisfy the requirement in real-time with good recovery results | Good | Yes | Yes | Yes |
| [132] (2019) | DCP based method with seven-stage pipelined hardware architecture | This method solves the problem of flicker in the video. However, results are over-brightened in long-range regions or sky regions. Frame rate is not so good for high-speed applications such as ADAS | Good | Yes | No | No |
| [170] (2019) | This approach consists of two modules: low complexity atmospheric light estimation (LAE) and independent transmission estimation (ITRE) without relying on airlight | (1) The dehazed image may be dark in presence of shadows (2) The hardware resources requirement is high and lacks video dehazing capability | Average | Yes | No | No |
| [171] (2019) | Presented a multi-spectral transmission map fusion method to enhance the quality of visible band images using near-infrared data | The low-cost hardware implementation makes this method suitable for real-time processing | Good | Yes | No | depending on opted method |
| [101] (2020) | Presented a computational efficient hardware architecture that consists of two modules: depth refinement transmission estimation (DRTE) and distribute airlight estimation (DAT) | This approach is superior in terms of energy, area and reduction of line buffers | Good | No | No | Yes |
| [172] (2020) | This algorithm is implemented on two hardware platforms: DSP processor and Zynq-706 with 14-stage pipeline structures | The proposed method cannot be applied to real-time video dehazing due to slow processing | Average | Yes | No | No |
| [133] (2020) | Proposed a VLSI architecture for the resource-constrained environment for real-time video dehazing | This method is computationally efficient and tested on different datasets. However, due to DCP and physical model, it is not valid when the objects in the image are similar to airlight | Good | Yes | No | Yes |
| [173] (2021) | Proposed a transposed filter algorithm, combined with parallel minimum filter and parallel mean filter algorithm to speed up the processing | This method is hard to implement in an embedded system due to more consumption of power in GPUs | Good | Yes | No | No |

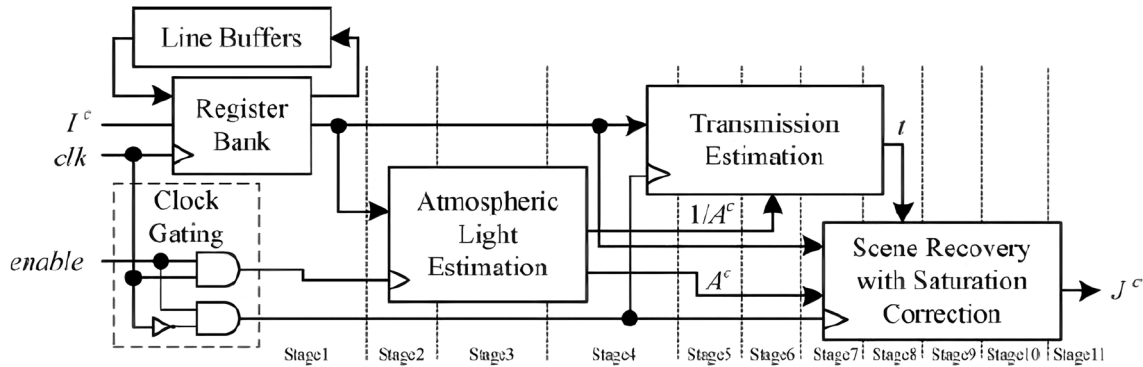


Fig. 14 General framework of Hardware based implementation [72]

require mapping of hazy and their corresponding GT image for training the model while other techniques do not need hazy images and corresponding haze-free images for training [76, 80, 81]. Several deep learning base techniques are reported, including multi-scale convolutional neural network (MSCNN) [73], Dehaze Net [74], All-in-One Dehazing Network (AOD-Net) [75], Cycle-Dehaze [76], Gated Fusion Network [77], Generic Model-Agnostic (GMAN) [78], back projected pyramid network [79], Double DIP [80] (Table 11).

In [82], proposed a variational and deep CNN based dehazing method for estimating transmission, airlight and dehazed image simultaneously. The deep CNN is employed to teach haze-relevant priors (fidelity terms and prior terms). Furthermore, an iterative optimization method based on gradient descent is utilized to solve the variational model.

The method [83] proposed a GAN based method that jointly learns the transmission and haze-free image using loss functions (perceptual loss and Euclidean distance). In the first step, the transmission is estimated by a hazy image and it is combined with high dimension features. Afterward, both features and transmission are fed to the Guided dehazing module to recover a haze-free image. This approach is shown in Fig. 15.

The traditional methods used hand-crafted features such as contrast maximization, dark channel, etc. The method [84] used an encoder-decoder based structure called gated context aggregation network (GCANet) to directly recover a haze-free image. This architecture utilized smoothed dilated convolution to avoid the artifact. Moreover, a subnetwork is proposed to fuse the features at different levels.

Zhang et al. [85] presented a multi-scale dehazing network called the perceptual pyramid deep network. This encoder and decoder-based method directly learn the mapping between a hazy and a clear image without estimating the transmission map. An encoder is constructed through the dense block and residual block while a decoder consists of a dense residual block with a pyramid pooling module

to retain contextual information of the scene, as shown in Fig. 16. The network is optimized by mean squared error and perceptual losses.

Qin et al. [86] proposed FFA-net (feature fusion attention network) to obtain a haze-free image. This method consists of three modules: feature attention module (which combines channel attention and pixel attention and focuses on thick haze removal), local residual learning (deal with thin haze) and feature fusion attention (adaptively learns the weights from the feature attention module). As shown in Fig. 17, a hazy image is provided input to a shallow feature extraction module. After that, it is fed into an N block structure with skip connection and output is fused into a feature fusion module. Finally, global residual learning is used to restore a haze-free image.

The prior based methods estimate the transmission on the basis of haze-relevant priors. As a result, dehazed image may suffer from darkened or brightened artifacts.

Recently, end to end CNN based deep learning methods had shown great potential in image dehazing. However, these methods fail to handle non-homogenous haze. In addition, the existing popular multi-scale approaches are utilized to solve various issues of dehazing, namely color distortions, artifacts and some of them also can handle dense haze, but they are not computationally and memory efficient. Deep learning methods produce a visually pleasing result for most hazy images. However, their performance relies heavily on several training samples and the quality of these sample images.

4.11 Miscellaneous Category

In this section, we present the miscellaneous category of dehazing methods. This category includes semi-supervised, unsupervised and ensemble network. In semi-supervised learning, both approaches supervised and unsupervised are utilized in deep CNN. For example, in [87] supervised learning is performed using supervised loss (mean squared,

Table 10 Comparison of existing traditional machine learning based methods

| Ref. (Year) | Key methodology | Performance/characteristics | Speed | Over enhancement | Artifacts | Dense fog removal |
|--------------|---|---|---------|------------------|-----------|-------------------|
| [26] (2016) | Gamma correction, Support vector machine, Histogram analysis, Bilateral texture filtering | Due to the color correction scheme in sky regions, brighter white objects are also processed in the same way and produce a color shift in the dehazed image | Average | Yes | No | No |
| [34] (2017) | Proposed two-layer Gaussian process regression and superpixel segmentation. A model is trained on various features such as dark channel, local maximum contrast, saturation and Gabor using superpixel | It is not applicable to remove dense haze | Poor | No | No | No |
| [174] (2017) | It proposed a kernel regression model (KRM) which considers local information in dehazing. Initial transmission is calculated using the DCP method and refined by KRM | Handles blocking artifacts. Removes two inherent problems of DCP: unsMOOTH and negligence of neighborhood information in the estimation of the transmission | Average | No | No | Yes |
| [118] (2017) | A support vector regression is utilized to estimate the transmission by learning seven haze-related features | This method is capable of suppressing noise amplification. However, not able to deal with dense haze | Good | Yes | No | No |
| [175] (2018) | Proposed multi-atmospheric veil, estimated by Radial basis function and brightness is adjusted by an activation function | This method can dehaze the image with sufficient brightness and texture details. However, it is not applicable to dense haze images | Average | No | No | No |
| [123] (2018) | Proposed a haze density model based on exponential inference with a universal airlight extractor (UAE). The UAE is designed to detect local lighting sources using support vector data description and exclude them from a hazy image in order to select airlight | This method removes the problem of local lighting. However, dehazing speed is poor | Poor | No | No | Yes |
| [176] (2018) | Proposed a dehazing method using conditional random field (CRF) which estimates the transmission in a pixel-wise manner | This method does not require refinement of the transmission. However, it is not efficient in terms of time complexity | Poor | No | No | Yes |

Table 11 Comparison of existing deep learning-based methods

| Ref. (Year) | Key methodology | Performance/characteristics | Speed | Over enhancement | Artifacts | Dense fog removal |
|--------------|---|---|---------|------------------|-----------|-------------------|
| [73] (2016) | Presented a multi-scale deep neural network to estimate the transmission | The method is not able to remove the haze well | Average | No | No | No |
| [74] (2016) | Proposed nonlinear regression by extracting various haze-relevant features like dark channel, hue disparity and color attenuation, etc. to estimate the transmission | The method is not able to remove the haze well | Average | No | No | No |
| [75] (2017) | Proposed a lightweight and end-to-end CNN based method by reformulating the physical model | This method does not estimate the transmission and airlight. Instead of it directly generates a haze-free image | Good | No | No | No |
| [76] (2018) | Proposed a Cycle-Dehaze which is an improved version of Cycle GAN. This method enhances the CycleGAN by combining perceptual loss and cycle consistency | Achieved higher values of PSNR and SSIM than Cycle GAN. However, color distortions are seen for real-world haze-free images | Average | Yes | No | No |
| [142] (2018) | Presented a densely connected pyramid dehazing network (DCPDN). This method directly takes the physical model of haze formation as an input to jointly learn the airlight and the transmission map | Its performance is satisfactory on synthetic hazy images. However, sometimes, it generates over-saturated results in long-range regions for real images | Average | Yes | No | No |
| [126] (2018) | Proposed a patch quality comparator (PQC) based on CNN. They generate dehazed image by comparing dehazed output patches with the hazy patches by binary search and comparator | However, dehazed images suffer from the problem of over-saturation due to incorrect estimation of the transmittance | Poor | Yes | No | No |
| [127] (2018) | It constructs an energy model using dark channel and transmission priors. The refinement is done through the iterative algorithm using deep architecture called proximal dehaze-net | The method is unable to remove the haze effect if an image is captured in night-time or dense hazy conditions | Average | Yes | No | No |
| [77] (2018) | Proposed an end-to-end network that consists of an encoder and a decoder. This fusion based method derived three inputs from the hazy image by applying gamma correction, white balancing and contrast-enhancing | This method is unable to handle noisy images under the dense haze | Average | Yes | No | No |
| [139] (2019) | Proposed two variants of a fully convolutional neural network named small and big version. The small version <i>i.e.</i> , FastNet is a single encoder-decoder structure for high resolution I/O-haze datasets dataset without reducing the size. The second variant <i>i.e.</i> , DualFastNet uses pair of encoder-decoder to estimate the transmission and airlight for the NYU depth dataset | Suffers from the problem of overfitting and leads to noticeable artifacts in dense hazy regions | Good | No | Yes | Yes |
| [78] (2019) | Proposed a fully agnostic CNN model to restore a haze-free image without considering the atmospheric scattering model. The method presents an encoder-decoder structure and consists of convolution, residual and deconvolutional blocks that consider two loss functions: MSE and perceptual loss | This method does not provide a generalized solution for all types of hazy images and also does not handle the noises and distortions in an image | Average | Yes | No | No |

Table 11 (continued)

| Ref. (Year) | Key methodology | Performance/characteristics | Speed | Over enhancement | Artifacts | Dense fog removal |
|--------------|---|---|---------|---------------------|-----------|----------------------------|
| [128] (2019) | Proposed a deep multimodal fusion network that combines multiple models. The dehazed results are obtained by the physical haze model and layer separation model. Finally, an attention mechanism fuses these two dehazed images | The method is not suitable for night-time hazy images | Average | No | No | Yes |
| [129] (2019) | Proposed a method called HR-dehazed. A high-resolution image dehazing based on encoder and decoder architecture | The method is able to maintain the semantic structure of input hazy images | Good | Yes | No | Yes |
| [177] (2020) | Proposed color transfer dehazing model using deep neural network | It restores the image with high fidelity, sharpness and brightness. However, it is unable to remove dense haze | Average | No | No | No |
| [83] (2020) | Proposed a GAN based method that jointly learns the transmission and haze-free image using loss functions (perceptual loss and Euclidean distance) | It suffers from the problem of over-saturations in dense haze regions | Average | Yes | Yes | Yes |
| [79] (2020) | Presented a back projected pyramid network. This network consists of UNet and pyramid pool block learning haze relevant features by incorporating local and global spatial context | This method is able to remove dense haze and non-homogeneous haze also. However, performance is dependent on the color space used in the training | Average | Yes (In dense haze) | No | Yes |
| [178] (2021) | Proposed a cyclic GAN model by incorporating a feature transformer within the generator | In presence of a thick haze, it is unable to recover the actual color of the image | Average | Yes | No | No |
| [179] (2021) | Proposed an encoder-decoder structure, where T-net is used to infer transmission and D-net recovers haze-free image. The T-net transfers the knowledge about transmission to D-net | This method produces artifact-free images and also can be utilized in computer vision tasks to improve object detection | Good | No | No | Yes |
| [180] (2021) | Consider both models physical based and learning based to remove haze. Introduced a model called ICycleGAN that follows an iterative generation process to achieve a haze-free image. Furthermore, a detail information consistency loss function is proposed to preserve texture and color details | Due to the mixed approach, it is inefficient in terms of computation speed. Moreover, for natural images, it is unable to increase the visibility in long-range regions in presence of dense haze | Average | No | No | Yes (for synthetic images) |

Fig. 15 A framework of the GAN based image dehazing method [83]

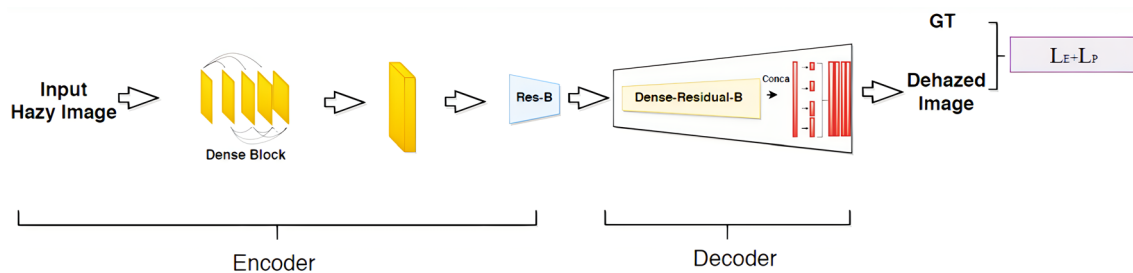
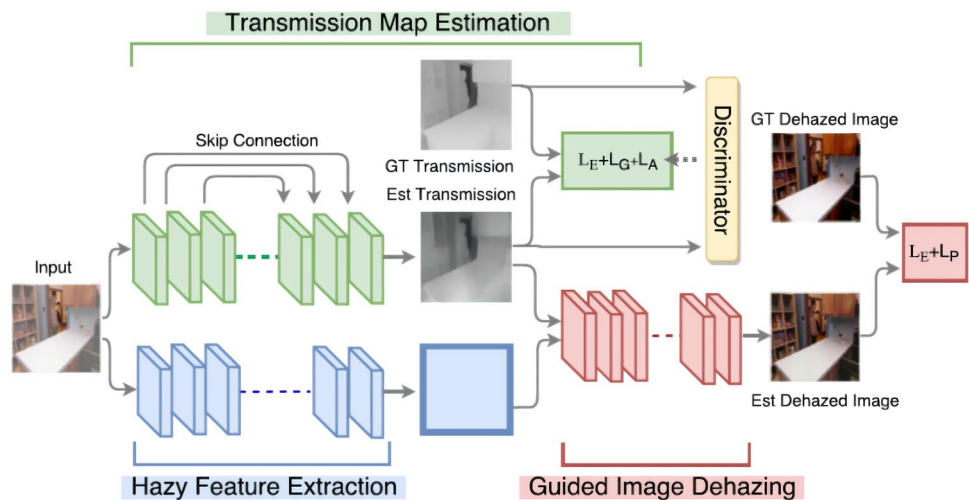


Fig. 16 Encoder-decoder structure framework of image dehazing [85]

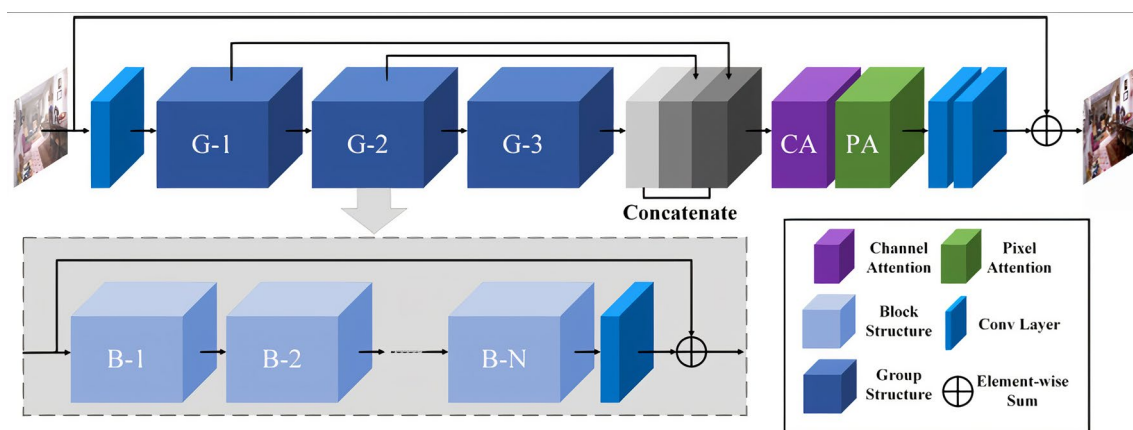


Fig. 17 Feature fusion attention network [86]

adversarial and perceptual loss) of clean image and hazy image for synthetic images and unsupervised learning is exploited using DCP and gradient prior on real images.

Unsupervised learning does not require the hazy and haze-free image pairs for training the deep neural network. These methods avoid the need for a large-scale synthetic dataset required for training the model. Recent

learning-based methods utilized a deep learning model to establish the relationship between hazy and clear images. However, it is difficult to collect a vast amount of hazy and clear images for the training. Therefore, these models are trained on synthetic images, generated using indoor images and corresponding depth images. The performance of these methods is degraded on outdoor hazy

images. Some research works use unsupervised learning which does not require hazy images and corresponding GT images during the training phase [88]. It uses only a single captured hazy image to learn and inference the haze-free image.

Another interesting category of image dehazing method is the ensemble, where multiple deep CNN are exploited. For example, in method [89], multiple neural networks were utilized to estimate the transmission to solve the problem of overfitting. Yu et al. [90] proposed three ensemble models: EDN-AT, EDN-EDU and EDN-3J. One of them, EDN-EDU is an ensemble (Encoder-decode and U-net) of two sequential hierarchical different dehazing networks. The ensemble networks can remove the non-homogeneous haze (Table 12).

The atmospheric model assumes the global airlight and scattering coefficient. Therefore, it introduces unrealistic color distortions in dehazed images. The method [91] proposed a color constrained dehazing model to produce a realistic haze-free image. This method solves the dehazing problem as an optimization problem where cost function considers color, local smoothness of transmission and airlight. Moreover, this method can be developed as a semi-supervised dehazing model. It is modeled as three networks by training on synthetic datasets for estimating airlight, transmission and haze-free image. The proposed loss function considers loss in the reconstruction of the hazy image, reconstruction loss of haze-free image, smoothing loss of airlight and transmission map. Golts et al. [92] proposed a deep energy method that offers an unsupervised energy function that replaces the supervised loss. This deep neural network performs training on real world input without the requirement of manually annotated labels. This method is used in three different tasks: Single image dehazing, image matting and seeded segmentation. Experiments are performed on RESIDE dataset.

Li et al. [93] proposed an unsupervised and untrained neural network for image dehazing, called as you only look yourself (YOLY). This method utilized three subnetworks to decompose the hazy image into three latent layers, *i.e.*, haze-free layer, transmission layer and airlight.

Figure 18 shows the input hazy image x is decomposed into three layers using three joint subnetworks. This approach feed x simultaneously into a haze-free estimation network (J-net), a transmission network (T-net) and airlight network (A-net). After that, a hazy image is reconstructed through an atmospheric scattering model. In this way, it is learned in an unsupervised manner, and networks are optimized by the loss function. For the J-net network, a loss function considers the minimization of loss by taking the difference of brightness and saturation.

4.12 Non-Homogeneous Haze

Although deep learning-based methods had been successfully implemented in image dehazing, one of the most challenging problems is to remove the non-homogeneous haze. Most of the method works effectively in presence of homogeneous haze. However, in a real scenario, haze is not homogeneous *i.e.*, not evenly distributed across the image. A dehazing method is required to enhance the visibility without color distortions under the non-uniform airlight (Table 13).

The traditional methods either directly recovering haze-free image (J) with image enhancement or fusion based methods or restoration-based method which estimate transmission map and airlight, fail in case of non-homogenous haze where there is an uneven distribution of haze in the image, *i.e.*, some part of the image is covered with denser haze and other parts with the thin haze. The method [94] takes advantage of both methods to estimate a weight map w . w combines the result of directly estimated J by a physical model. This architecture uses one encoder and four decoders to estimate dehazing parameters J , A , t and w , as shown in Fig. 19. Channel attention is added to generate unique feature maps for these decoders. Moreover, dilation inception is proposed to fill the missing information by non-local features.

Wu et al. [95] proposed a knowledge transfer dehazing network (KTTD) which consists of two networks, *i.e.*, teacher network and dehazing network, as shown in Fig. 20. The teacher network learns the knowledge about clear image and transfers this knowledge to the dehazing network. Furthermore, a feature attention module comprises channel attention and pixel attention is employed to extract important details of the image. Finally, an enhancing module is developed to refine the texture details.

5 Datasets Used for Image Dehazing

At the beginning of this field, there were very limited datasets available and also the size of these datasets was very small. The researcher used only a few images for validating the performance of their proposed haze removal algorithm. They download the hazy images from the Internet for the dehazing task. The drawback of this approach is that these images do not contain the ground truth images. The lack of ground truth images manifests a great challenge for the researchers in evaluating their methods qualitatively and quantitatively. Therefore, various blind dehazing metrics were introduced but these metrics were not accepted by the global community to conclude due to a lack of haze-free images.

Table 12 Comparison of miscellaneous category

| Category | Ref. (Year) | Key methodology | Performance/characteristics | Speed | Over-enhancement | Artifacts | Dense fog removal |
|-----------------|--------------|---|--|---------|------------------|-----------|-------------------|
| Semi-Supervised | [87] (2019) | A semi-supervised dehazing method consisting of both supervised and unsupervised learning. In supervised learning, a CNN is used while in unsupervised learning; two priors, namely dark channel and gradient prior are exploited to calculate the loss | This method produces good results for mild hazy images. However, its performance is degraded on dense hazy images | Average | Yes | No | No |
| | [91] (2020) | Proposed a color-constrained dehazing model to produce a realistic haze-free image | This method solves the dehazing problem as an optimization problem where cost function considers color, local smoothness of transmission and airlight | Average | No | No | Yes |
| Unsupervised | [80] (2019) | This method proposed a deep image prior to unsupervised layer decomposition | It treats the image dehazing problem as a layer separation problem where the first layer is a haze-free image and the second layer is airlight. However, it is unable to remove the haze effect completely | Average | Yes | No | No |
| | [181] (2019) | This method employed a cycle generative adversarial network called CycleGAN. A haze-free image is obtained by combining cycle consistency loss and adversarial loss | It uses two generators G and F and a discriminator D | Average | No | No | No |
| | [81] (2020) | This methodology is called zero shot image dehazing as it does not require the hazy and haze-free image pairs for training the deep neural network; instead, it uses only a captured hazy image to perform learning and inference | It has comparable performance with the supervised method. However, it suffers from limitation, such as slow inference speed | Poor | No | No | Yes |
| Ensemble | [182] (2020) | A deep prior ensemble that integrates both knowledge and information from training data to address the image enhancement problem | This method is applicable to various enhancement related tasks such as super resolution, image dehazing, underwater, etc. However, in image dehazing, the restored image has a residual haze | Average | No | No | Yes |
| | [89] (2021) | Proposed a method using superpixel and non-linear regression. To estimate the accurate transmission, multiple neural networks are trained | This method removes the problem of color distortions and artifacts in haze-free images with a small number of training examples | Average | No | No | No |

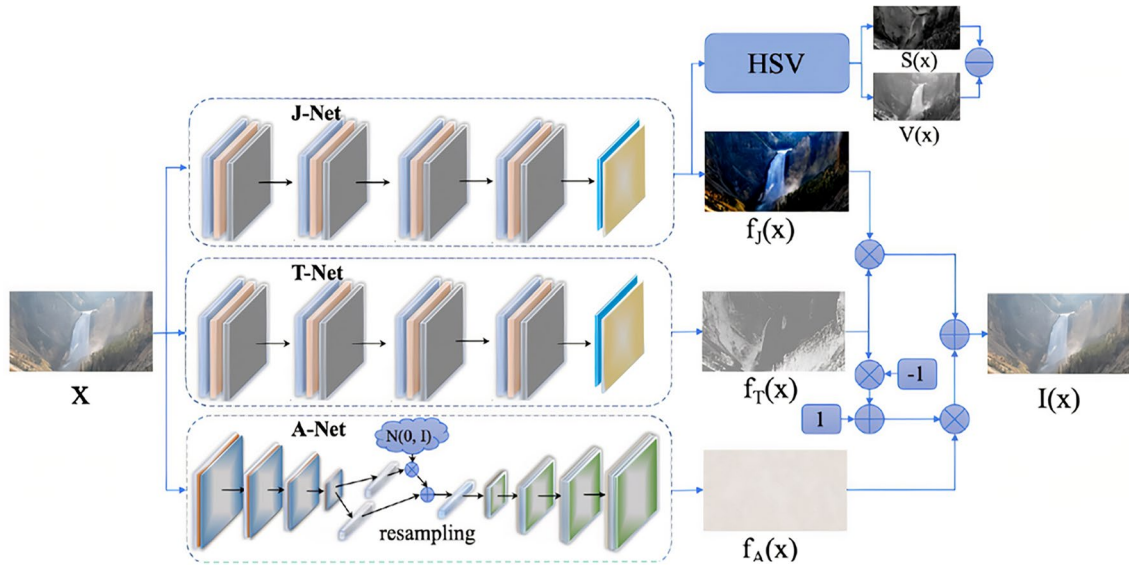


Fig. 18 General framework of unsupervised image dehazing [93]

Now a day, two types of datasets are used in this field: a natural hazy image without reference image known as a real image and a synthetic hazy image along with the depth image or ground truth image. The assessment methods are also different for both types of hazy images, which will be discussed in the next section. We discuss all the datasets used in this field based on various parameters, namely the process of hazy image generation, number of images, types of hazy images, etc. The performance of different dehazing methods on these datasets is also explained in the experiment and results section.

5.1 Frida Dataset [96]

The dataset foggy road image database consists of 90 synthetic images of 18 urban road scenes. Frida2 comprises 330 synthetic images of 66 diverse road scenes. Each fog-free image contains 4 foggy images and a depth map, as shown in Fig. 21. The dataset considers four types of fog: uniform fog, heterogeneous fog, cloudy fog, and cloudy heterogeneous fog. Uniform fog is synthesized according to the physical model and Perlin's noise between 0 and 1 is added to simulate heterogeneous fog. This dataset is helpful to improve the performance of a camera-based driver assistance systems whose objective is to provide a clearer view of the road in the presence of fog to minimize accidents.

5.2 Fattal's Dataset [97]

This is the most popular dataset available to the research community for the assessment of dehazing capability. This dataset provided 12 synthetic hazy images along with 31

realistic hazy images. This dataset contains various benchmarks hazy images, consisting of several challenges: nighttime haze, heavily dense haze, white objects, depth discontinuities, different illumination conditions, sky regions, etc. Some sample images from this dataset are shown in Fig. 22a.

5.3 Waterloo IVC [98]

The dataset consists of 25 realistic hazy images of diverse scenes in an outdoor and indoor environment. There are 22 outdoor real-world hazy images, captured in different haze concentrations while 3 indoor images are simulated using physical mode. This dataset is widely used in single image dehazing to evaluate performance. Some sample images from this dataset are shown in Fig. 22b.

5.4 500 Foggy Images [99]

The dataset consists of 500 natural foggy images, used in many research papers for evaluation of their method. These images comprise different sizes, different fog densities ranging from light fog to dense fog, and diverse image contents. Some sample images from this dataset are shown in Fig. 22c.

5.5 D-Hazy [100]

This dataset contains 1400+ pairs of synthetic hazy and haze-free images of indoor scenes. This dataset is generated using Middlebury and NYU depth datasets, containing their corresponding depth maps. For each image, the transmission map is computed based on atmospheric light and the scattering coefficient. Atmospheric light is assumed

Table 13 Comparison of Non-homogeneous haze removal

| Ref. (Year) | Key methodology | Performance/characteristics | Speed | Over enhancement | Artifacts | Dense fog removal |
|--------------|--|---|---------|------------------|-----------|-------------------|
| [90] (2020) | Proposed an ensemble method to solve the problem of non-homogenous haze. This method utilized three models: EDN-3J, EDN-AT and EDN-EDU | EDN-AT and EDN-EDU models perform better in terms of fidelity and perceptual quality | Average | Yes | No | Yes |
| [94] (2020) | The proposed method takes the advantage of both direct dehazing and restoration-based method to remove non-homogeneous haze. A spatially varying weight map (w) is used to combine the results of both methods | To further improve the result, it requires post-processing | Average | No | No | Yes |
| [95] (2020) | Proposed a knowledge transfer dehazing network (KTTD) which consists of two networks, <i>i.e.</i> , teacher network and dehazing network | This method is able to restore non-homogeneous dense hazy images. However, it is unable to restore the original colors of the image | Average | Yes | No | Yes |
| [183] (2020) | Proposed a fast-deep multi-patch hierarchical network having a different number of patches at each level | The number of levels and patches at each level are decided manually | Good | No | No | Yes |
| [184] (2021) | Proposed a skyGAN method for removal of haze from aerial images by combining HSI guidance and multi-cue color | The method is applicable to aerial images of different haze densities under non-homogeneous environment | Poor | No | No | Yes |

to be pure white [101] and the scattering coefficient is set by default as 1. Some sample images from this dataset are shown in Fig. 23a.

5.6 Semantic Understanding of Foggy Scenes [102]

Sakaridis et al. [102] presented two distinct datasets: foggy cityscapes and foggy driving. The foggy cityscapes dataset was derived from the cityscape dataset and contains outdoor synthetic hazy images with different scattering coefficients. It preserves the semantic annotation of the original images. Foggy driving was comprised of 101 real-world foggy road scenes with annotation and a maximum resolution of 960*1280 pixels, as shown in Fig. 23b.

5.7 Haze RD Dataset [103]

This dataset contains 15 outdoor scenes with realistic hazy conditions. Each hazy scene is simulated with five different weather conditions, ranging from thin haze to dense haze and visible range from 50 to 1000 m, as shown in Fig. 24. These images are of high resolutions and justify the scattering theory of the physical model. A depth map of each hazy scene is estimated by fusing structure from motion and lidar.

5.8 I-Haze Dataset [104]

The dataset contains 35 indoor image pairs of hazy and corresponding haze-free images. The real haze appearance is produced by a professional haze machine and captured in a controlled environment under the same illumination for both hazy and haze-free images. Some sample images along with their GT images from this dataset are shown in Fig. 25a.

5.9 O-Haze [105]

This dataset is an outdoor scene dataset comprised pairs of real hazy and corresponding haze-free images. O-haze contains 45 different outdoor scenes in which real haze is produced by a professional haze machine that simulates a hazy environment. These scenes were captured on cloudy days, morning, sunset or when wind speed was below 3 km/h. Some sample images along with GT images from this dataset are shown in Fig. 25b.

5.10 Dense-Haze [106]

Ancuti et al. [106] proposed a Dense-haze dataset containing real-world hazy images, characterized by dense and homogeneous haze. It consists of 33 pairs of real hazy and their corresponding haze-free images. Some sample images along with GT images from this dataset are shown in Fig. 25c.

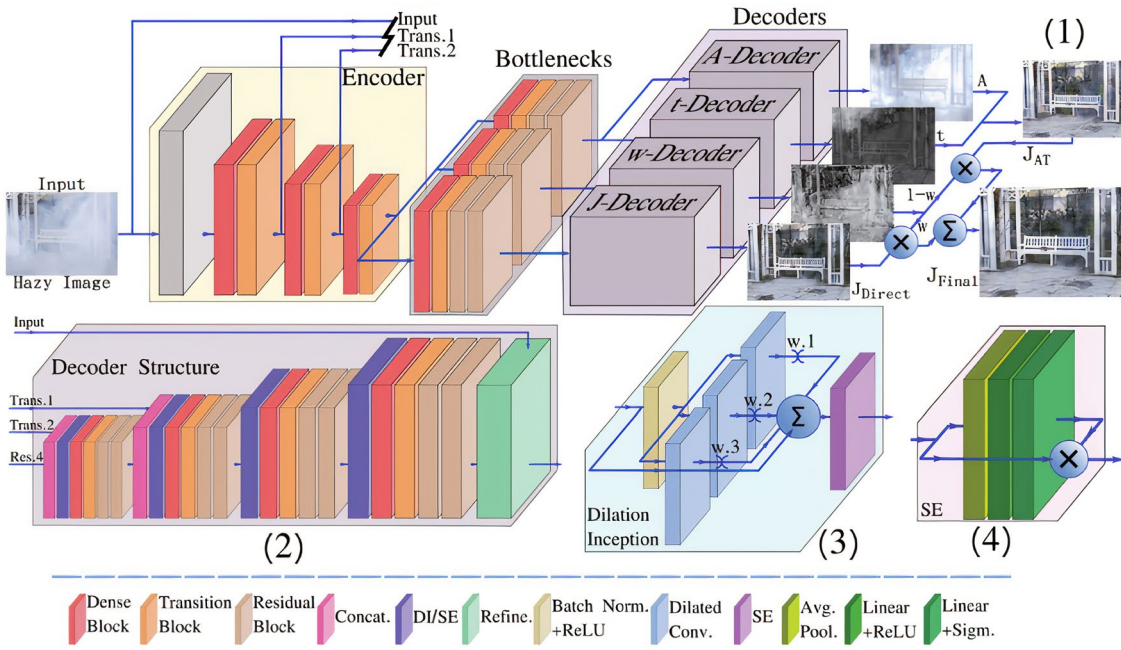
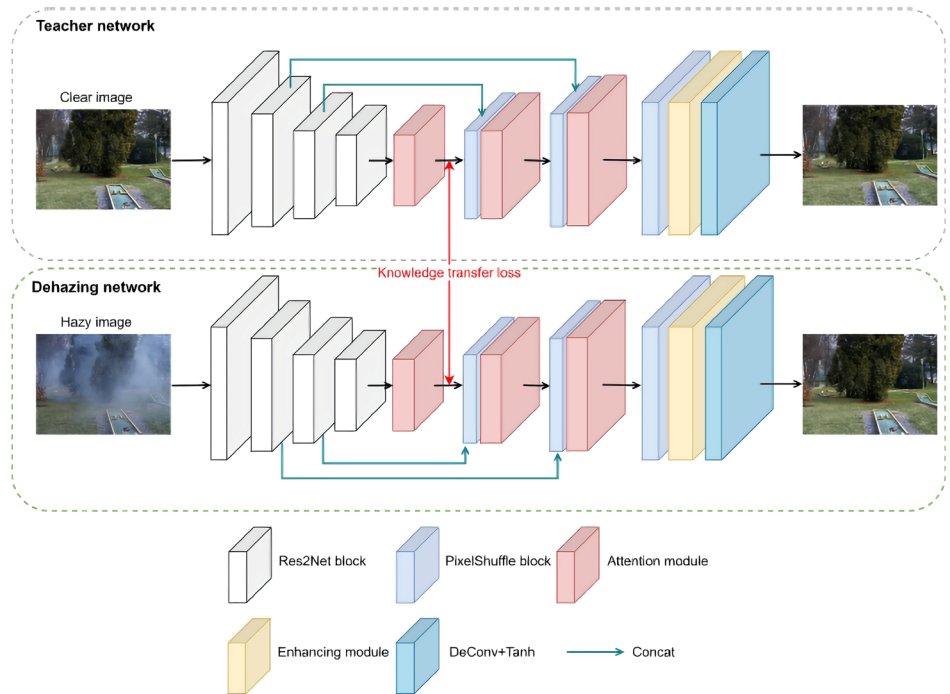


Fig. 19 U-net structure for non-homogeneous haze removal [94]

Fig. 20 The dual network (knowledge transfer dehazing network) for non-homogeneous haze removal [95]



5.11 RESIDE [107]

This is the recent and large-scale dataset of hazy images containing both synthetic and realistic hazy images, called realistic single image dehazing (RESIDE). This dataset is available in RESIDE standard and RESIDE- β . The standard RESIDE contains three subsets: indoor training test (ITS),

synthetic objective testing set (SOTS), and hybrid subjective testing set (HSTS). The ITS contains 13,990 synthetic hazy images generated using 1399 haze-free images from NYU2 and Middlebury stereo indoor datasets. For each haze-free image, 10 synthetic hazy images are generated. Atmospheric light is taken uniformly randomly in between [0.7, 1.0] and the scattering coefficient is also randomly uniform

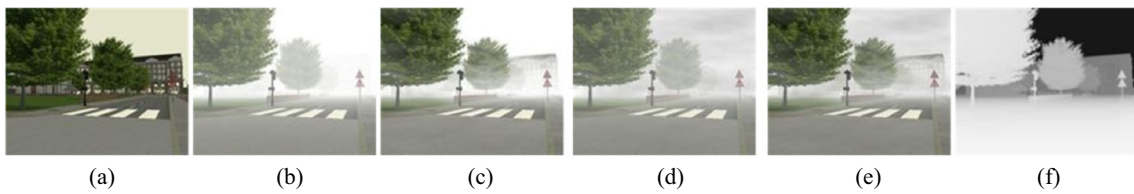


Fig. 21 Images **a** without fog, **b** with uniform fog, **c** with inhomogeneous fog, **d** with fog and clouds, **e** with clouds and inhomogeneous, **f** Depth map

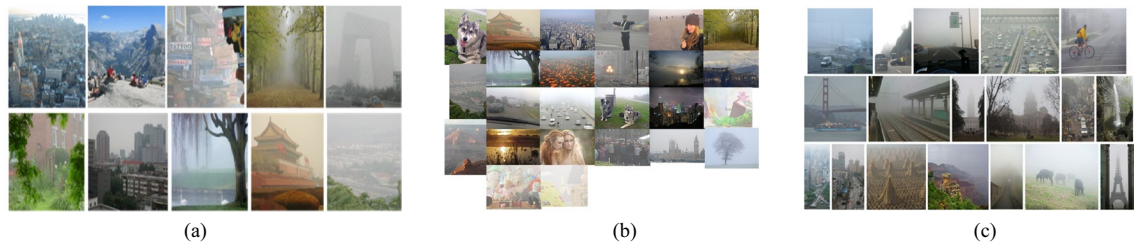


Fig. 22 Sample images of datasets **a** [97], **b** [98], **c** [99]



Fig. 23 Haze images from datasets, **a** [100], **b** varying visibility scenes from foggy Cityscapes [55]

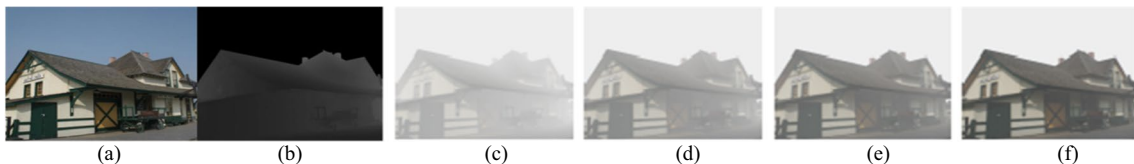


Fig. 24 HazeRD samples from left to right, **a** Haze-free image, **b** depth map, simulated hazy images with the visual range of **c** 50 m, **d** 100 m, **e** 200 m, and **f** 500 m, respectively

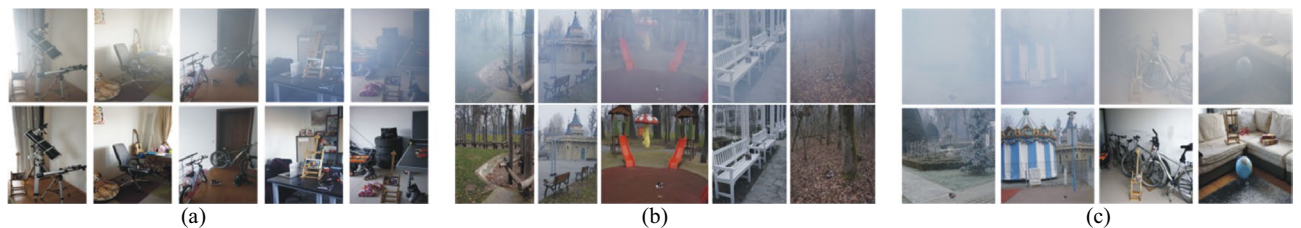


Fig. 25 Sample hazy images along with GT images from **a** [104], **b** [105], **c** [106]

in between [0.6, 1.8]. Testing sets are designed for evaluation purposes. The SOTS contains 500 different images with white scenes and dense haze synthesized from NYU2 which are not used in the training set. HSTS selects 10 synthetic outdoor hazy images, together with 10 realistic hazy images. Besides, RESIDE- β provides two more subsets: outdoor training set (OTS) and real-world task-driven testing set (RTTS). The OTS contains 72,135 hazy images and RTTS contains 4322 images.

This dataset provided a new dimension in the single image dehazing for the evaluation of various dehazing methods on a large-scale dataset in terms of full reference metric, no-reference metric, and human subjective rating in visual analysis. The sample images from each part of the RESIDE datasets are shown in Fig. 26.

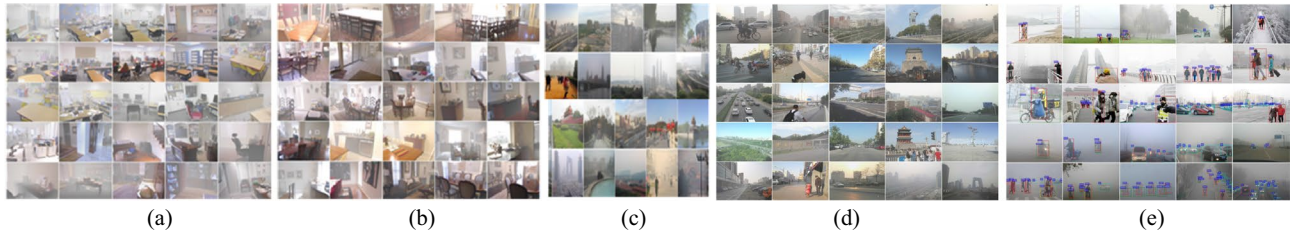


Fig. 26 Sample images from different category of RESIDE dataset [107] **a** ITS, **b** SOTS, **c** HSTS, **d** OTS, **e** RTTS

Fig. 27 Non-homogenous hazy image and GT image from [108], **a** hazy images, **b** GT images



Table 14 Standard datasets description

| Dataset (Reference, year) | Synthetic | | Real | |
|------------------------------------|-----------|---------|---------|-----------|
| | Indoor | Outdoor | Outdoor | Annotated |
| (1) Frida ([96], 2012) | — | 420 | — | — |
| (2) Fattal ([97], 2014) | 4 | 8 | 31 | — |
| (3) Waterloo IVC ([98], 2015) | 3 | — | 22 | — |
| (4) 500 Foggy images ([99], 2015) | — | — | 500 | — |
| (6) D-Hazy ([100], 2016) | 1449 | — | — | — |
| (5) Foggy Cityscapes ([102], 2017) | — | 25,000 | 101 | 101 |
| (7) HazeRD ([103], 2017) | — | 14 | — | — |
| (8) I-HAZE ([104], 2018) | 35 | — | — | — |
| (9) O-HAZE ([105], 2018) | — | 45 | — | — |
| (10) Dense-Haze ([106], 2019) | — | 33 | — | — |
| (11) RESIDE ([107], 2019) | 14,490 | 72,135 | 9129 | 4322 |
| (12) NH-Haze ([108], 2020) | — | 55 | — | — |

dataset used by the recent methods, we found that Fattal's dataset [97] and RESIDE [107] are the first choices for real and synthetic images, respectively.

6 Evaluation Metrics

There are several evaluation metrics used for testing the capability of the dehazing algorithms (DHA). At present, the images used in assessment can be divided into two categories: when ground truth image is available and when ground truth image is not available. Therefore, two categories of quantitative metrics depending upon the availability of images are introduced: full reference metric and no-reference metric, as shown in Fig. 28. Since it is difficult to obtain a haze-free image of the same scene. Therefore, no-reference metrics are often used for the assessment of DHA.

During dehazing, various issues may remain unresolved, including residual haze, structure damage, color distortions, over enhancement, halo artifacts, noise amplification, blurring effects, edge preservation, etc. To measure these distortions, many dehazing quality assessment methods were introduced in the literature. In this section, we will explore all these metrics.

6.1 No-Reference Metrics

A good DHA must ensure the following qualities in the dehazed image: improved visibility, removal of artifacts, over enhancement, contrast enhancement, structure preservation, and edge preservations. By considering all these qualities,

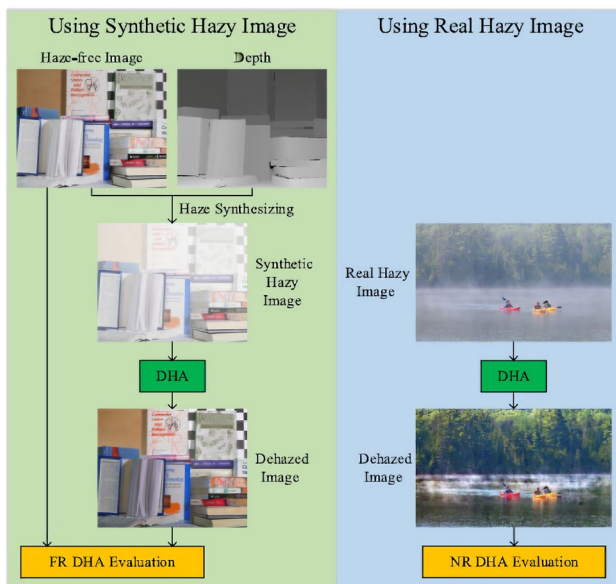


Fig. 28 Assessment criteria of real and synthetic hazy images [9]

many dehazing metrics were introduced. Unfortunately, there is no single DHA that can test all the dehazing capabilities. In this section, we discuss some well-known and dehazing metrics introduced in recent years.

6.1.1 Blind Contrast Enhancement Assessment [110]

The contrast of the image under adverse weather conditions is reduced significantly due to the scattering of the particles. This method is widely accepted in many dehazing works where the reference image is not available. This method is based on the assessment of contrast in terms of visible edges before and after restoration. It uses three descriptors: rate of new visible edges (e), the gain of visibility level (r), and saturated pixel ratio (σ). The value of the e metric specifies the ability of the dehazing method in terms of new visible edges in the restored image that are not seen in the original hazy image. It is calculated as follows:

$$e = \frac{n_{hf} - n_h}{n_h} \quad (14)$$

where n_h and n_{hf} represent the cardinality of visible edges in hazy and haze-free images, respectively.

The second metric r is the ratio of the visibility level of objects in the restored image and the visibility level of objects in a hazy image. This metric considers visible and invisible edges both in the hazy image as follows:

$$\bar{r} = e^{-\left(\frac{1}{n_{hf}} \sum_{p_i \in \psi_{hf}} \log r_i\right)} \quad (15)$$

where ψ_{hf} represents the set of visible edges in a haze-free image and r_i is the gradient of p_i and the corresponding pixels in a hazy image.

The third metric is the saturated pixel ratio. This metric talks about pixels which become saturated (black or white) after applying the dehazing process.

$$\sigma = \frac{n_s}{\text{dim}_x \times \text{dim}_y} \quad (16)$$

where n_s is the number of saturated pixels and dim_x and dim_y represent the width and height of the image, respectively.

A high value of e and r indicates good quality of a dehazed image in terms of edges preservation and contrast enhancement while a small value of σ is an indication that a dehazed image has fewer saturated pixels or color distortions than a hazy image.

6.1.2 Non-Reference Image Quality Assessment based Blockiness and Luminance Change (BALC) [111]

This metric is designed to measure the two distortions in an image: blocking artifacts and improper luminance change.

It is a no-reference metric and obtains the quality score of a dehazed image based on these distortions. These distortions in the dehazed image are estimated based on gradient. Usually, halo artifacts appear in the image at depth discontinuities. This method divides the image into 8×8 non-overlapping blocks. The blockiness of a block is measured by taking the average of discontinuities along the four boundaries of the block. For luminance change or blurring effect, it calculates the average of gradients inside the block. Finally, two measures are combined into a single metric as follows:

$$BALC = B_{hf} * L_{hf}^{-\lambda} \quad (17)$$

where B_{hf} and L_{hf} denote artifact and blurring effect of the haze-free image. $\lambda \geq 0$ is a parameter, used to adjust the importance of these two distortions.

A small value of BALC indicates the good quality of the haze-free image in terms of artifacts and blurring effects.

6.1.3 Blur Metric [112]

After the dehazing process, some methods introduce a blurring effect in the haze-free image. To check the quality of the dehazed image in terms of blur perception, many recent works used this metric.

This metric applies the low-pass filter on the dehazed image to obtain a blurred version of this image. The comparison of intensity variations between two images (the dehazed image and the blurred dehazed image) indicates blur annoyance. Thus, a high variation in intensity values between these two images signifies that the dehazed image

is not blurred whereas a small difference indicates that the dehazed image is blurred.

Blur metric provides a score ranging from 0 to 1 which represents the best and the worst quality, respectively in aspects of blur perception.

6.1.4 Blind Image Quality Assessment (BLIIND-II) [113]

BLIIND-II is a no-reference image quality assessment metric based on a probabilistic model that predicts the quality score of an image. This metric uses the natural scene statistics (NSS) model which relies on discrete cosine transform coefficients. NSS model is built from undistorted natural scenes and requires a small number of training examples. The estimation of the predicted score consists of four stages. In the first stage, the image is divided into $n \times n$ blocks, then computing the DCT coefficients for each block. In the second stage, a generalized Gaussian density model is applied to each block that provides the model parameters. Four features: shape parameter, coefficient of variation, energy sub-band ratio measure and orientation features are extracted in the third stage from model parameters. Finally, the fourth stage consists of a Bayesian model that predicts the perceptual quality of the dehazed image. The steps for the computation of this metric are shown in Fig. 29.

It considers various types of distortions, such as artifacts, white noise, Gaussian blur, fast fading channel, etc. in the estimation of a quality score. The values of this metric are in the range of [0, 100]. A higher value of BLIIND-II indicates the poor quality or distortions in the image. During dehazing, many periodic patterns (checkerboard

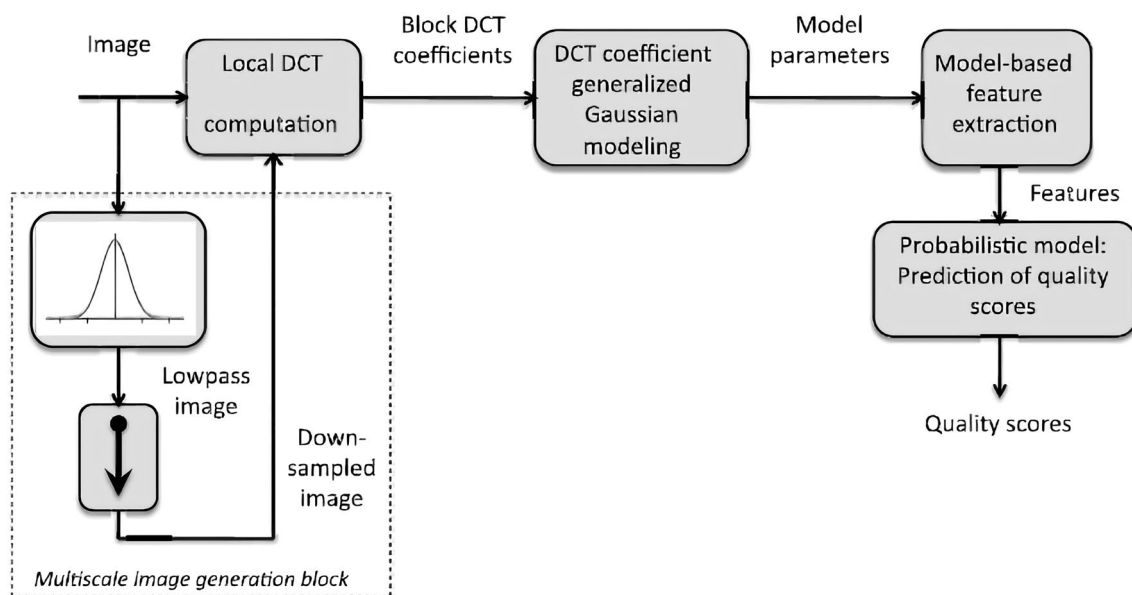


Fig. 29 Steps of computing BLIIND-II [113] metric

and blocking artifacts) are generated in the haze-free image. Therefore, this metric can be used to identify these distortions in the image.

6.1.5 Blind/No-Reference Image Spatial Quality Evaluator (BRISQUE) [114]

Mittal et al. [114] proposed a blind/no-reference image spatial quality evaluator (BRISQUE) metric which measures the losses of naturalness of an image without calculating the distortion-specific features, such as blocking, artifacts, blur, ringing artifacts, etc. It computes the local luminance coefficients and observed that these normalized luminance coefficients follow a Gaussian distribution for the natural scene. They extracted 36 natural scene statistics features at 2 scales-18 features per scale, used to identify all types of distortions. Finally, a regression module, support vector regression is used to calculate the quality score of an image. This model is tested on a LIVE IQA database which consists of 29 reference images and 779 distorted images spanning different types of distortions.

6.1.6 Fog Aware Density Evaluator (FADE) [99]

This metric is specially designed for the evaluation of DHA to judge the visibility of the restored image. This fog-aware density evaluator (FADE) metric does not consider the various approaches used previously, such as estimation of the transmission, salient region, human-related opinion, etc. This makes the judgment of visibility based on deviations in the spatial domain, seen in hazy and haze-free images. A set of fog-aware statistical features, namely MSCN (mean subtracted contrast normalized) coefficients, sharpness, contrast energy, colorfulness, color saturation, image entropy and dark channel prior are extracted from foggy images. It used 500 foggy and 500 fog-free images to extract these features. A test foggy image is divided into p^*p patches and average feature values for statistical features for each patch are extracted. A multivariate Gaussian (MVG) probability density in the d dimension is computed between a test foggy image and 500 natural fog-free images as follows:

$$MVG(f) = \frac{1}{(2\pi)^{d/2} |\mu|^{1/2}} \exp\left(-\frac{1}{2}(f - \sigma)^t \mu^{-1}(f - \sigma)\right) \quad (18)$$

where f represents fog aware features while μ and σ denote mean and covariance, respectively. In the next step, the Mahalanobis distance measure is computed between the MVG fit to features extracted from a test foggy image and the MVG model of 500 fog-free images as follows:

$$D_f(\mu_1, \mu_2, \sigma_1, \sigma_2) = \sqrt{(\mu_1 - \mu_2)^t \left(\frac{\sigma_1 + \sigma_2}{2}\right)^{-1} (\mu_1 - \mu_2)} \quad (19)$$

where μ_1, μ_2 and σ_1, σ_2 are the mean and covariance of the MVG model of the 500 fog-free images and a test foggy image, respectively. Similarly, D_{ff} is calculated between the MVG of 500 foggy images and a test image. Finally, the fog density of a hazy image is calculated as follows:

$$D = \frac{D_f}{D_{ff} + 1} \quad (20)$$

Constant 1 is added to the denominator to prevent divide by zero exception. Smaller values of D represent lower fog density, i.e. A DHA is improving the visibility of the hazy image to great extent.

A smaller FADE value indicates less residual haze present in the dehazed result. The residual haze, artifacts and noises, on images reduce the FADE scores. However, the bright scenes may be mistaken as residual haze by FADE and increase the value of FADE.

6.1.7 Natural Image Quality Evaluator (NIQE) [115]

This is another no-reference metric used in DHA for measuring the distortion during the dehazing process. This metric provides a natural image quality evaluator based on quality-aware features of the natural scene statistics model. These features are extracted from a corpus of undistorted natural images. The 36 features are extracted from a dehazed image (whose quality is to be analyzed) by dividing the image into p^*p patches and then comparing its MVG fit to the MVG model.

6.1.8 Dehazing Quality (DHQ) [116]

Min et al. [116] proposed an objective measure for the quantitative evaluation of dehazed images. To assess overall dehazing quality, first, they constructed a database of 1750 dehazed images generated from 250 real hazy images using 7 dehazing algorithms of different haze densities. Afterward, subjective quality evaluation is conducted on this dataset. Finally, the regression module predicts the dehazing quality (DHQ) by extracting several features from a dehazed image. The overall dehazing quality is measured in three aspects: haze removal, preservation of structure and over enhancement, as shown in Fig. 30.

Haze removing features aim to design haze-relevant descriptors to evaluate haze removing effect. It considers five features: pixel wise DCP, image entropy, local variance, normalized local variance and contrast energy. Another important parameter is structure preservation

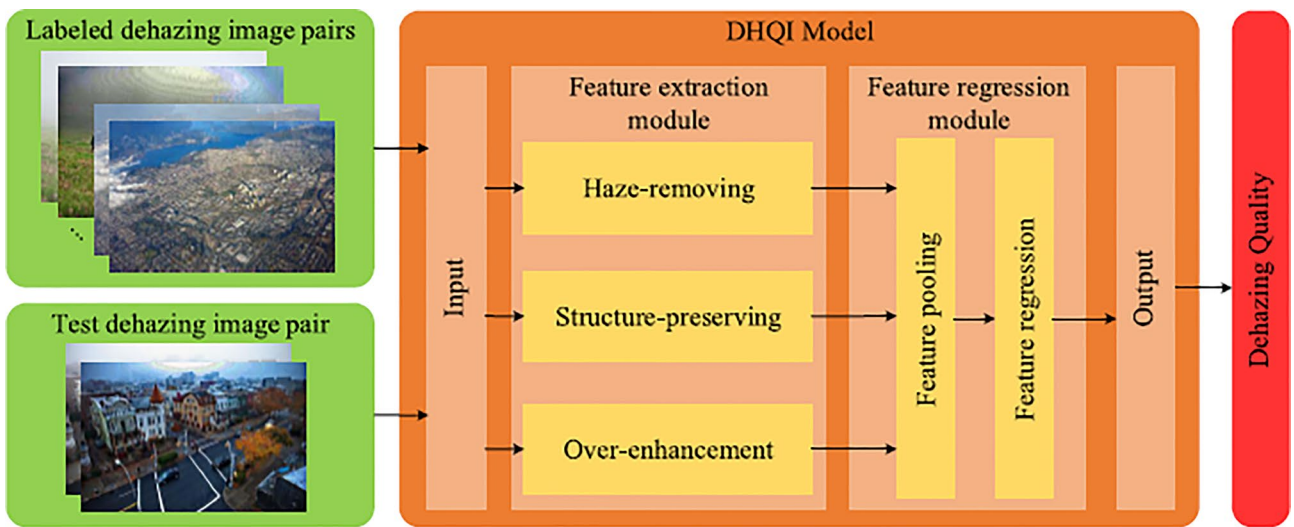


Fig. 30 Quantitative evaluation to measure overall issues of dehazing in real hazy images using non-reference based metric DHQ [116]

used to judge the quality of the dehazed image. The dehazing process sometimes can introduce structure degradation or artifacts. To account for structure preservation, various features, such as variance similarity, normalized variance similarity and normalized image similarity are used. The third important quality indicator of the dehazing process is the identification of over enhancement problem in dehazed images. During the dehazing process, details in low contrast areas are darkened; colors are distorted or may introduce structural artifacts. It is measured in the form of low contrast areas and blockiness.

6.2 Full-Reference Metrics

Full-reference metrics are used to evaluate a method when a GT image is available. This method is applicable to test the performance of synthetic images. Recently, several metrics: PSNR, SSIM, LPIPS, CIEDE 2000 and SHRQ had been utilized in many works. In this section, we have explored all such metrics.

6.2.1 Learned Perceptual Image Patch Similarity Metric (LPIPS) [117]

Pixel-wise metrics such as PSNR and SSIM disagree with human judgment in assessing the perceptual quality of the dehazed image. Therefore, Zhang et al. [118] proposed a learned perceptual image patch similarity metric (LPIPS) that establishes the perceptual similarity between two images that resemble human opinion. It is based on deep features, trained on some well-known deep learning frameworks like supervised, self-supervised, unsupervised, etc. This metric can identify a wide range of distortions in the image, including photometric (color shift, contrast, saturation), noise (white, artifacts), blur, and compression. Three network architectures including AlexNet, SqueezeNet and VGG are considered for supervised training. The overall framework of this metric is shown in Fig. 31.

This diagram shows how the distance between two patches x (patch of GT image) and x_0 (patch of dehazed image) is calculated by a network F . The features are extracted from many layers, normalize in channel dimension,

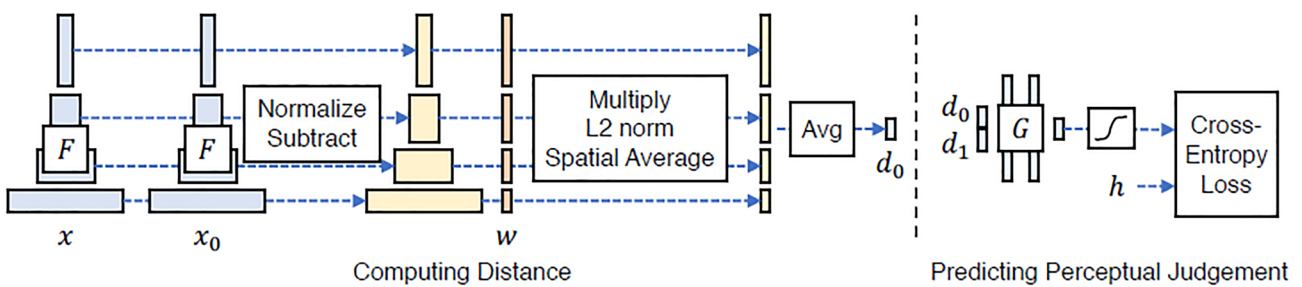


Fig. 31 Deep learning framework to measure perceptual quality of the dehazed image

scale each channel by vector w and compute the l_2 norm. Finally, the average of spatial and channel-wise is taken. G is a network trained to predict perceptual quality h from distance pair d_0 and d_1 .

The lower LPIPS score indicates a higher similarity between the two images.

6.2.2 Peak Signal to Noise Ratio (PSNR) [119]

Peak signal to noise ratio (PSNR) measures the degree of signal distortion between a haze-free image obtained by a DHA and GT image. A high value of PSNR signifies the good quality of the dehazed image. It is calculated as:

$$PSNR = 10 \log_{10} \left(\frac{255^2}{MSE} \right) \quad (21)$$

where MSE is used to calculate the error between dehazed image and ground truth image. It must be minimized and calculated as follows:

$$MSE = \frac{1}{M \times N} \sum_{i=1}^M \sum_{j=1}^N (G(i,j) - I_{hf}(i,j))^2 \quad (22)$$

where G and I_{hf} are the ground truth and dehazed images, respectively.

6.2.3 Structural Similarity Index Metric (SSIM) [120]

Since PSNR is not effective in terms of human visual judgment. Therefore, many researchers utilized the structural similarity index metric (SSIM) which evaluates the dehazing performance in terms of contrast, luminance and structure between ground truth and dehazed images. It is calculated as follows:

$$SSIM(r, i) = \left(\frac{2\mu_r\mu_i + c_1}{\mu_r^2 + \mu_i^2 + c_1} \right) \left(\frac{2\mu_{ri} + c_2}{\sigma_r^2 + \sigma_i^2 + c_2} \right) \quad (23)$$

Here, μ_r and μ_i are means of r (restored image) and i (GT image), respectively. σ_r^2 and σ_i^2 are the variances of r and i and μ_{ri} is the cross-variance between r and i . Default values of c_1 and c_2 are 0.01 and 0.03.

SSIM yields a decimal score between 0 and 1. The score value of 1 indicates that the two images are identical. SSIM is highly sensitive to variations of contrast and illumination. Therefore, it can judge the issues of dehazing, such as incomplete haze removal or over-saturation of pixels.

6.2.4 CIEDE 2000 [121, 122]

During the dehazing process, color distortions may be introduced in a restored image. It cannot be reliably evaluated

by PSNR or SSIM. Therefore, researchers in this field also used an accurate color difference metric CIEDE 2000 which assesses dehazing in terms of color restoration closer to human eye perception in color difference.

It yields values in the range [0,100] with smaller values indicating better color preservation, and values less than 1 corresponding to imperceptible by the human eye. A value of 100 indicates that colors are the opposite of two images.

6.2.5 Synthetic Haze Removing Quality (SHRQ) [9]

Min et al. [123] proposed a full reference metric called synthetic haze removing quality (SHRQ) to evaluate the overall quality of a dehazed image. The proposed dehazing quality evaluator integrates many quality parameters raised during the dehazing process. These issues of dehazing are structure recovery, color rendition and over-enhancement. The author first creates an SHRQ database that consists of two subsets: regular and aerial images. The regular image dataset consists of 45 haze-free images while the aerial dataset contains 30 high-quality aerial images. The ASM model is utilized to get the synthetic hazy images. These hazy images are processed by eight state-of-the-art methods. The overall quality of a dehazed image is estimated as follows:

$$Q = \frac{1}{z} \sum_{i,j} S_{sim}(i,j) \cdot [C_{ren}(i,j)]^\alpha \cdot O \quad (24)$$

where S_{sim} is the structure map, C_{ren} is the color rendition map and O represents over-enhancement in low contrast areas. z represents the total number of pixels, α is set empirically to adjust the importance of color information.

7 Experimental Results

In this section, experimental results are presented in three ways. First, we evaluate the recent state-of-the-art methods based on dehazing assessment criteria. Second, we discuss the qualitative or visual analysis of dehazing methods. Finally, we discuss the performance of different methods quantitatively on different datasets.

7.1 Comparison of the State-of-the-art Methods based on Dehazing Assessment

This section presents the assessment criteria of different dehazing methods based on parameter setting during experimentation, dataset(s) selected and evaluation metrics used for the assessment. For comparison, we have collected this data from their manuscript. This analysis is illustrated in Table 15.

Table 15 Comparison of experimental analysis of existing methods using different parameters

| Category | Ref. | Year | Dataset | Parameter | Evaluation Metric |
|--------------------------------------|-------|--------|--|--|--|
| Deep learning | [23] | (2020) | RESIDE | $r=0.4$, learning rate = 0.0001, and a batch size of 32, $n=3$ (DWT iteration) | PSNR, SSIM, FADE |
| | [124] | (2020) | SOTS, Fattal | Training 140 epochs, loss function: $\lambda_E = \lambda_A = \lambda_p = \lambda_G = 1$, batch size = 5, Adam optimizer, learning rate = 2×10^{-4} | Full-reference: SSIM, PSNR, VIF, UQI, LPIPS, MSE, MS-SSIM, SIMIndex, CIEDE 2000, |
| | [55] | (2020) | O-Haze, Dense- Haze | CycleGAN $\lambda_{cycle}=10$, learning rate 0.0002, L_1 loss $\lambda_l=100$, Perceptual loss $\lambda_p=5$ | PSNR, SSIM, BRISQUE, NIQE |
| | [179] | (2021) | Sample images from RESIDE, I-Haze and O-Haze | Training 20 epochs, Adam optimizer learning rate = 2×10^{-4} , $\lambda_H = 0.5\lambda_G = 10$, $\lambda_p = 0.5\lambda_B = 10^{-2}$, $\lambda_{GAN} = 1$, $B=0.1$, $K=20$, and $\sigma^2 = 3 * 10^{-3}$ | PSNR, SSIM, SSEQ, and BLIINDS-II |
| Image fusion-based methods | [19] | (2017) | Natural and synthetic images | Scaling factors: $\lambda_1 = \lambda_2 = \lambda_3 = 5$, Gamma correction γ , penalizing parameter $\varepsilon = 10^{-6}$, η | No reference: TV-Error, NIQE, BLIINDS II, and BRISQUE |
| | [52] | (2017) | 7 benchmark images | Scale $\sigma=0.1$, mean filter = $20*20$, patch size in BTM = 15, Level of decomposition = 7, neighborhood $r=13$, regularization term $\lambda=3$ | e, r, contrast gain, IVM, VCM, SSIM |
| | [61] | (2019) | Sample images from NYU2 Depth, Middlebury, I-Haze and SOTS-indoor and outdoor databases from FRIDA2, HazeRD, O-Haze and SOTS outdoor | $\lambda_t = 10^{-6}$, $\tau = 0.138$, $s=3$ | PSNR, SSIM, VSNR, FSIMc |
| | [56] | (2020) | Subset of RESIDE, Remote Sensing Images, Under water image, etc | Patch size 7*7, Local detail enhancement $\beta=1.1$, structural information σ_D , σ_B , and α are set to 0.12, 0.5, and 6.25 | SSIM, FADE, Entropy, Gradient-based performance metric (QG), Nonlinear correlation information entropy ($QNCE$), Chen-Blum metric (QCB), Visual information fidelity ($QVIF$), Peak signal-to-noise ratio (PSNR) |
| Miscellaneous Category: Unsupervised | [81] | (2020) | RESIDE, | Adam optimizer, 140 epochs, learning rate = 0.001, $\lambda_1 = 0.1$ and $\lambda_2 = 0.005$ | PSNR and SSIM |
| Hardware | [133] | (2020) | Middlebury, NYU2, SOTS-Indoor, and SOTS-Outdoor | Patch size = 3*3 and 15*15 for bright white objects, $th=40$, $\alpha = 0.05$ to 0.1 | PSNR, SSIM and CIEDE2000 |
| DCP based methods | [44] | (2019) | NYU depth dataset | Contrast saturation α , patch size = 15*15 | RMSE, CIEDE2000, Weibull-Edge, SSIM and F&T |
| | [88] | (2020) | RESIDE, real-world images | Loss function parameters: $\lambda=10^{-4}$, $\varepsilon=10^{-6}$, $\omega=0.95$, $t_0=0.1$, DCP patch size: 15*15, and soft matting patch size: 3*3 | PSNR, SSIM |
| | [164] | (2020) | O-Haze, RESIDE | - | PSNR, SSIM, CIEDE2000 |

Table 15 (continued)

| Category | Ref. (Year) | Dataset | Parameter | Evaluation Metric |
|---------------------------------------|--------------|--|---|---|
| Restoration based methods with priors | [64] (2015) | Real and synthetic images | $r=15, \beta=1.0, \theta_0=0.121779, \theta_1=0.959710, \theta_2=-0.780245$ and $\sigma=0.041337$ | MSE and SSIM |
| | [40] (2019) | Subset of FRIDA, FRIDA2, RESIDE, D-Hazy, IVC | Mask size of GPP is $3*3$ | e, r, C_g , PSNR, SSIM, Perceptual haze density (D_h), σ |
| | [157] (2020) | 500 Foggy Images, O-Haze and I-Haze | Patch size = $6*6$, Neighborhood size = $30*30$ | SSIM, FADE, SCORE, UCIQE |
| | [138] (2020) | Natural images, RESIDE | Positive constants ϵ_1 and ϵ_2 set to 10^{-5} , correction factor $\Gamma = 0.5$, regulation constant $\lambda = 0.5$ | FADE, e , SSIM, and MSE |
| | [66] (2020) | Natural images and O-Haze | Color cluster N = 1000, Number of angles, $k = 40$, the number of different atmospheric light candidates is $M = 1/\Delta A$, where $\Delta A = 0.02$, threshold = 0.02, the number of different haze-lines is Q = 1000, $\lambda = 0.1$ | SSIM and CIEDE2000 |
| | [136] (2021) | Real and synthetic images and images from I-Haze, O-Haze | $p_1 = -0.397, p_2 = 0.07747, \epsilon = 0.02, \delta = 4, s = 75 * 75$ | r , NIQE, PSNR, FADE |
| Image Enhancement based methods | [22] (2017) | Fattai's Dataset | Patch size $8*8$ and decomposition level = 2 | e, σ and r |
| | [30] (2017) | 8 real hazy images | Control factor δ and filter window $15*15$ | MSE, PSNR and SSIM |
| | [33] (2018) | Real hazy images | $\lambda = 1/2048, \gamma = 2048, \theta = 13/8$, and $\epsilon = 1/64$ | FADE |
| | [24] (2019) | Real images, I-haze and O-haze | multilevel parameter = 2, weighting parameter λ is set according to atmospheric light | e, σ, r , PSNR, SSIM |
| | [43] (2020) | Real hazy images and D-hazy | Dehazing controlling $\tau = 0.8$ for outdoor and $\tau = 0.7$ for indoor and $k = 0.4-0.6$ | NRM, FADE, e, r , NIQE, BRISQUE, FRM-CID, Delta E, SSIM |

Table 15 demonstrates the datasets and metrics used by the respective dehazing method. We can notice in the table; the recent state-of-the-art methods utilize a variety of dehazing metrics including full reference and no reference metrics for comparison purposes. Most of the methods focus on selecting the number of metrics for evaluation. In this regard, the method [43, 56, 124] utilized sufficient metrics for evaluation. Besides, a good DHA must be tested on diverse datasets of different haze concentrations including dense haze, non-homogeneous haze, sky regions, night-time hazy conditions, mild haze, etc. The method [40, 61] is tested on a large number of datasets as compared to other methods. We can also notice in this table that all DHA requires some parameters to be adjusted adaptively or manually, irrespective of their category. The number of parameters increases the overhead and reduces the efficiency of a method. Hence, they must be minimized as methods [40, 125].

7.2 Qualitative Evaluation

Figure 32 shows the visual analysis of restoration-based methods with prior on two hazy images from HSTS of RESIDE dataset along with GT image. We can observe in this figure that all the methods are unable to preserve the color and contrast of the image. All the dehazed images in the sky regions are darker than the GT image. In addition to

color distortions, the DCP [63] also suffers from halo artifacts. However, the dehazed image by [47] has fewer color distortions as compared to other methods and resembles the GT image.

Furthermore, Fig. 33 shows the qualitative results of different machine learning and deep learning methods on the HSTS dataset along with the GT image. It is observed in this figure that dehazed result by the Deep DCP method has residual haze. The methods [73, 75], and [76] have color distortions in the image. The other methods [74] and [126] have fewer color distortions. The dehazed image obtained by [89] resembles the GT and also all the details are visible.

Figure 34 shows a visual comparison of state-of-the-art methods on two hazy images taken from O-Haze datasets. We can notice in this figure that NLD [66], PDN [127] highly distort the color of the image. The AOD-net and DCPDN are unable to remove haze completely. The method GFN [77] is managed to remove haze and also has fewer color distortions. The dehazed image achieved by method [128] is much closer to the GT image.

The visual analysis in Fig. 35 reveals that removing dense haze is still a challenging task. The performance of most of the methods (deep learning and prior based) on this dataset is not satisfactory. The details of the images are imperceptible under the dense haze. All earlier methods [73–75] and [85] are unable to remove the haze. However, the

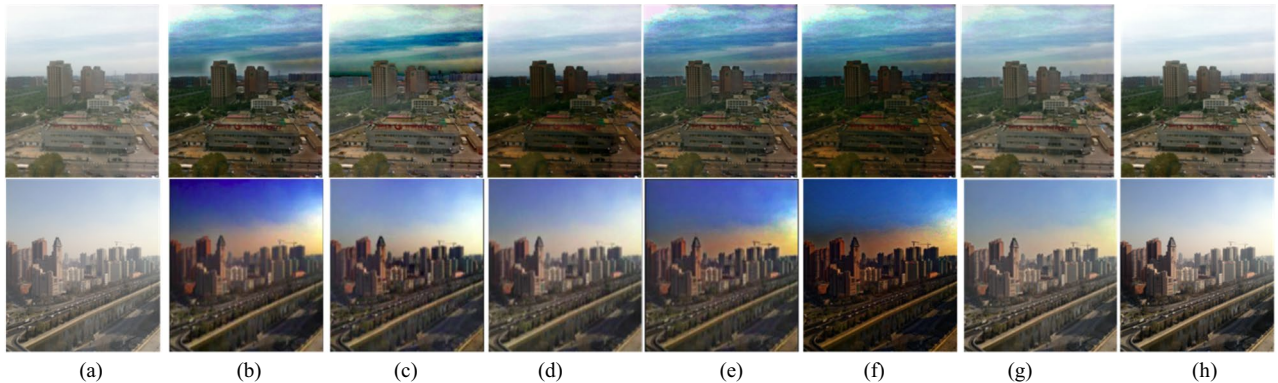


Fig. 32 Reside HSTS: Prior based restoration methods, **a** Hazy image, **b** DCP [63], **c** NLD [66], **d** CAP [64], **e** BCCR [49], **f** CEP [67], **g** LBF [47], **h** GT

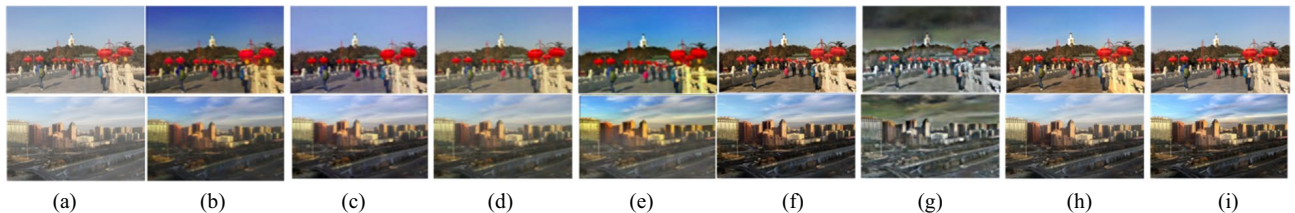


Fig. 33 RESIDE HSTS: learning based methods, **a** hazy image, **b** AOD net [75], **c** DehazeNet [74], **d** deep DCP [88], **e** MSCNN [73], **f** PQC [126], **g** cycle-dehaze [76], **h** DFIDSE [89], **i** GT

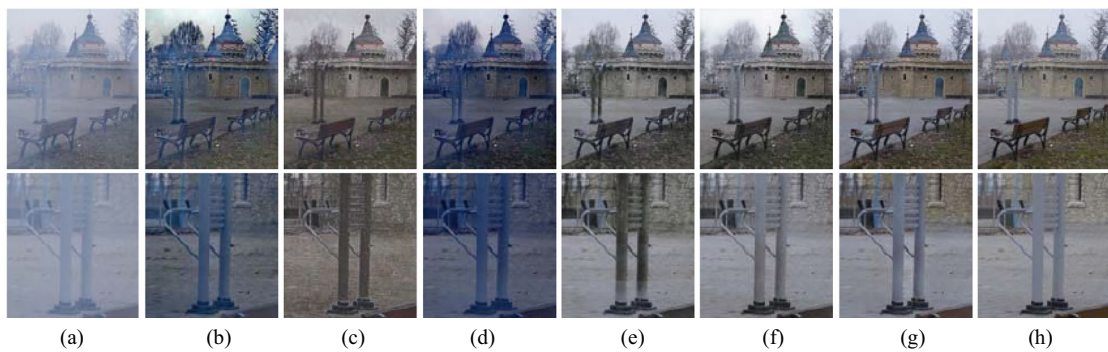


Fig. 34 Haze removal results by various methods on hazy images from O-HAZE **a** hazy image, **b** NLD [66], **c** AOD-net [75], **d** PDN [127], **e** GFN [77], **f** DCPDN [142], **g** DM²F-Net [128], **h** GT

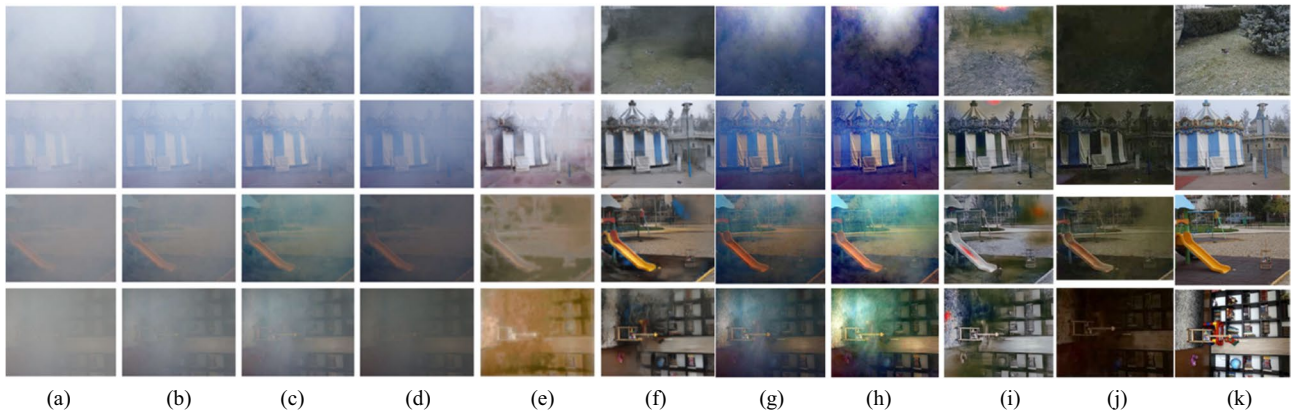


Fig. 35 Qualitative comparison of results on images from the Dense-Haze dataset. **a** Hazy image, **b** DehazeNet [74], **c** MSCNN [73], **d** AOD-Net [75], **e** PPDNet [85], **f** HR-Dehazer [129], **g** DCP [63], **h** NLD [66], **i** BPPNet [79], **j** GCANet [84], **k** GT

restoration-based method DCP and NLD attempt to remove the haze at the cost of high color distortions. The method [84] produces dark images in which details are not visible. The method [79] and [129] perform better than other methods except for the first image.

Figure 36 represents non-homogeneous hazy images, different from other dehazing datasets in which haze is characterized by homogeneous haze. The performance of most state-of-the-art methods drops significantly due to the non-homogeneous nature. The color distortions problem is noticed in dehazed images by the DCP method due to the homogeneous assumption of the physical model. In addition to color distortions, the method [74] also introduced the noise in the dehazed image. The AOD and GCA net are unable to remove the haze in dense hazy regions. The DCPDN is succeeded to remove the haze without color distortion. However, some artifacts are observed. The method [95] generates pleasing results and is able to deal with non-homogeneous haze in presence of dense haze to some extent.

Figure 37 shows the qualitative analysis of different methods on a sample image taken from HazeRD datasets.

The results of DCP, CAP, PDN and DehazeNet suffer from color distortions while the haze-free obtained by the method DCPDN and GFN are over brightened as compared to GT. The MSCNN and NLD leave some haze in the dehazed result. The method [130] and [75] perform satisfactorily. However, they are also not able to restore the color of sky regions in addition to other methods.

In Fig. 38, hardware architecture-based methods are tested on three real images from Fattal's dataset. The methods [72] and [131] used the simple concept of DCP to remove the haze. Therefore, their dehazed images are having the problem of color distortions and over-saturation of pixels. The dehazed images of the method [132] are over brightened also suffer from over-saturation of pixels. The method of [133] generates pleasing results. However, visibility in long-range regions is not up to the mark.

Finally, we present dehazing results on some sample images from the dataset [99] in Fig. 39. The quantitative results are also illustrated in Table 22. Here, we consider four popular categories of methods: image enhancement [22], image fusion [13], and [62], machine learning:

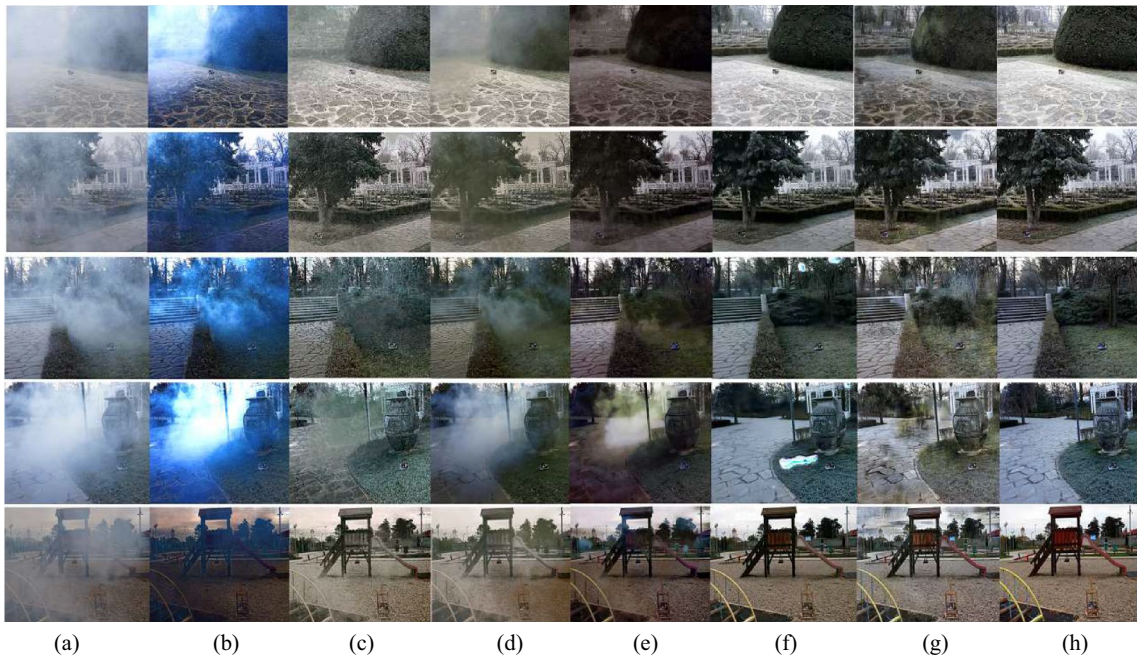


Fig. 36 Quantitative comparisons of the state-of-the-art dehazing methods on NTIRE-2020 challenge: NH-HAZE. **a** Hazy image, **b** DCP [63], **c** DehazeNet [74], **d** AOD net [75], **e** GCAAnet [84], **f** DCPDN [142], **g** KTDN [95], **h** GT

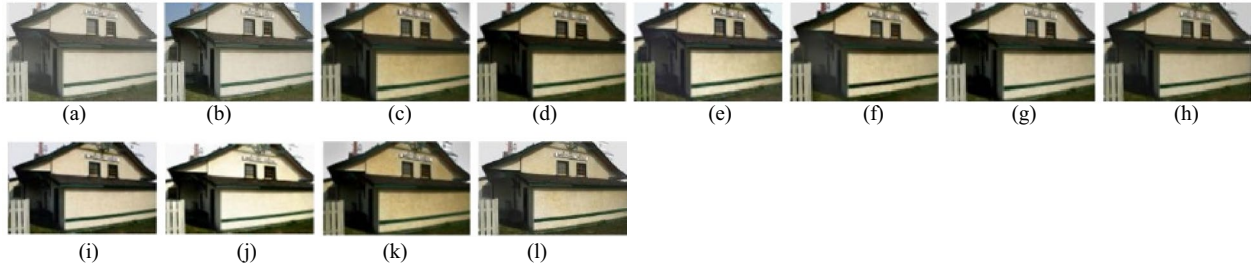


Fig. 37 Comparison with state-of-the-art methods on a hazy image from HazeRD dataset. **a** hazy image, **b** GT, **c** DCP [63], **d** CAP [64], **e** NLD [66], **f** MSCNN [73], **g** DehazeNet [74], **h** AOD-net [75], **i** GFN [77], **j** DCPDN [142], **k** PDN [127], **l** DHRNT [130]

[134] and [64] and restoration with priors [63, 66] and [51]. Fusion based method [13] distorts the color also leaves haze in some parts of the images while another method [62] better preserves the color in nearby regions and enhances the visibility in faraway regions. Machine learning methods [134] and [64] do not distort the color but they failed to remove the haze completely. In comparison to restoration with prior methods, DCP has pleasing results as compared to NLD with fewer color distortions. The RASD method better handles the artifacts but it blurs the details of dehazed images due to gradient residual minimization. The enhancement-based method [22] on DCP has a better-dehazed image as compared to the restoration-based method.

7.3 Quantitative Evaluation

This section provides a comparison of recent and popular methods of dehazing on different standard datasets. Tables 16, 17, 18, 19, 20, 21, 22, provide the quantitative evaluation of HazeRD, RESIDE, I-Haze, O-Haze, Dense-haze and D-Hazy, respectively. Since all these datasets are having GT images. Their assessment is done using full-reference metrics: PSNR and SSIM. Moreover, Table 22 provides the quantitative analysis of the real images used in Fig. 39. GT images are not available for these images; therefore, evaluation is done by a variety of non-reference metrics including FADE, Blur, BALC, σ , e, r, NIQE, BRISQUE, BLIINDSII and BIQI.

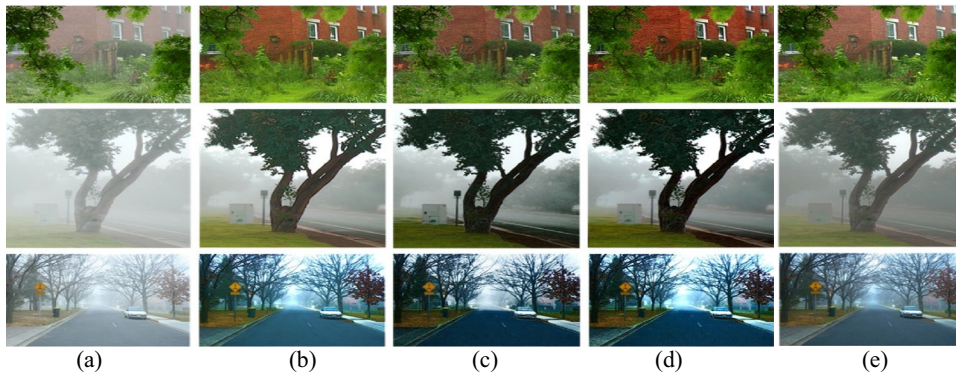


Fig. 38 Hardware based methods **a** Hazy image, **b** Shiau et al. [72], **c** Zhang et al. [131], **d** Shiau et al. [132], **e** Kumar et al. [133]

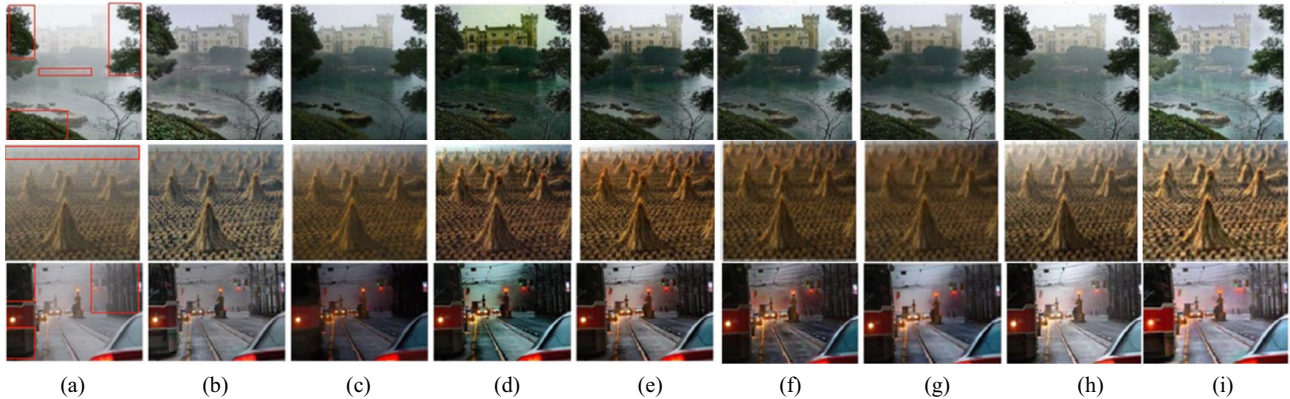


Fig. 39 Hazy images with sky region and their dehazed images by different methods **a** Hazy image, **b** AMEF [13], **c** CAP [64], **d** NLD [66], **e** ESIDD [22], **f** DCP [63], **g** RASD [51], **h** MLP [134], **i** The JCDF method [62]

We have opted for different methods in comparison tables because we have considered the top performers in respective datasets. We conclude from the quantitative analysis of datasets that a method that is ranked no 1 on one dataset is not the best on other datasets too. The haze density is also different when moving from one dataset to another dataset. Considering this fact in the mind, the performance of methods differs according to the level of the haze.

Table 16 illustrates the performance of the most popular and recent dehazing method on the HazeRD dataset. This dataset contains synthetic images of different haze concentrations. For the assessment of dehazing quality, we use two metrics: PSNR and SSIM. Most of the methods have lower PSNR and SSIM values except for one or two methods. The lower PSNR and SSIM values indicate that these methods are not able to remove the haze completely or there is a higher color distortion. The higher values of PSNR and SSIM indicate that the dehazed image by the method LDP [82] is visually closer to the GT images and is ranked no 1 among all the compared methods.

Table 17 illustrates the performance of recent dehazing methods on the most popular RESIDE dataset. This dataset contains both real and synthetic images with a mild haze. The table presents the results of the SOTS indoor and SOTS outdoor part of RESIDE dataset. The evaluation metric used is PSNR and SSIM. We can observe that DCP suffers from the problem of color distortions due to invalidity of prior for white brighter objects or high depth regions. AOD-Net has residual haze and dehazed images are having low brightness. The dehazed images by the Dehazenet method are over brightened as compared to the GT. GCANet has higher PSNR and SSIM values and indicates better-dehazed images as compared to other methods except for FFA-Net [86] and DM2F-Net [128]. However, its performance is degraded at high-frequency components such as edges or blue sky. The dehazed result of [86] and [129] are better than state-of-the-art methods with a large margin of PSNR and SSIM values. GMAN method [78] performs better on SOTS outdoor but average on SOTS indoor. The performance of DM²F-Net [128] is also noticeable on SOTS indoor which is in the

Table 16 PSNR and SSIM comparison of existing techniques on HazeRD dataset

| Methods | PSNR | SSIM |
|----------------|-------|------|
| DCP [63] | 14.64 | 0.78 |
| CAP [64] | 14.15 | 0.74 |
| NLD [66] | 14.58 | 0.81 |
| MSCNN [73] | 15.62 | 0.82 |
| DehazeNet [74] | 15.30 | 0.79 |
| AOD-Net [75] | 15.64 | 0.80 |
| GFN [77] | 13.73 | 0.67 |
| DCPDN [142] | 15.86 | 0.77 |
| PDN [127] | 14.48 | 0.75 |
| LDP [82] | 17.51 | 0.85 |

Table 17 PSNR and SSIM comparison of existing techniques on RESIDE dataset

| Method | SOTS Outdoor | | SOTS Indoor | |
|-----------------------------|--------------|------|-------------|------|
| | PSNR | SSIM | PSNR | SSIM |
| DCP [63] | 19.13 | 0.82 | 16.62 | 0.82 |
| AOD-Net [75] | 20.29 | 0.88 | 19.06 | 0.85 |
| DehazeNet [74] | 22.46 | 0.85 | 21.14 | 0.85 |
| GFN [77] | 21.55 | 0.84 | 22.30 | 0.88 |
| FFA-Net [86] | 33.57 | 0.98 | 35.77 | 0.98 |
| GMAN [78] | 28.19 | 0.96 | 20.53 | 0.81 |
| Deep DCP [88] | 24.08 | 0.93 | 19.25 | 0.83 |
| CAP [64] | 22.30 | 0.91 | 19.05 | 0.84 |
| MSCNN [73] | 21.73 | 0.83 | 17.57 | 0.81 |
| NLD [66] | 18.07 | 0.80 | 17.29 | 0.75 |
| BCCR [49] | 15.49 | 0.78 | 16.88 | 0.79 |
| Y-NET [23] | 26.61 | 0.95 | — | — |
| Deep Energy (Network) [92] | 24.07 | 0.93 | — | — |
| Improved CycleGAN [178] | 21.78 | 0.80 | — | — |
| GCANet [84] | — | — | 30.23 | 0.98 |
| HIDEGAN [185] | 25.54 | 0.88 | 24.71 | 0.87 |
| RYFNet [186] | — | — | 21.44 | 0.87 |
| DM ² F-Net [128] | — | — | 34.29 | 0.98 |
| DPDP-Net [141] | — | — | 20.18 | 0.88 |

second position after the FFANet [86]. The dehazing capability of other methods is not satisfactory. The FFANet has good dehazing capability on both datasets and ranked no 1 and deals with many problems of sky regions, avoiding darkening of colors, color fidelity and image details.

Tables 18 and 19 illustrate the PSNR and SSIM values of recent and popular dehazing methods on I-Haze and O-Haze datasets, respectively. These datasets contain high-resolution images with a mild haze density. The restoration-based methods [63, 66, 135–137] and [138] again suffer from the problem of color distortions and are unable to preserve the

Table 18 PSNR and SSIM comparison of existing techniques on I-Haze dataset

| Method | PSNR | SSIM |
|--------------------------|-------|--------|
| DCP [63] | 14.43 | 0.752 |
| CAP [64] | 12.24 | 0.606 |
| MSCNN [73] | 15.22 | 0.7545 |
| NLD [66] | 14.12 | 0.653 |
| AOD-Net [75] | 13.98 | 0.732 |
| PPDNet [85] | 22.53 | 0.870 |
| BPPNet [79] | 22.56 | 0.899 |
| Feature Forwarding [139] | 18.56 | 0.809 |
| IDE [136] | 15.77 | — |
| NCC [137] | 15.84 | 0.534 |
| NRIS [135] | 12.62 | 0.574 |
| ICycleGAN [180] | 15.92 | 0.745 |
| CFCEMD [152] | 15.21 | 0.698 |
| DCPDN [142] | 14.37 | 0.724 |
| GFN [77] | 11.87 | 0.527 |
| Cycle-Dehaze [76] | 14.89 | 0.744 |
| DehazeNet [74] | 16.73 | 0.626 |
| DFIN [140] | 16.04 | 0.633 |
| IDGCP [138] | 16.10 | — |

Table 19 PSNR and SSIM comparison of existing techniques on O-Haze dataset

| Method | PSNR | SSIM |
|-----------------------------|-------|------|
| DCP [63] | 16.78 | 0.65 |
| CAP [64] | 16.08 | 0.60 |
| MSCNN [73] | 17.56 | 0.65 |
| NLD [66] | 15.98 | 0.58 |
| AOD-Net [75] | 15.03 | 0.54 |
| PPDNet [85] | 24.24 | 0.72 |
| BPPNet [79] | 24.27 | 0.89 |
| Feature Forwarding [139] | 22.07 | 0.75 |
| IDE [136] | 14.19 | — |
| AMEF [13] | 8.31 | 0.00 |
| NRIS [135] | 7.37 | 0.35 |
| Cycle-Dehaze [76] | 19.62 | 0.67 |
| Doble-DIP [80] | 18.82 | — |
| ICycleGAN [180] | 18.22 | 0.85 |
| CFCEMD [152] | 16.06 | 0.62 |
| DCPDN [142] | 14.52 | 0.59 |
| GFN [77] | 17.18 | 0.62 |
| Cycle-Dehaze [76] | 17.35 | 0.86 |
| DehazeNet [74] | 17.90 | 0.55 |
| DFIN [140] | 17.46 | 0.53 |
| IDGCP [138] | 15.71 | — |
| DM ² F-Net [128] | 25.19 | 0.78 |
| HR-Dehazer [129] | 21.46 | 0.69 |

Table 20 PSNR and SSIM comparison of existing techniques on Dense-Haze dataset

| Method | PSNR | SSIM |
|--------------------------|-------|-------|
| DCP [63] | 14.56 | 0.398 |
| BCCR [49] | 14.62 | 0.352 |
| DCL [97] | 12.11 | 0.326 |
| DehazeNet [74] | 11.36 | 0.374 |
| NTDF [200] | 13.67 | 0.306 |
| NLD [66] | 13.18 | 0.358 |
| MSCNN [73] | 12.52 | 0.369 |
| Feature Forwarding [139] | 16.37 | 0.569 |
| BPPNet [79] | 17.01 | 0.613 |
| AOD-Net [75] | 12.79 | 0.423 |
| HR-Dehazer [129] | 16.47 | 0.518 |
| PPDNet [85] | 12.04 | 0.428 |

Table 21 PSNR and SSIM comparison of existing techniques on D-Hazy dataset

| Method | D-Hazy-NYU | | D-Hazy-MB | |
|----------------|------------|------|-----------|------|
| | PSNR | SSIM | PSNR | SSIM |
| DCP [63] | 11.56 | 0.67 | 12.13 | 0.68 |
| CAP [64] | 13.29 | 0.73 | 14.36 | 0.75 |
| DehazeNet [74] | 13.02 | 0.73 | 13.78 | 0.73 |
| MSCNN [73] | 13.67 | 0.74 | 13.97 | 0.75 |
| AOD-Net [75] | 12.44 | 0.71 | 13.48 | 0.75 |
| DFIN [140] | 18.11 | 0.83 | 15.63 | 0.73 |
| DPDP-Net [141] | – | – | 18.76 | 0.91 |

structure of the image due to the invalidity of priors. Earlier, simple machine learning and deep learning methods: [64, 73–77], etc. are unable to remove the haze effect completely. In comparison with other methods, the overall results of [79, 85, 139] and [128] are better with higher PSNR and SSIM values. From Tables 18 and 19, we conclude that BPPNet [79] is the top performer on the I-Haze dataset while DM2F-Net [128] is the best among all the methods on the O-Haze dataset.

Table 20 shows the results of the comparison on the Dense-Haze dataset. This dataset greatly differs from other datasets (I-Haze and O-Haze) in terms of increased haze levels. This dataset contains hazy images with very dense fog. The state-of-the-art methods are generally trained on images having sparse haze. For example, the method [85] is trained on O-Haze (Mild hazy images). Therefore, its performance is degraded when tested on dense hazy images, as indicated by the PSNR and SSIM values of PPDNet. Moreover, PSNR and SSIM values of most of the methods are very low indicating higher color distortions and incapable

to deal with dense haze except for two or three methods. In comparison with other methods, BPPNet, HR-Dehazer and Feature Forwarding methods have got the satisfactory values of PSNR and SSIM because these methods are trained on dense hazy images. BPPNet is ranked no 1 and capable to remove the dense haze. However, the color restoration of dehazed images does not resemble the GT images. The quantitative analysis of the Dense-Haze dataset confirms the qualitative analysis in Fig. 35.

Furthermore, we compared the state-of-the-art methods on the D-Hazy dataset. The D-Hazy dataset is divided into two parts: NYU depth and Middlebury (MB) portions. This dataset contains synthetic images with medium haze. Table 21 presents the quantitative results. The analysis of this table demonstrates that the dehazing results of a learning-based method [73–75, 140] and [141] are better than prior based methods [63] and [64]. In the comparison of PSNR and SSIM values, DFIN [140] and DPDP-Net [141] are ranked no 1 in NYU-depth and MB portion, respectively.

Furthermore, we have analyzed the performance of the state-of-the-art methods on natural images using multiple metrics, to identify the pitfalls of these methods, available as non-reference image quality assessment. The dehazing results are better suggested by FADE. A smaller FADE indicates less residual haze present in the dehazed result; BLIINDS-2 and BRISQUE are the indicators of perceptually pleasing results; a higher Gradient Ratio implies that more edge details are preserved after dehazing. The small value of NIQE represents that the haze-free image is more natural and realistic.

Finally, Table 22 shows the quantitative results of the real images shown in Fig. 39 using different metrics listed in the table. In this table, the red color of numbers denotes the first position, the green color the second position and the blue color represents the third position. The smaller values of all metrics except the e and r metrics denote the good dehazing capability in terms of distortions (blur, BALC), perceptual quality (NIQE, BLIINDSII, etc.), visibility after haze removal (FADE score), preservation of edges in restored images (e and r), color distortions (saturated pixel ratio). Different categories of methods are involved in the comparison. We can notice in this table that method [62] is at the first position in the overall quality of the dehazed image. The dehazed image has improved visibility, with no over-saturation of pixels and artifacts. In the second place, the DCP method is there with good perceptual quality and preservation of edges. However, it suffers from the halo artifacts problem at depth discontinuities. The performance of the NLD method is reported at the third position with the highest FADE score (no residual haze). However, it suffers from the problem of over-saturation of pixels and lacks perceptual quality. The performance of other methods is average.

Table 22 Quantitative Comparison of different methods using well known no reference quality assessment metrics

| S.No | Metric | AMEF [13] | CAP [64] | NLD [66] | ESIDD [22] | DCP [63] | RASD [51] | MLP [134] | JCDF [62] |
|------|----------------------|------------|----------|----------|------------|----------|-----------|-----------|-----------|
| 1 | FADE ↓ | 0.224 | 0.267 | 0.110 | 0.242 | 0.209 | 0.390 | 0.258 | 0.214 |
| | | 0.371 | 0.328 | 0.196 | 0.293 | 0.300 | 0.463 | 0.366 | 0.312 |
| | | 0.231 | 0.316 | 0.114 | 0.154 | 0.151 | 0.274 | 0.184 | 0.115 |
| 2 | Mean FADE values | 0.275 | 0.304 | 0.140 | 0.230 | 0.220 | 0.376 | 0.269 | 0.214 |
| | | Blur ↓ | 0.163 | 0.164 | 0.153 | 0.180 | 0.171 | 0.183 | 0.160 |
| | | 0.278 | 0.294 | 0.286 | 0.300 | 0.289 | 0.353 | 0.287 | 0.302 |
| 3 | Mean Blur values | 0.216 | 0.240 | 0.221 | 0.271 | 0.228 | 0.249 | 0.215 | 0.213 |
| | | 0.219 | 0.233 | 0.220 | 0.250 | 0.229 | 0.262 | 0.221 | 0.227 |
| | | BALC ↓ | 0.552 | 1.239 | 1.588 | 1.122 | 1.617 | 1.647 | 0.749 |
| 4 | Mean BALC values | 1.935 | 1.573 | 2.268 | 1.937 | 2.079 | 1.828 | 1.908 | 2.228 |
| | | 1.307 | 2.102 | 1.605 | 1.785 | 1.940 | 1.985 | 1.607 | 0.638 |
| | | 1.265 | 1.638 | 1.821 | 1.615 | 1.879 | 1.820 | 1.421 | 0.972 |
| 5 | σ ↓ | 0.430 | 0.020 | 0.290 | 0.120 | 0.020 | 0.030 | 0.080 | 0.000 |
| | | 0.090 | 0.050 | 0.150 | 0.200 | 0.060 | 0.050 | 0.170 | 0.010 |
| | | 0.000 | 5.600 | 0.320 | 1.330 | 0.140 | 0.420 | 0.270 | 0.000 |
| 6 | Mean σ values | 0.173 | 1.890 | 0.253 | 0.550 | 0.073 | 0.167 | 0.173 | 0.003 |
| | | e ↑ | 0.460 | 0.400 | 0.810 | 0.250 | 0.540 | 0.150 | 0.320 |
| | | 0.370 | 0.220 | 0.620 | 0.260 | 0.530 | 0.140 | 0.260 | 0.580 |
| 7 | Mean e values | 0.910 | 1.210 | 1.260 | 1.060 | 1.430 | 0.800 | 0.800 | 1.420 |
| | | 0.580 | 0.610 | 0.897 | 0.523 | 0.833 | 0.363 | 0.460 | 0.897 |
| | | r ↑ | 1.840 | 1.160 | 1.870 | 1.260 | 1.820 | 1.070 | 1.420 |
| 8 | Mean r values | 1.940 | 1.020 | 1.950 | 1.320 | 1.760 | 1.100 | 1.270 | 2.780 |
| | | 2.330 | 0.980 | 2.490 | 1.990 | 1.670 | 1.220 | 1.870 | 4.520 |
| | | 2.037 | 1.053 | 2.103 | 1.523 | 1.750 | 1.130 | 1.520 | 3.220 |
| 9 | NIQE ↓ | 3.299 | 3.208 | 3.261 | 3.253 | 2.862 | 2.735 | 3.371 | 3.140 |
| | | 2.410 | 2.853 | 2.456 | 2.628 | 2.479 | 3.058 | 2.413 | 2.349 |
| | | 3.582 | 3.592 | 3.880 | 4.381 | 3.712 | 3.368 | 3.563 | 3.629 |
| 10 | Mean NIQE values | 3.097 | 3.218 | 3.199 | 3.421 | 3.017 | 3.054 | 3.116 | 3.039 |
| | | BRISQUE ↓ | 32.216 | 25.376 | 35.929 | 31.805 | 25.994 | 17.691 | 27.695 |
| | | 14.709 | 17.816 | 17.214 | 18.581 | 15.044 | 19.861 | 15.163 | 15.026 |
| 11 | Mean BRISQUE values | 13.528 | 13.018 | 13.365 | 22.095 | 12.482 | 9.854 | 13.058 | 13.762 |
| | | 20.151 | 18.737 | 22.169 | 24.160 | 17.840 | 15.802 | 18.639 | 18.586 |
| | | BLIINDS2 ↓ | 11.000 | 9.000 | 17.500 | 26.000 | 5.500 | 7.500 | 12.000 |
| 12 | Mean BLIINDS2 values | 3.000 | 15.000 | 9.000 | 18.500 | 12.000 | 16.000 | 7.000 | 8.000 |
| | | 12.000 | 13.500 | 12.500 | 34.500 | 12.500 | 13.000 | 13.000 | 18.000 |
| | | 8.667 | 12.500 | 13.000 | 26.333 | 10.000 | 12.167 | 10.667 | 11.167 |
| 13 | BIQI ↓ | 45.944 | 31.035 | 47.024 | 25.650 | 39.868 | 19.761 | 38.707 | 41.288 |
| | | 27.115 | 19.930 | 30.340 | 30.652 | 27.440 | 26.991 | 26.901 | 28.494 |
| | | 26.718 | 46.322 | 41.917 | 36.291 | 53.668 | 32.936 | 33.812 | 40.487 |
| 14 | Mean BIQI values | 33.259 | 32.429 | 39.760 | 30.864 | 40.325 | 26.563 | 33.140 | 36.757 |

8 Conclusions and Future Direction

The haze removal methods have drawn the attention of researchers in the recent years due to the various applications in computer vision, especially in video surveillance and transportation systems. In this paper, the recent haze removal methods are investigated. First, for better understanding, these methods are grouped into different categories

based on their similar characteristics. From each group, the prominent methods are selected for analysis on various issues of dehazing. It also introduces many recent categories including non-homogeneous haze removal, hardware architecture, superpixels, ensemble, etc. Then, this survey paper explores most of the evaluation metrics and datasets used by the recent works. Finally, qualitative and quantitative analysis on many datasets including Reside, I-Haze, O-Haze,

D-Hazy, Dense-Haze conducted. Although, this field has achieved remarkable progress. However, many problems or open challenges need to be addressed as follows:

(1) In most of the dehazing methods, a large number of parameters are selected empirically or manually. It limits the dehazing performance and may suffer from various issues of dehazing, such as incomplete haze removal, color distortions or halo artifacts when they are tested on hazy images of different haze concentrations. Adaptive selection of these parameters can cope up with these issues.

(2) There are very limited metrics available and designed especially for dehazing. The researcher in this field used many individual metrics for the assessment of their method. In the future, a single image quality assessment method is required to design that can deal with residual haze, over enhancement, artifacts, color distortions, structure damage, perceptual quality, etc. instead of using multiple metrics.

(3) After a literature study, we found that there exists no single method which can handle different weather conditions such as dense fog, night-time, non-homogeneous, etc. Most of the existing methods are capable to remove mild fog or homogeneous fog. Therefore, fusion based methods and ensemble learning methods may be investigated to meet these challenges that will integrate the advantages of restoration based and deep learning-based methods.

(4) Most of the methods focus on the removal of fog from a single image. There are limited methods that remove the fog of the video with a moving camera. Video fog removal (e.g., video surveillance and transportation system) requires good recovery results with real-time processing. In this direction, hardware implementation-based methods require more attention which processes high-resolution video with low-cost hardware and power consumption.

Declarations

Conflict of interest On behalf of all authors, the corresponding author states that there is no conflict of interest.

References

- Kumar R, Kaushik BK, Balasubramanian R (2017) FPGA implementation of image dehazing algorithm for real time applications. In: Proc SPIE 10396, applications of digital image processing XL. <https://doi.org/10.1117/12.2274682>
- Narasimhan SG, Nayar SK (2002) Vision and the atmosphere. *Int J Comput Vis* 48:233–254
- Li Y, You S, Brown MS, Tan RT (2017) Haze visibility enhancement: A Survey and quantitative benchmarking. *Comput Vis Image Underst* 165:1–16
- Wang W, Yuan X (2017) Recent advances in image dehazing. *IEEE/CAA J Automat Sin* 4(3):410–436. <https://doi.org/10.1109/JAS.2017.7510532>
- Singh D, Kumar VA (2019) Comprehensive review of computational dehazing techniques. *Arch Comput Methods Eng* 26:1395–1413. <https://doi.org/10.1007/s11831-018-9294-z>
- Babu GH, Venkatram N (2020) A survey on analysis and implementation of state-of-the-art haze removal techniques. *J Visu Commun Image Represent* 72:102912. <https://doi.org/10.1016/j.jvcir.2020.102912>
- Das B, Ebenezer JP, Mukhopadhyay SA (2020) Comparative study of single image fog removal methods. *Vis Comput*. <https://doi.org/10.1007/s00371-020-02010-4>
- <https://www.ndtv.com/topic/fog-accident>
- Min X et al (2019) Quality evaluation of image dehazing methods using synthetic hazy images. *IEEE Trans Multimedia* 21(9):2319–2333. <https://doi.org/10.1109/TMM.2019.2902097>
- Shen L, Zhao Y, Peng Q, Chan JC, Kong SG (2019) An iterative image dehazing method with polarization. *IEEE Trans Multimedia* 21(5):1093–1107. <https://doi.org/10.1109/TMM.2018.2871955>
- Ancuti C, Ancuti CO, De Vleeschouwer C, Bovik AC (2020) Day and night-time dehazing by local airlight estimation. *IEEE Trans Image Process* 29:6264–6275. <https://doi.org/10.1109/TIP.2020.2988203>
- Chen W, Ding J, Kuo S (2019) PMS-net: Robust haze removal based on patch map for single images. In: 2019 IEEE/CVF conference on computer vision and pattern recognition (CVPR), Long Beach, CA, USA, pp 11673–11681. <https://doi.org/10.1109/CVPR.2019.01195>
- Galdran A (2018) Image dehazing by artificial multiple-exposure image fusion. *Signal Process* 149:135–147
- Fu X, Wang J, Zeng D, Huang Y, Ding X (2015) Remote sensing image enhancement using regularized-histogram equalization and dct. *IEEE Geosci Remote Sens Lett* 12(11):2301–2305
- Chen BH, Huang SC, Ye JH (2015) Hazy image restoration by bi-histogram modification. *ACM Tran Intell Syst Technol TIST* 6(4):50
- He S, Yang Q, Lau RW, Yang MH (2016) Fast weighted histograms for bilateral filtering and nearest neighbor searching. *IEEE Trans Circ Syst Video Technol* 26(5):891–902
- Mi Z, Zhou H, Zheng Y, Wang M (2016) Single image dehazing via multi-scale gradient domain contrast enhancement. *IET Image Process* 10(3):206–214
- Zheng L, Shi H, Gu M (2017) Infrared traffic image enhancement algorithm based on dark channel prior and gamma correction. *Mod Phys Lett B* 31:1740044
- Gao Y, Chen H, Li H, Zhang W (2017) Single image dehazing using local linear fusion. *IET Image Proc* 12:637–643
- Ju M, Ding C, Zhang D, Guo YJ (2018) Gamma-correction-based visibility restoration for single hazy images. *IEEE Signal Process Lett* 25(7):1084–1088. <https://doi.org/10.1109/LSP.2018.2839580>
- Wang J, Lu K, Xue J, He N, Shao L (2018) Single image dehazing based on the physical model and MSRCR algorithm. *IEEE Trans Circ Syst Video Technol* 28(9):2190–2199. <https://doi.org/10.1109/TCSVT.2017.2728822>
- Liu X, Zhang H, Cheung Y, You X, Tang YY (2017) Efficient single image dehazing and denoising: an efficient multi-scale correlated wavelet approach. *Comput Vis Image Underst* 162:23–33
- Yang H, Yang CH, Tsai YJ (2020) Y-net: multi-scale feature aggregation network with wavelet structure similarity loss function for single image dehazing. In: ICASSP 2020–2020 IEEE international conference on acoustics, speech and signal processing (ICASSP), Barcelona, Spain, pp 2628–2632. <https://doi.org/10.1109/ICASSP40776.2020.9053920>
- He J, Xing FZ, Yang R, Zhang C (2019) Fast single image dehazing via multilevel wavelet transform based optimization. *arXiv: 1904.08573*

25. Singh D, Garg D, Singh Pannu H (2017) Efficient landsat image fusion using fuzzy and stationary discrete wavelet transform. *Imaging Sci J* 65(2):108–114
26. Liu C, Zhao J, Shen Y et al (2016) Texture filtering based physically plausible image dehazing. *Vis Comput* 32:911–920. <https://doi.org/10.1007/s00371-016-1259-3>
27. Singh D, Kumar V (2019) Image dehazing using Moore neighborhood-based gradient profile prior. *Signal Process Image Commun* 70:131–144
28. Tarel JP, Hautiere N, Cord A, Gruyer D, Halmaoui H (2010) Improved visibility of road scene images under heterogeneous fog. In: Proc IEEE Intell Veh Symp, pp 478–485
29. Tarel JP, Hautiere N (2009) Fast visibility restoration from a single color or gray level image. In: Proceedings of the IEEE 12th international conference on computer vision. IEEE, Kyoto, Japan, pp 2201–2208
30. Wang W, Yuan X, Wu X, Liu Y (2017) Fast image dehazing method based on linear transformation. *IEEE Trans Multimedia* 19(6):1142–1155. <https://doi.org/10.1109/TMM.2017.2652069>
31. Salazar-Colores S, Cabal-Yepez E, Ramos-Arreguin JM, Botella G, Ledesma-Carrillo LM, Ledesma S (2019) A fast image dehazing algorithm using morphological reconstruction. *IEEE Trans Image Process* 28(5):2357–2366. <https://doi.org/10.1109/TIP.2018.2885490>
32. Bi G, Ren J, Fu T, Nie T, Chen C, Zhang N (2017) Image dehazing based on accurate estimation of transmission in the atmospheric scattering model. *IEEE Photon J* 9(4):1–18. <https://doi.org/10.1109/JPHOT.2017.2726107>
33. Li Z, Zheng J (2018) Single image de-hazing using globally guided image filtering. *IEEE Trans Image Process* 27(1):442–450. <https://doi.org/10.1109/TIP.2017.2750418>
34. Fan X, Wang Y, Tang X, Gao R, Luo Z (2017) Two-layer Gaussian process regression with example selection for image dehazing. *IEEE Trans Circuits Syst Video Technol* 27(12):2505–2517. <https://doi.org/10.1109/TCSVT.2016.2592328>
35. Riaz I, Yu T, Rehman Y, Shin H (2016) Single image dehazing via reliability guided fusion. *J Vis Commun Image Represent* 40:85–97
36. Xiao J, Shen M, Lei J, Zhou J, Klette R, Sui HG (2020) Single image dehazing based on learning of haze layers. *Neurocomputing* 389:108–122
37. Jiang B, Meng H, Ma X et al (2018) Nighttime image Dehazing with modified models of color transfer and guided image filter. *Multimed Tools Appl* 77:3125–3141. <https://doi.org/10.1007/s11042-017-4954-9>
38. He K, Sun J, Tang X (2013) Guided image filtering. *IEEE Trans Pattern Anal Mach Intell* 35(6):1397–1409
39. Li Z, Zheng J, Zhu Z, Yao W, Wu S (2015) Weighted guided image filtering. *IEEE Trans Image Process* 24(1):120–129
40. Singh D, Kumar V, Kaur M (2019) Single image dehazing using gradient channel prior. *Appl Intell* 49:4276–4293. <https://doi.org/10.1007/s10489-019-01504-6>
41. Nandal S, Kumar S (2019) Single image fog removal algorithm in spatial domain using fractional order anisotropic diffusion. *Multimed Tools Appl* 78:10717–10732. <https://doi.org/10.1007/s11042-018-6576-2>
42. Ancuti CO, Ancuti C (2013) Single image dehazing by multi-scale fusion. *IEEE Trans Image Process* 22(8):3271–3282
43. Vazquez-Corral J, Galdran A, Cyriac P et al (2020) A fast image dehazing method that does not introduce color artifacts. *J Real-Time Image Proc* 17:607–622. <https://doi.org/10.1007/s11554-018-0816-6>
44. Liu P, Horng S, Lin J, Li T (2019) Contrast in haze removal: configurable contrast enhancement model based on dark channel prior. *IEEE Trans Image Process* 28(5):2212–2227. <https://doi.org/10.1109/TIP.2018.2823424>
45. Baig N, Riaz MM, Ghafoor A, Siddiqui AM (2016) Image dehazing using quadtree decomposition and entropy-based contextual regularization. *IEEE Signal Process Lett* 23(6):853–857. <https://doi.org/10.1109/LSP.2016.2559805>
46. Yuan H, Liu C, Guo Z, Sun Z (2017) A region-wised medium transmission based image dehazing method. *IEEE Access* 5:1735–1742
47. Raikwar SC, Tapaswi S (2020) Lower bound on transmission using non-linear bounding function in single image dehazing. *IEEE Trans Image Process* 29:4832–4847. <https://doi.org/10.1109/TIP.2020.2975909>
48. Zhang S, He F, Ren W et al (2020) Joint learning of image detail and transmission map for single image dehazing. *Vis Comput* 36:305–316. <https://doi.org/10.1007/s00371-018-1612-9>
49. Meng G, Wang Y, Duan J, Xiang S, Pan C (2013) Efficient image dehazing with boundary constraint and contextual regularization. In: Proceedings of the IEEE international conference on computer vision, pp 617–624
50. Cui T, Tian J, Wang E, Tang Y (2017) Single image dehazing by latent region-segmentation based transmission estimation and weighted L 1-norm regularization. *IET Image Proc* 11(2):145–154
51. Chen C, Do MN, Wang J (2016) Robust image and video dehazing with visual artifact suppression via gradient residual minimization. In: European conference on computer vision. Springer, pp 576–591
52. Wang X, Ju M, Zhang D (2017) Image haze removal via multi-scale fusion and total variation. *J Syst Eng Electron* 28(3):597–605. <https://doi.org/10.21629/JSEE.2017.03.19>
53. Liu Q, Gao X, He L, Lu W (2018) Single image dehazing with depth-aware non-local total variation regularization. *IEEE Trans Image Process* 27(10):5178–5191. <https://doi.org/10.1109/TIP.2018.2849928>
54. Wu Q, Zhang J, Ren W, Zuo W, Cao X (2020) Accurate transmission estimation for removing haze and noise from a single image. *IEEE Trans Image Process* 29:2583–2597. <https://doi.org/10.1109/TIP.2019.2949392>
55. Park J, Han DK, Ko H (2020) Fusion of heterogeneous adversarial networks for single image dehazing. *IEEE Trans Image Process* 29:4721–4732. <https://doi.org/10.1109/TIP.2020.2975986>
56. Zhu Z, Wei H, Hu G, Li Y, Qi G, Mazur N (2021) A novel fast single image dehazing algorithm based on artificial multiexposure image fusion. *IEEE Trans Instrum Meas* 70:1–23. <https://doi.org/10.1109/TIM.2020.3024335>
57. Yuan F, Zhou Y, Xia X, Shi J, Fang Y, Qian X (2020) Image dehazing based on a transmission fusion strategy by automatic image matting. *Comput Vis Image Underst* 194:102933
58. Ma Z, Wen J, Zhang C, Liu Q, Yan D (2016) An effective fusion defogging approach for single sea fog image. *Neuro-computing* 173:1257–1267
59. Son C, Zhang X (2018) Near-infrared fusion via color regularization for haze and color distortion removals. *IEEE Trans Circuits Syst Video Technol* 28(11):3111–3126. <https://doi.org/10.1109/TCSVT.2017.2748150>
60. Shibata T, Tanaka M, Okutomi M (2019) Unified image fusion framework with learning-based application-adaptive importance measure. *IEEE Trans Comput Imaging* 5(1):82–96. <https://doi.org/10.1109/TCI.2018.2879021>
61. Zhao D, Xu L, Yan Y, Chen J, Duan L-Y (2019) Multi-scale optimal fusion model for single image dehazing. *Signal Process* 74:253–265
62. Agrawal SC, Jalal AS (2021) A joint cumulative distribution function and gradient fusion-based method for dehazing of long shot hazy images. *J Vis Commun Image Represent* 77:103087

63. He K, Sun J, Tang X (2010) Single image haze removal using dark channel prior. *IEEE Trans Pattern Anal Mach Intell* 33(12):2341–2353
64. Zhu Q, Mai J, Shao L et al (2015) A fast single image haze removal algorithm using color attenuation prior. *TIP* 24(11):3522–3533
65. Zhenfei Gu, Mingye Ju, Zhang D (2017) A single image dehazing method using average saturation prior. *Math Probl Eng.* <https://doi.org/10.1155/2017/6851301>
66. Berman D, Treibitz T, Avidan S (2020) Single image dehazing using haze-lines. *IEEE Trans Pattern Anal Mach Intel* 42(3):720–734. <https://doi.org/10.1109/TPAMI.2018.2882478>
67. Bui TM, Kim W (2018) Single image dehazing using color ellipsoid prior. *IEEE Trans Image Process* 27(2):999–1009. <https://doi.org/10.1109/TIP.2017.2771158>
68. Mei K, Jiang A, Li J, Li J, Wang M (2019) Progressive feature fusion network for realistic image dehazing. In: Asian conference on computer vision. https://doi.org/10.1007/978-3-030-20887-5_13
69. Salazar-Colores S, Ramos-Arreguín JM, Pedraza-Ortega JC et al (2019) Efficient single image dehazing by modifying the dark channel prior. *J Image Video Proc* 2019:66. <https://doi.org/10.1186/s13640-019-0447-2>
70. Zhang L, Wang S, Wang X (2018) Saliency-based dark channel prior model for single image haze removal. *IET Image Process* 12(6):1049–1055
71. Zhu M, He B, Wu Q (2018) Single image dehazing based on dark channel prior and energy minimization. *IEEE Signal Process Lett* 25(2):174–178. <https://doi.org/10.1109/LSP.2017.2780886>
72. Shiau Y, Yang H, Chen P, Chuang Y (2013) Hardware implementation of a fast and efficient haze removal method. *IEEE Trans Circ Syst Video Technol* 23(8):1369–1374. <https://doi.org/10.1109/TCSVT.2013.2243650>
73. Ren W, Liu S, Zhang H, Pan J, Cao X, Yang M-H (2016) Single image dehazing via multi-scale convolutional neural networks. In: ECCV, 2016
74. Cai B, Xu X, Jia K, Qing C, Tao D (2016) Dehazenet: an end-to-end system for single image haze removal. *IEEE Trans Image Process* 25(11):5187–5198
75. Li B, Peng X, Wang Z, Xu J, Feng D (2017) Aod-net: all-in-one dehazing network. In: Proceedings of the IEEE international conference on computer vision, pp 4770–4778
76. Engin D, Genc A, Ekenel HK (2018) Cycle-dehaze: enhanced CycleGAN for single image dehazing. In: 2018 IEEE/CVF conference on computer vision and pattern recognition workshops (CVPRW), Salt Lake City, UT, pp 938–9388. <https://doi.org/10.1109/CVPRW.2018.00127>
77. Ren W, Ma L, Zhang J, Pan J, Cao X, Liu W, Yang M-H (2018) Gated fusion network for single image dehazing. In: Proceedings of the IEEE conference on computer vision and pattern recognition, pp 3253–3261
78. Liu Z, Xiao B, Alrabeiah M, Wang K, Chen J (2019) Single image dehazing with a generic model-agnostic convolutional neural network. *IEEE Signal Process Lett* 26(6):833–837
79. Singh A, Bhate A, Prasad DK (2020) Single image dehazing for a variety of haze scenarios using back projected pyramid network. In: European conference on computer vision workshops
80. Gandelsman Y, Shocher A, Irani M (2019) Double-DIP: unsupervised image decomposition via coupled deepimage-priors. In: CVPR
81. Li B, Gou Y, Liu JZ, Zhu H, Zhou JT, Peng X (2020) Zero-shot image dehazing. *IEEE Trans Image Process* 29:8457–8466. <https://doi.org/10.1109/TIP.2020.3016134>
82. Liu Y, Pan J, Ren J, Su Z (2019) Learning deep priors for image dehazing. In: Proceedings of the IEEE/CVF international conference on computer vision (ICCV), pp 2492–2500
83. Zhang H, Sindagi V, Patel VM (2020) Joint transmission map estimation and dehazing using deep networks. *IEEE Trans Circ Syst Video Technol* 30(7):1975–1986
84. Chen D, He M, Fan Q, Liao J, Zhang L, Hou D, Yuan L, Hua G (2019) Gated context aggregation network for image dehazing and deraining. In: 2019 IEEE winter conference on applications of computer vision (WACV), pp 1375–1383
85. Zhang H, Sindagi V, Patel VM (2018) Multi-scale single image dehazing using perceptual pyramid deep network. In: 2018 IEEE/CVF conference on computer vision and pattern recognition workshops (CVPRW), Salt Lake City, UT, pp 1015–101509. <https://doi.org/10.1109/CVPRW.2018.00135>
86. Qin X, Wang Z, Bai Y, Xie X, Jia H (2019) Ffa-net: feature fusion attention network for single image dehazing. [arXiv:1911.07559](https://arxiv.org/abs/1911.07559)
87. Li L, Dong Y, Ren W, Pan J, Gao C, Sang N, Yang MH (2019) Semi-supervised image dehazing. *IEEE Trans Image Process.* <https://doi.org/10.1109/TIP.2019.2952690>
88. Golts A, Freedman D, Elad M (2020) Unsupervised single image dehazing using dark channel prior loss. *IEEE Trans Image Process* 29:2692–2701. <https://doi.org/10.1109/TIP.2019.2952032>
89. Agrawal SC, Jalal AS (2022) Distortion-free image dehazing by superpixels and ensemble neural network. *Vis Comput* 38:781–796. <https://doi.org/10.1007/s00371-020-02049-3>
90. Yu M, Cherukuri V, Guo T, Monga V (2020) Ensemble dehazing networks for non-homogeneous haze. In: 2020 IEEE/CVF conference on computer vision and pattern recognition workshops (CVPRW), Seattle, WA, USA, pp 1832–1841. <https://doi.org/10.1109/CVPRW50498.2020.00233>
91. Zhang S, Wu Y, Zhao Y, Cheng Z, Ren W (2020) Color-Constrained Dehazing Model. In: 2020 IEEE/CVF conference on computer vision and pattern recognition workshops (CVPRW), Seattle, WA, USA, pp 3799–3807. <https://doi.org/10.1109/CVPRW50498.2020.00443>
92. Golts A, Freedman D, Elad M Deep-energy: unsupervised training of deep neural networks. <https://arxiv.org/abs/1805.12355>
93. Li B, Gou Y, Gu S, Liu JZ, Zhou JT, Peng X (2020) You only look yourself: Unsupervised and untrained single image dehazing neural network. [http://arxiv.org/abs/2006.16829](https://arxiv.org/abs/2006.16829)
94. Metwaly K, Li X, Guo T, Monga V (2020) NonLocal channel attention for nonhomogeneous image dehazing. 2020 IEEE/CVF conference on computer vision and pattern recognition workshops (CVPRW), Seattle, WA, USA, pp 1842–1851. <https://doi.org/10.1109/CVPRW50498.2020.00234>
95. Wu H, Liu J, Xie Y, Qu Y, Ma L (2020) Knowledge transfer dehazing network for non-homogeneous dehazing. In: Proceedings of the IEEE/CVF conference on computer vision and pattern recognition (CVPR) workshops, pp 478–479
96. Tarel J, Hautiere N, Caraffa L, Cord A, Halmaoui H, Gruyer D (2012) Vision enhancement in homogeneous and heterogeneous fog. *IEEE Intel Transport Syst Mag* 4(2):6–20. <https://doi.org/10.1109/MITS.2012.2189969>
97. Fattal R (2014) Dehazing using color-lines. *ACM Trans Graph* 34(1):13
98. Ma K, Liu W, Wang Z (2015) Perceptual evaluation of single image dehazing algorithms. In: 2015 IEEE international conference on image processing (ICIP), Quebec City, QC, pp 3600–3604. <https://doi.org/10.1109/ICIP.2015.7351475>
99. Choi LK, You J, Bovik AC (2015) Referenceless prediction of perceptual fog density and perceptual image defogging. *IEEE Trans Image Process* 24(11):3888–3901. <https://doi.org/10.1109/TIP.2015.2456502>

100. Ancuti C, Ancuti CO, De Vleeschouwer C (2016) D-HAZY: a dataset to evaluate quantitatively dehazing algorithms. In: 2016 IEEE international conference on image processing (ICIP), Phoenix, AZ, pp 2226–2230. <https://doi.org/10.1109/ICIP.2016.7532754>
101. Lee Y-H, Tang S-J (2021) A Design of Image Dehazing Engine Using DTE and DAE Techniques. *IEEE Trans Circ Syst Video Technol.* <https://doi.org/10.1109/TCSVT.2020.3034250>
102. Sakaridis C, Dai D, Van Gool L (2017) Semantic foggy scene understanding with synthetic data. [arXiv:1708.07819](https://arxiv.org/abs/1708.07819)
103. Zhang Y, Ding L, Sharma G (2017) Hazerd: an outdoor scene dataset and benchmark for single image dehazing. In: 2017 IEEE international conference on image processing (ICIP). IEEE, pp 3205–3209
104. Ancuti CO, Ancuti C, Timofte R, De Vleeschouwer C (2018) I-HAZE: a dehazing benchmark with real hazy and haze-free indoor images. *ArXiv e-prints*
105. Ancuti CO, Ancuti C, Timofte R, De Vleeschouwer C (2018) O-HAZE: a dehazing benchmark with real hazy and haze-free outdoor images. In: 2018 IEEE/CVF conference on computer vision and pattern recognition workshops (CVPRW), Salt Lake City, UT, pp 867–8678. <https://doi.org/10.1109/CVPRW.2018.00119>.
106. Ancuti CO, Ancuti C, Sbert M, Timofte R (2019) Dense haze: a benchmark for image dehazing with dense-haze and haze-free images. In: IEEE international conference on image processing (ICIP)
107. Li B et al (2019) Benchmarking single-image dehazing and beyond. *IEEE Trans Image Process* 28(1):492–505. <https://doi.org/10.1109/TIP.2018.2867951>
108. Ancuti CO, Ancuti C, Timofte R (2020) NH-HAZE: an image dehazing benchmark with non-homogeneous hazy and haze-free images. In: Proceedings of the IEEE/CVF conference on computer vision and pattern recognition workshops, pp 444–445
109. Borkar K, Mukherjee S (2020) Single image dehazing by approximating and eliminating the additional airlight component. *Neurocomputing* 400:294–308
110. Hautiere N, Tarel JP, Aubert D, Dumont E (2008) Blind contrast enhancement assessment by gradient ratioing at visible edges. *Image Anal Stereol* J 27(2):87–95
111. Zhan Y, Zhang R (2017) No-reference JPEG image quality assessment based on blockiness and luminance change. *IEEE Signal Process Lett* 24(6):760–764. <https://doi.org/10.1109/LSP.2017.2688371>
112. Crete-Roffet F, Dolmire T, Ladret P, Nicolas M (2007) The blur effect: perception and estimation with a new no-reference perceptual blur metric. In: SPIE
113. Saad MA, Bovik AC, Charrier C (2012) Blind image quality assessment: a natural scene statistics approach in the DCT domain. *IEEE Trans Image Process* 21(8):3339–3352. <https://doi.org/10.1109/TIP.2012.2191563>
114. Mittal A, Moorthy AK, Bovik AC (2012) No-reference image quality assessment in the spatial domain. *IEEE Trans Image Process* 21(12):4695–4708
115. Mittal A, Soundararajan R, Bovik AC (2013) Making a “completely blind” image quality analyzer. *IEEE Signal Process Lett* 20(3):209–212. <https://doi.org/10.1109/LSP.2012.2227726>
116. Min X, Zhai G, Gu K, Yang X, Guan X (2019) Objective quality evaluation of dehazed images. *IEEE Trans Intell Transport Syst* 20(8):2879–2892. <https://doi.org/10.1109/TITS.2018.2868771>
117. Zhang R, Isola P, Efros AA, Shechtman E, Wang O (2018) The unreasonable effectiveness of deep features as a perceptual metric. In: Proc CVPR
118. Luan Z, Shang Y, Zhou X, Shao Z, Guo G, Liu X (2017) Fast single image dehazing based on a regression model. *Neurocomputing* 245:10–22
119. Wang Z, Bovik AC (2006) Modern image quality assessment. *Synth Lect Image Video Multimedia Process.* <https://doi.org/10.2200/S00010ED1V01Y200508IVM003>
120. Wang Z, Bovik AC, Sheikh HR, Simoncelli EP (2004) Image quality assessment: from error visibility to structural similarity. *IEEE Trans Image Process* 13(4):600–612
121. Sharma G, Wu W, Dalal E (2005) The ciede2000 color difference formula: Implementation notes, supplementary test data, and mathematical observations. *Color Res Appl.* <https://doi.org/10.1002/col.20070>
122. Westland S, Ripamonti C, Cheung V (2005) Computational colour science using matlab, 2nd edn. Wiley, New York
123. Shi L et al (Sept. 2018) Removing haze particles from single image via exponential inference with support vector data description. *IEEE Trans Multimedia* 20(9):2503–2512. <https://doi.org/10.1109/TMM.2018.2807593>
124. Sharma P, Jain P, Sur A (2020) Scale-aware conditional generative adversarial network for image dehazing. In: Proceedings of the IEEE/CVF winter conference on applications of computer vision (WACV), pp 2355–2365
125. <https://timesofindia.indiatimes.com/india/over-10000-lives-lost-in-fog-related-road-crashes/articleshow/67391588.cms>
126. Santra S, Mondal R, Chanda B (2018) Learning a patch quality comparator for single image dehazing. *IEEE Trans Image Process* 27(9):4598–4607. <https://doi.org/10.1109/TIP.2018.2841198>
127. Yang D, Sun J (2018) Proximal dehaze-net: a prior learning-based deep network for single image dehazing. In: ECCV, pp 702–717
128. Deng Z, Zhu L, Hu X, Fu C-W, Xu X, Zhang Q, Qin J, Heng P-A (2019) Deep multi-model fusion for single-image dehazing. In: Proceedings of the IEEE/CVF international conference on computer vision (ICCV), pp 2453–2462
129. Bianco S, Celona L, Piccoli F, Schettini R (2019) High-resolution single image dehazing using encoder-decoder architecture. In: 2019 IEEE/CVF conference on computer vision and pattern recognition workshops (CVPRW), Long Beach, CA, USA, pp 1927–1935. <https://doi.org/10.1109/CVPRW.2019.00244>
130. Agrawal SC, Jalal AS (2022) Dense haze removal by non-linear transformation. *IEEE Trans Circuits Syst Video Technol* 32(2):593–607. <https://doi.org/10.1109/TCSVT.2021.3068625>
131. Zhang B, Zhao J (2017) Hardware implementation for real-time haze removal”. *IEEE Trans Very Large Scale Integr Syst* 25(3):1188–1192
132. Shiau Y-H, Kuo Y-T, Chen P-Y, Hsu F-Y (2019) VLSI design of an efficient flicker-free video defogging method for real-time applications. *IEEE Trans Circuits Syst Video Technol* 29(1):238–251
133. Kumar R, Balasubramanian R, Kaushik BK (2020) Efficient method and architecture for real-time video defogging. *IEEE Trans Intell Transp Syst.* <https://doi.org/10.1109/TITS.2020.2993906>
134. Salazar-Colores S, Cruz-Aceves I, Ramos-Arreguin J (2018) Single image dehazing using a multilayer perceptron. *J Electron Imaging.* <https://doi.org/10.1117/1.JEI.27.4.043022>
135. Zhu Y, Tang G, Zhang X, Jiang J, Tian Q (2018) Haze removal method for natural restoration of images with sky. *Neurocomputing* 275:499–510
136. Ju M, Ding C, Ren W, Yang Y, Zhang D, Guo YJ (2021) IDE: image dehazing and exposure using an enhanced atmospheric scattering model. *IEEE Trans Image Process* 30:2180–2192. <https://doi.org/10.1109/TIP.2021.3050643>

137. Sahu G, Seal A, Krejcar O, Yazidi A (2021) Single image dehazing using a new color channel. *J Visual Commun Image Represent* 74:103008
138. Ju M, Ding C, Guo YJ, Zhang D (2020) IDGCP: image dehazing based on gamma correction prior. *IEEE Trans Image Process* 29:3104–3118. <https://doi.org/10.1109/TIP.2019.2957852>
139. Morales P, Klinghofer T, Lee SJ (2019) Feature forwarding for efficient single image dehazing. In: Proceedings of the IEEE/CVF conference on computer vision and pattern recognition (CVPR) workshops
140. Zheng X, et al. (2018) Strong baseline for single image dehazing with deep features and instance normalization. In: BMVC
141. Yang A, Wang H, Ji Z, Pang Y, Shao L (2019) Dual-path in dual-path network for single image dehazing. In: Proceedings of the twenty-eighth international joint conference on artificial intelligence main track, pp 4627–4634. <https://doi.org/10.24963/ijcai.2019/643>
142. Zhang H, Patel VM (2018) Densely connected pyramid dehazing network. In: CVPR, pp 3194–3203
143. Galdran A, Vazquez-Corral J, Pardo D, Bertalmio M (2017) Fusion-based variational image dehazing. *IEEE Signal Process Lett* 24(2):151–155. <https://doi.org/10.1109/LSP.2016.2643168>
144. Zheng M, Qi G, Zhu Z, Li Y, Wei H, Liu Y (2020) Image dehazing by an artificial image fusion method based on adaptive structure decomposition. *IEEE Sens J* 20(14):8062–8072. <https://doi.org/10.1109/JSEN.2020.2981719>
145. Gao Y, Su Y, Li Q, Li H, Li J (2020) Single image dehazing via self-constructing image fusion. *Signal Process* 167:107284
146. Wang B, Wei B, Kang Z et al (2020) Fast color balance and multi-path fusion for sandstorm image enhancement. SIViP. <https://doi.org/10.1007/s11760-020-01786-1>
147. Huo F, Zhu X, Zeng H, Liu Q, Qiu J (2021) Fast fusion-based dehazing with histogram modification and improved atmospheric illumination prior. *IEEE Sens J* 21(4):5259–5270. <https://doi.org/10.1109/JSEN.2020.3033713>
148. Hong S, Kim M, Kang MG (2021) Single image dehazing via atmospheric scattering model-based image fusion. *Signal Process* 178:107798
149. Wang R, Li R, Sun H (2016) Haze removal based on multiple scattering model with superpixel algorithm. *Signal Process* 127:24–36
150. Jiang Y, Sun C, Zhao Y, Yang L (2017) Image dehazing using adaptive bi-channel priors on superpixels. *Comput Vis Image Understand* 165:17–32
151. Yang M, Liu J, Li Z (2018) Superpixel-based single nighttime image haze removal. *IEEE Trans Multimedia* 20(11):3008–3018. <https://doi.org/10.1109/TMM.2018.2820327>
152. Wang P, Fan Q, Zhang Y, Bao F, Zhang C (2019) A novel dehazing method for color fidelity and contrast enhancement on mobile devices. *IEEE Trans Consum Electron* 65(1):47–56. <https://doi.org/10.1109/TCE.2018.2884794>
153. Hassan H, Bashir AK, Ahmad M et al (2020) Real-time image dehazing by superpixels segmentation and guidance filter. *J Real-Time Image Proc.* <https://doi.org/10.1007/s11554-020-00953-4>
154. Wang LZSWX (2021) Single image dehazing based on bright channel prior model and saliency analysis strategy. *IET Image Proc* 15(3):1023–1031
155. Tan Y, Wang G (2020) Image haze removal based on superpixels and Markov random field. *IEEE Access* 8:60728–60736. <https://doi.org/10.1109/ACCESS.2020.2982910>
156. Yuan F, Huang H (2018) Image haze removal via reference retrieval and scene prior. *IEEE Trans Image Process* 27(9):4395–4409. <https://doi.org/10.1109/TIP.2018.2837900>
157. Mandal S, Rajagopalan AN (2020) Local proximity for enhanced visibility in haze. *IEEE Trans Image Process* 29:2478–2491
158. Reda M, Zhao Y, Chan JC-W (2017) polarization guided autoregressive model for depth recovery. *IEEE Photon J* 9(3):1–16
159. Haofeng Hu, Zhao L, Li X, Wang H, Yang J, Li K, Liu T (2018) Polarimetric image recovery in turbid media employing circularly polarized light. *Opt Express* 26:25047–25059
160. Li X et al (2019) Pseudo-polarimetric method for dense haze removal. *IEEE Photon J* 11(1):1–11. <https://doi.org/10.1109/JPHOT.2018.2890771>
161. Tian Y, Liu B, Su X, Wang L, Li K (2019) Underwater imaging based on LF and polarization. *IEEE Photon J* 11(1):1–9. <https://doi.org/10.1109/JPHOT.2018.2890286>
162. Liang Z, Ding X, Mi Z, Wang Y, Fu X (2022) Effective polarization-based image dehazing with regularization constraint". *IEEE Geosci Remote Sens Lett*. <https://doi.org/10.1109/LGRS.2020.3023805>
163. Zhang L, Yin Z, Zhao K, Tian H (2020) Lane detection in dense fog using a polarimetric dehazing method. *Appl Opt* 59:5702–5707
164. Kim SE, Park TH, Eom IK (2020) Fast single image dehazing using saturation based transmission map estimation. *IEEE Trans Image Process* 29:1985–1998. <https://doi.org/10.1109/TIP.2019.2948279>
165. Lu Z, Long B, Yang S (2020) Saturation based iterative approach for single image dehazing. *IEEE Signal Process Lett* 27:665–669. <https://doi.org/10.1109/LSP.2020.2985570>
166. Gao Y, Hu H, Li B, Guo Q, Pu S (2019) Detail preserved single image dehazing algorithm based on airlight refinement. *IEEE Trans Multimedia* 21(2):351–362. <https://doi.org/10.1109/TMM.2018.2856095>
167. Wang A, Wang W, Liu J, Gu N (2019) AIPNet: image-to-image single image dehazing with atmospheric illumination prior. *IEEE Trans Image Process* 28(1):381–393. <https://doi.org/10.1109/TIP.2018.2868567>
168. Hu H, Zhang H, Zhao Z, Li B, Zheng J (2020) Adaptive single image dehazing using joint local-global illumination adjustment. *IEEE Trans Multimedia* 22(6):1485–1495. <https://doi.org/10.1109/TMM.2019.2944260>
169. Dhara SK, Roy M, Sen D, Biswas PK (2021) Color cast dependent image dehazing via adaptive airlight refinement and non-linear color balancing. *IEEE Trans Circ Syst Video Technol*. <https://doi.org/10.1109/TCSVT.2020.3007850>
170. Lee Y, Wu B (2019) Algorithm and architecture design of a hardware-efficient image dehazing engine. *IEEE Trans Circuits Syst Video Technol* 29(7):2146–2161. <https://doi.org/10.1109/TCSVT.2018.2862906>
171. Kumar R, Kaushik BK, Balasubramanian R (2019) Multi-spectral transmission map fusion method and architecture for image dehazing. *IEEE Trans Very Large-Scale Integr Syst* 27(11):2693–2697
172. Soma P, Jatoh RK (2020) Implementation of a novel, fast and efficient image de-hazing algorithm on embedded hardware platforms. *Circuits Syst Signal Process*. <https://doi.org/10.1007/s00034-020-01517-4>
173. Wu X, Wang K, Li Y, Liu K, Huang B (2021) Accelerating haze removal algorithm using CUDA. *Remote Sens* 13(1):85. <https://doi.org/10.3390/rs13010085>
174. Xie CH, Qiao WW, Liu Z et al (2017) Single image dehazing using kernel regression model and dark channel prior. SIViP 11:705–712. <https://doi.org/10.1007/s11760-016-1013-3>
175. Chen B, Huang S, Li C, Kuo S (2018) Haze removal using radial basis function networks for visibility restoration applications. *IEEE Trans Neural Netw Learn Syst* 29(8):3828–3838. <https://doi.org/10.1109/TNNLS.2017.2741975>
176. Kang C, Kim G (2018) Single image haze removal method using conditional random fields. *IEEE Signal Process Lett* 25(6):818–822. <https://doi.org/10.1109/LSP.2018.2827882>

177. Yin JL, Huang YC, Chen BH, Ye SZ (2020) Color transferred convolutional neural networks for image dehazing. *IEEE Trans Circuits Syst Video Technol* 30(11):3957–3967. <https://doi.org/10.1109/TCSVT.2019.2917315>
178. Chaitanya BSNV, Mukherjee S (2021) Single image dehazing using improved cycleGAN. *J Visual Commun Image Represent* 74:103014
179. Li Y, Liu Y, Yan Q, Zhang K (2021) Deep dehazing network with latent ensembling architecture and adversarial learning. *IEEE Trans Image Process* 30:1354–1368. <https://doi.org/10.1109/TIP.2020.3044208>
180. Sun Z, Zhang Y, Bao F, Shao K, Liu X, Zhang C (2021) ICycleGAN: Single image dehazing based on iterative dehazing model and CycleGAN. *Comput Vis Image Understand* 203:1031332
181. Huang L, Yin J, Chen B, Ye S (2019) Towards unsupervised single image dehazing with deep learning. In: 2019 IEEE international conference on image processing (ICIP), Taipei, Taiwan, pp 2741–2745. <https://doi.org/10.1109/ICIP.2019.8803316>.
182. Liu R, Ma L, Wang Y, Zhang L (2019) Learning converged propagations with deep prior ensemble for image enhancement. IEEE Trans Image Process 28(3):1528–1543. <https://doi.org/10.1109/TIP.2018.2875568>
183. Das SD, Dutta S (2020) Fast deep multi-patch hierarchical network for nonhomogeneous image dehazing. In: Proceedings of the IEEE/CVF conference on computer vision and pattern recognition (CVPR) workshops, pp 482–483
184. Mehta A, Sinha H, Mandal M, Narang P (2021) Domain-aware unsupervised hyperspectral reconstruction for aerial image dehazing. In: Proceedings of the IEEE/CVF winter conference on applications of computer vision (WACV), pp 413–422
185. Mehta A, Sinha H, Narang P, Murari (2020) HIDEGAN: a hyperspectral-guided image Dehazing GAN Mandal. In: Proceedings of the IEEE/CVF conference on computer vision and pattern recognition (CVPR) workshops, pp 212–213
186. Dudhane A, Murala S (2020) RYF-net: deep fusion network for single image haze removal. *IEEE Trans Image Process* 29:628–640. <https://doi.org/10.1109/TIP.2019.2934360>

Publisher's Note Springer Nature remains neutral with regard to jurisdictional claims in published maps and institutional affiliations.